COOLABILITY BEHAVIOUR OF TOP AND BOTTOM FLOODED MOLTEN CORIUM POOL WITH MOLTEN CORE –CONCRETE INTERACTION

By

PARIMAL PRAMOD KULKARNI

ENGG0120074017

Bhabha Atomic Research Centre

A thesis submitted to the
Board of Studies in Engineering Sciences

In partial fulfilment of requirements

For the Degree of

Doctor of Philosophy

of

HOMI BHABHA NATIONAL INSTITUTE

July 2015

Homi Bhabha National Institute

Recommendations of the Viva Voce Board

As members of the Viva Voce Board, we certify that we have read the dissertation prepared by Parimal Pramod Kulkarni entitled “Coolability Behaviour of Top and Bottom Flooded Molten Corium Pool with Molten Core –Concrete Interaction” and recommend that it may be accepted as fulfilling the dissertation requirement for the Degree of Doctor of Philosophy.

____**Date:**
Chairman- Dr (Smt) S. B. Roy

____**Date:**
Guide: Dr A. K. Nayak

____**Date:**
Examiner Prof. S. V. Prabhu

____**Date:**
Member -1 Dr D. Srivastava

____**Date:**
Member -2 Dr (Smt) S. Mukhopadhyay

____**Date:**
Member -3 Dr Rajeev Kapoor

Final approval and acceptance of this dissertation is contingent upon the candidate’s submission of the final copies of the dissertation to HBNI.

I hereby certify that I have read this dissertation prepared under my direction and recommend that it may be accepted as fulfilling the dissertation requirement.

Date:

Place:

Guide (Dr A. K. Nayak)

STATEMENT BY AUTHOR

This dissertation has been submitted in partial fulfilment of requirements for an advanced degree at Homi Bhabha National Institute (HBNI) and is deposited in the Library to be made available to borrowers under rules of the HBNI.

Brief quotations from this dissertation are allowable without special permission, provided that accurate acknowledgement of source is made. Requests for permission for extended quotation from or reproduction of this manuscript in whole or in part may be granted by the Competent Authority of HBNI when in his or her judgment the proposed use of the material is in the interests of scholarship. In all other instances, however, permission must be obtained from the author.

Parimal Pramod Kulkarni

DECLARATION

I, hereby declare that the investigation presented in the thesis has been carried out by me. The work is original and has not been submitted earlier as a whole or in part for a degree / diploma at this or any other Institution / University.

Parimal Pramod Kulkarni

List of Publications Resulting out of this thesis

Journal

1. "Study on coolability of melt pool with different strategies" P. P. Kulkarni, A. K. Nayak, *Nuclear Engineering and Design*, **2014**, *270*, 379–388
2. "Quenching Behaviour of Top Flooded Molten Pool", P. P. Kulkarni , A. K. Nayak, *International Journal of Nuclear Energy Science and Engineering*, **2014**, , *4(1),* 20-25.
3. "A simple model to understand physics of melt coolability under bottom flooding" P. P. Kulkarni, A. K. Nayak, Nuclear Engineering and Design, **2013**, *262*, 81– 87.
4. "Experimental Investigation of Coolability Behaviour of Irregularly Shaped Particulate Debris Bed", P. P. Kulkarni, M. Rashid, R. Kulenovic and A. K. Nayak, *Nuclear Engineering Design,* **2010**, *240*, 3067-3077.
5. "A Numerical and Experimental Study of Water Ingression Phenomena in Melt Pool Coolability", A. K. Nayak, R. K. Singh, P. P. Kulkarni and Bal Raj Sehgal, *Nuclear Engineering Design*, **2009,** 1285-1293.

Conferences

1. "Assessment of Capability of Models for Prediction of Pressure Drop and Dryout Heat Flux in a Heat Generating Particulate Debris Bed", P. P. Kulkarni, M. Rashid, R. Kulenovic and A. K. Nayak, , 13th International Topical Meeting on Nuclear Reactor Thermal Hydraulics (NURETH-13) Kanazawa, Japan, September 27-October 2, **2009**. (Paper No N13P1023)

2. "Understanding the Corium Coolability Phenomena: Know Better, Gain Better", P.P. Kulkarni, R.K. Singh, A.K. Nayak, P. K. Vijayan, A. Rama Rao, D. Saha, International Conference on Topical Issues in Nuclear Installation Safety: Ensuring Safety for Sustainable Nuclear Development, Mumbai, India, 17 – 21 November, **2008**.

3. "Physics of Coolability of Top Flooded Molten Corium", P.P. Kulkarni, R. K. Singh, A. K. Nayak, P. K. Vijayan, D. Saha and R. K. Sinha, The 14th International Topical Meeting on Nuclear Reactor Thermal hydraulics, NURETH-14, Toronto, Ontario, Canada, September 25-30, **2011**, paper No 328

DEDICATED TO

जननी जन्मभूमिश्च स्वर्गादपि गरियसी .

THE BELOVED NATION WHICH IS ON THE PATH OF NUCLEAR

SELF SUFFICIENCY

Acknowledgment

First of all, I would like to thank Dr R. K. Sinha, Chairman, AEC for inculcating research culture in me which enabled me to pursue Ph.D.

I am thankful to Dr. P. K. Vijayan, Director, RD&DG for allowing me to register for Ph.D, carry out project work in RD&DG and supporting me throughout the project.

And, most importantly, I would like to take this opportunity to pay my profound gratefulness and express my sincere gratitude to my guide, **Dr. A. K. Nayak,** without whose continuous guidance, encouragement, support and perseverance this report would not have been completed.

I am grateful to Director, NRG for allowing me to utilize their facilities and carry out experiments at NRG.

I express my sincere thanks to Dr G. Sugilal, TDD for the support he has extended for carrying out experiments at WIP.

I extend my gratitude towards Dr Ing Rudi Kulenovic, IKE for allowing me to work on the DEBRIS facility which imparted a lot of knowledge to me.

I also thank the Chairman and the members of Doctoral committee for critically evaluating my performance and giving valuable guidance over the period of my Ph.D.

I am thankful to Shri D. G. Belokar, Shri S. P. Limaye and Dr R. D. Kulkarni for extending invaluable guidance and support for carrying out experiments.

I am also thankful to all the workshop, instrumentation and WIP operation staff without whom this work would not have been completed.

I am grateful to my colleagues from room no 101 with whom I have learnt so many things which were useful to complete my Ph.D.

Finally, I thank my family for supporting me through thick and thin and extending moral support to carry out this research.

Contents

Abstract

In a postulated core melt accident in a light water reactor, the barriers for the release of radioactivity start failing leading to melting of fuel and formation of a molten mass. In ex-vessel scenario, the melt will form a pool in the containment cavity on the base material. If this melt is not quenched in time, it starts attacking the concrete base which causes ablation of the concrete. This leads to liberation of a lot of non-condensable gases like CO, CO_2, H_2 and water vapour which pose a threat of containment pressurization and explosion. Besides, if basemat melt-through occurs, there is a potential danger of ground and water contamination by radiological waste.

The ultimate aim of any severe accident management strategy is termination of the accident as quickly as possible. A severe accident is said to be stabilized and terminated only when the core melt has been cooled and quenched and kept in the latter state for a long time and there is no release of radioactivity to the environment. However, the phenomena of quenching of melt pool is much more complex involving multiphase multi-component flow with heat, mass and momentum transfer associated with wide variation of thermophysical properties of the melt such as the viscosity, the melting point, thermal conductivity, modulus of elasticity, tensile strength and linear thermal expansion coefficient. In order to devise a strategy for arresting further progression of severe accident, understanding of coolability in such scenarios is utmost important.

The main objective of this thesis is to understand the physics of coolability of top and bottom flooded molten corium pool with molten core –concrete interaction.

Top flooding is the simplest strategy to tackle the core melt situation where ample amount of melt is flooded on the top of the pool. The coolability of molten pool under top flooding strongly depends on the water ingression inside the crust. However, the phenomenology of water ingression in melt pool is not yet understood. As a first exercise, the only existing

model in literature was assessed for its capability to predict the water ingression and coolability of an experiment from literature in which corium simulant (Cao + B_2O_3) at 1200 ^oC was poured in a test section and flooded from top with water. The model was a 1 –D steady state model based on creep for water ingression into hot rocks beneath the sea extended for melt coolability in ex vessel scenarios. It was observed that the model was unable to predict the behavior owing to the facts that, water ingression in geological reservoir depends upon strain rate and is definitely appropriate for the large scale and long time frame events whereas for. However, the phenomena in corium coolability are catastrophic and time scales are much smaller than that in geological phenomena whereas the phenomena in corium coolability are catastrophic and time scales are much smaller than that in geological phenomena. Hence, considering the need of development of new model, postulation of melt coolability phenomena was carried out considering the heat transfer in the melt pool, crust growth, crust failure by thermal stresses and subsequent water ingression. A new mechanistic model based on the governing equations was developed considering above postulations. The model was tested with the same experimental data and was found to not only simulate the data in good agreement but also explain the physics satisfactorily.

In order to quantify the effect of property changes during the molten core concrete interaction and uncertainties on water ingression, simulations have been carried out by varying thermo-physical properties of corium. A new dimensionless parameter called as crust break parameter, given as $E\alpha/\sigma$ was conceived and it was demonstrated that water ingression was appropriately scaled by this crust break parameter.

In actual reactor conditions, corium mixes with concrete which has high silica content. The resulting mixture contains metal silicates which act as a brittle glassy material. Besides, the temperature dependent properties of the mixture material (CaO + B_2O_3) were not fully known. Hence, it was decided to use glass as a simulant material, whose properties are known for simulating water ingression test. Accordingly, an experiment was carried out wherein molten sodium borosilicate glass at 1200 ^{o}C was poured in a test section and flooded from top with water. It was observed that water could ingress only upto 10 mm depth and it took a lot of time to cool the melt. Analysis with our model showed that the crust break parameter was very low and the stresses never exceeded the fracture stress which did not cause any water ingression and the water ingression was only due to surface interaction with the melt. The model was able to predict the temperature history quite well. This exercise corroborated the fact that top flooding alone is not a suitable strategy to achieve complete coolability.

Experimental as well as theoretical investigation on top flooding corroborated the fact that, top flooding is not a reliable strategy to achieve complete coolability in case of core melt accidents. Hence, efforts were made to study the melt coolability behaviour under an alternative strategy, i.e. bottom flooding. While, a few small scale experiments showed evidence of better coolability under bottom flooding condition, there is lack of understanding of the phenomenology of melt coolability under bottom flooding. There are no mechanistic models in literature for predicting coolability under bottom flooding. Hence, similar to top flooding, phenomena of melt coolability under bottom flooding was postulated and a model was developed considering the heat transfer from water at bottom to the melt, steam formation and pressurization at the bottom, steam eruption through melt, porous zone formation and subsequent coolability of the melt. The model was validated with experimental data from literature. In order to test the melt coolability in siliceous material, and experiment was carried out wherein molten sodium borosilicate glass at 1200 ^{o}C was poured in a test section and was flooded from bottom through nozzles. It was observed that the melt got quenched within few minutes as a result of formation of large porous structure in the melt after steam erupted through the melt. Our model was able to predict the temperature history quite well.

Similar to top and bottom flooding, external vessel cooling is also employed as a strategy to tackle core melt accident. In indirect cooling techniques, the core melt is often collected in an external vessel containing sacrificial material or contained inside the RPV and the vessel is then cooled externally by water. In order to have a comparison of all the three cooling techniques commonly used for melt coolability, an additional experiment on indirect cooling was carried out using same melt material, initial temperature and same mass as that was used in top and bottom flooding experiment. It was observed that, the moment the melt was poured in the vessel, the melt adjacent to the vessel solidified immediately and formed a crust. Owing to the poor thermal conductivity of the crust, the heat transfer to the surrounding water was very poor and in fact, the water did not boil at all and no steam was observed. It took long time to cool the melt. Also comparison of all these experiment showed that bottom flooding is the most important strategy of all.

As it was observed in experiments, in both, top flooding as well as bottom flooding, a porous debris bed is formed which continues to generates heat. Ensuring further long term coolability of such heat generating debris beds is very much important in the context of safety of the reactor. Coolability of such heat generating debris beds is determined by many factors like size of the particles, porosity of the debris, operating conditions spatial distribution of the bed porosity etc. Coolability of such debris bed is expressed in terms of dryout heat flux and two phase pressure drop. Dryout characteristics of debris bed consisting of irregular shaped particles at top and bottom flooding condition at different pressure were studied experimentally. Also, pressure Drop characteristics experiments for top and bottom flooding were carried out. Assessment of existing models from literature for prediction of dryout heat flux and two phase pressure drop was carried out and the most suitable model was selected.

Finally, after developing models for melt coolability, an integration of all these models has been carried out and a conceptual design of a core catcher for an LWR has also been presented. The integrated model was used to evaluate the coolability of melt pool relocated in the core catcher.

Nomenclature

d	Particle diameter (m)
g	Gravitational acceleration (m/s^2)
h	Heat transfer coefficient (W/m^2 K)
h	Enthalpy (kJ/kg)
h_{bed}	Bed height (m)
h_{fg}	Latent heat of vaporization (J/kg)
h_{fs}	Liquid saturation enthalpy (J/kg)
h_{fus}	Latent heat of fusion (J/kg)
h_{in}	Inlet enthalpy (J/kg)
h_{lv}	Latent heat of vaporization (J/kg)
k	Thermal Conductivity (W/m K)
l	Crack length (m)
p	Pressure (Pa)
q’’	Heat flux (W/m^2)
q’’’	Volumetric heat generation rate (W/m^3)
r	Radial direction (m)
t	Time (s)
t_{cr}	Crust thickness (m)
u	Displacement in radial direction (m)
v	Velocity (m/s)
w	Displacement in axial direction (m)
z	Axial direction (m)
A	Cross section area (m^2)
A_{ch}	Area of openings

Cp	Specific heat capacity at constant pressure (J/kg K)
D_n	Diameter of nozzle
E	Young's modulus (N/m^2)
F	Interfacial drag force (N/m^3)
G	Mass flux ($kg/m^2.s$)
J	Superficial velocity (m/s)
K	Permeability
L_b	Length of the opening
M	Mass (kg)
N_n	Number of inlet nozzles
Q	Volumetric heat generation (W/m3)
T	Temperature (K)
V	Volume (m^3)
V_p	Volume in porous region

Greek letters

α	Void fraction
α_l	Linear expansion coefficient (K^{-1})
ε	Bed porosity
ε_s	Emissivity
γ	Density of openings per unit area
γ_s	Surface Energy (N/m)
η	Bed passability
κ	Bed permeability
μ	Viscosity (Pa.s)

ν	Poisson's ratio
ρ	Density (kg/m^3)
σ	Normal stress (N/m^2)
σ_b	Bending stress (N/m^2)
σ_{max}	Fracture stress(N/m^2)
σ_{mc}	Surface tension between melt and steam
σ_{th}	Thermal stress (N/m^2)
σ_{ST}	Surface tension (N/m)
σ_1	Maximum stress (N/m^2)
ξ	Critical Taylor wavelength
ψ	Number of eruption channels
τ	Shear stress (N/m^2)
Γ	Vapour generation rate (kg/s)

Subscripts

c	crust
c	critical
d	dryout
f	fluid
fb	Film boiling
g	Gas
i	Interfacial
in	inlet
l	liquid

m	melt
nb	Nucleate boiling
p	particle
r	radial
rad	radiation
rel	Relative
s	solid
sat	saturation
sat	Saturated
st	steam
sub	subcooled
sup	superheated
v	vapor
w	water
z	axial
0	inlet

List of Figures

List of Tables

1. Introduction

1.1 Background

As the demand for energy is increasing day by day, nuclear energy is clearly emerging as a viable and clean source of energy. Many reactors equipped with innovative technologies and enhanced safety features are being developed. The question that arises is, where does the nuclear energy stand in terms of public and environmental safety? In the history of commercial nuclear power so far, three major accidents leading to damage of reactor core, have taken place: first one at Three Mile Island (1979) [1], second one at Chernobyl (1986) [2] and the recent one at Fukushima (2011) [3]. Research on severe accidents had started since the TMI-2 accident and after the recent accident in Fukushima; the research has been further intensified. Even after roughly three decades of research, there are still several severe accidents issues which remain unresolved. One of the most important of unresolved issues is the ex vessel melt/debris coolability [4].

1.2 Ex Vessel Corium coolability

In a postulated core melt accident, the barriers for the release of radioactivity start failing. The severity of the accident depends upon the failure of multiple barriers. In a limited core damage accident, only single fuel rod may melt and be relocated in the core itself. There may not be further propagation of the accident. But in a severe core damage accident, large number of rods may melt and form a molten mass. In vessel type reactors, this mass can be relocated at the lower head of the vessel keeping the pressure boundary intact giving rise to an in-vessel scenario. This was the case in TMI2 where molten core was relocated inside the RPV. One of the easiest ways to arrest the progression of the accident is to flood the entire core with water inside vessel. Sufficient flooding will ensure the coolability of the melt inside vessel. However, if the cooling arrangement is not sufficient, the vessel will fail due to large thermal gradient and the melt will come out of the vessel and form a pool in the cavity on the base material. Similar may be the case with vertical pressure tube type reactors where the melt will directly come onto the basemat. Here we have to deal with an ex-vessel scenario. If there is water lying on the cavity, the pool may breakup in debris bed. If the debris bed is not quenched, it will again remelt due to the decay heat. The melt starts attacking the concrete base which is termed as the molten coolant- concrete interaction (MCCI). The heat transfer from the hot melt to the concrete causes ablation of the concrete. Further, the melt start reacting with the water vapor and may release Hydrogen. This has manifold impacts as the chemical reactions add a lot of heat into the system, generation of non-condensable gases because of concrete decomposition (i.e. CO, CO_2, H_2 and water vapor) and pose a threat of containment pressurization. The hydrogen generated has a potential danger of explosion. Besides, if basemat melt-through occurs, there is a potential danger of ground and water contamination by radiological waste. The final barrier is the containment. In any case, the containment barrier should not be breached.

The ultimate aim of any severe accident management strategy should be management and termination of the accident as quickly as possible. A severe accident is said to be stabilized and terminated only when the core melt has been cooled and quenched and kept in the latter state for a long time and there is no release of radioactivity in the environment. According to Sehgal [5], the release of fission products stops at around 1000 ^{o}C and if containment cooling is sufficient, the integrity of containment will not be challenged any more. However, the phenomena of quenching of melt pool is much more complex involving multiphase multi-component heat, mass and momentum transfer associated with wide variation of thermo-physical properties of the melt. Hence, in order to devise a strategy for arresting further progression of severe accident, understanding of coolability in such scenarios is utmost important.

1.3 Issues in corium coolability

The most convenient accident management strategy in ex-vessel scenario is cool the melt pool by flooding it from the top with ample amount of water. However, the question arises that, to what extent the water can ingress in the corium melt pool to quench it? When the cavity is flooded with water from top, immediately a crust is formed on the upper surface of the melt pool, which is found to limit the access of the water over-layer to the melt pool below the crust. Initially, due to the intense stirring because of gases liberating during MCCI, the crust will not be stable and bulk cooling will take place [6]. But after some time, as the gas flow rate decreases, a stable crust will prevail. After the stable crust is formed, the crust may anchor to the sidewalls of the vessel which may result in a considerable drop in the heat transfer rate due to induced gap [7] in between the crust and the melt pool lying below. Although, the crust limits the water inflow, cooling may occur by different mechanisms like mechanical breach of crust due to its own weight, volcanic eruptions in the crust and water ingression. Water ingresses through the gaps and fissures of the crust enhancing the coolability. Very little information is available at present on the knowledge of mechanism of water ingression or why the water ingression stops after certain depth is reached. Besides, during the accident progression, the properties of corium such as the viscosity, the melting point, thermal conductivity, modulus of elasticity, tensile strength and linear thermal expansion coefficient can change drastically due to its interactions with the in-vessel and ex-vessel structures and also with the concrete basement. The influence of these parameters on coolability is still unknown.

Apart from top flooding, another strategy to cool the melt is flooding the melt pool from bottom [8]. Bottom flooding has an advantage that when the water is flooded from bottom, the steam erupts through the melt making porous zones inside the melt and steam and water both flow upward taking away the heat and which excludes the possibility of counter current flow limit. However, there are some unresolved issues like

- Under what conditions this steam eruption takes place, since the water has to overcome the melt hydrostatic head.
- If there is a crust formation at the bottom before the water in injected, will the water be able to penetrate the melt?
- The location and of the size of eruption?
- The particle diameter and porosity of the resulting debris?
- Parameters influencing the melt eruption?
- Whether the eruption sufficient for complete melt coolability?

These issues are still unresolved.

In top flooding, after water ingression into the crust, as well as in bottom flooding, following steam eruption through the melt, a porous heat generating debris bed is formed. If the containment is wet, the melt may fragment and form a debris bed. It is very important to remove the decay heat from such heat generating debris bed for sufficiently longer period of time to prevent it from remelting and further propagation of the accident. The coolability of such heat generating debris beds is also complex one influenced by many factors like

- bed porosity and its distribution
- particle diameters
- flooding conditions such as water flooding from the top or the bottom of the debris bed
- Water temperature and containment pressure
- The magnitude of non-condensable gases generated during Core-Concrete Interaction (CCI)

Downward flow of water is opposed by upward movement of steam leading to counter current flooding limitation ultimately leading to dryout. In view of this, studies on the thermal hydraulic behavior of such particulate debris beds is important in the context of safety assessment with respect to coolability as well as failure of cooling, re-melting and subsequent attack of structures.

1.4 Literature survey

In order to gain some information about melt coolability phenomenon in ex-vessel situation, a detailed survey of existing literature was carried out. The findings from the literature are cited below.

1.4.1 Experimental investigations

A series of coolability experiments were conducted at Argonne National Laboratory under MACE (Melt Attack and Coolability Experiments) test program [9]. The principal objective was to explore the benefits of addition of large quantity of water on the molten core concrete interaction already in progress for quenching and stabilizing the heat generating core melt, and arresting or even terminating basemat ablation. Four operationally successful integral experiments were conducted in this program. Firs two tests were conducted with 70 % oxidized PWR melt compositions, while the later tests were conducted with fully oxidized core melts. Core melt masses in these various scale tests ranged from 130 to 1950 kg. The important finding from the test was that, the crust was anchored to the sidewalls of the vessels. The crust remained at the elevation where it initially formed. As the MCCI progressed downward, an intervening gap formed between the melt and crust, which most likely terminated efficient heat transfer processes between the debris and water thus limiting the coolability

In COTELS experiments [10], a total of 10 reactor material experiments were carried out to investigate melt and debris coolability. In these tests, prototypic melts of mass around 50 kg was poured in the test section laden with concrete and it was flooded from top with a water jet. Out of the 10 tests, in three tests, a large debris mass was observed at the interface and complete coolability was observed. In three tests, a small debris bed was observed and in remaining tests, solid mass was observed. This solidified corium mass was found to contain cracks and crevices which axially spanned the depth of the layer. The test results indicate that water was able to penetrate into these cracks and crevices during the test, in addition to penetrating into the intervening gap formed at the sidewall corium-concrete interface. However, the relative contributions of water ingression at the sidewall versus that in the central region to the overall debris cooling rate was not quantified. Besides, the tests had very low power density

SWISS experiments were carried out at Sandia National Laboratory [11]. In these experiments, coolability of stainless steel melts interacting with limestone/common sand (LCS) concrete was tested. Test results indicated that, water addition had little influence on the basemat erosion rate. Posttest examinations indicated that a bridge crust ranging from 5.1 to 6.4 cm thick had formed which was anchored to the test section sidewalls spanning the entire vessel diameter. As a result, an intervening gap developed between the melt and crust severely affecting the coolability.

The WETCOR tests [12] were carried out in similar manner as SWISS tests except the melt material was a mixture of oxides (76.8/16.9/4.0/0.9/0.5 wt% Al2O3/CaO/SiO2/Fe2O3/MgO). Decay heat of the order of 0.61 MW/m^3 was provided by side heating elements. The results showed that, after the initial intense heat transfer period, a stable crust formed thereby reducing the heat transfer to the overlying coolant.

Farmer et al. [13] have reported possible evidence of a sequential cooling mechanisms starting from the bulk cooling mechanism due to mixing by the gases coming out of the melt concrete interaction followed by a stable crust formation. Water ingression was found to augment the coolability. In addition, the tests also showed presence of melt eruptions. These tests do show a plausible mechanism of cooling, but complete understanding of coolability mechanism is not explained with the help of these tests. For example, there is an evidence of formation of debris bed over the melt pool due to the crust breakage and eruptions, which might had limited the inflow of water due to counter current flooding limitations.

COMECO tests [14] were carried out to study role of water ingression on coolability on the melt consisting of CaO and B_2O_3. In the experiment, molten simulant at 1200 deg C was poured in the test section and was flooded from top. Decay heat of the order of 1.33 MW/m^3 was simulated. The results indicate that water could hardly ingress up to a depth of 10 cm beneath the top of the pool thereby limiting further coolability.

Farmer et al. [15] have reported the results of the ex-vessel debris coolability and two dimensional molten core concrete interactions under both wet and dry cavity conditions. It was found that, the radial ablation is a key element of overall cavity erosion process.

All these experiments showed that, the top crust formation together with the separation of the melt pool from the crust due to the concrete erosion marked a sharp decline in the corium coolability.

To counter this, the bottom flooding concept was first demonstrated in COMET series of tests at FZK and ANL [16-19]. In these experiments, simulants as well as actual corium material of masses ranging from few kilograms to hundreds of kilograms were used. In these tests, molten material was spread onto a layer of sacrificial concrete material. The melt eroded this layer and finally reached a matrix of plastic water injectors buried in this layer. Upon contact with the molten core material, the plastic plugs melted and water was injected into the molten material. The driving water pressure was due to the location of the water reservoir above the containment cavity. In the COMET experiments, the melt was found to quench in a relatively short time to a porous, easily penetrable debris, with continued access of water. Different variants of COMET tests were conceived which used injection nozzles as well as percolation through a layer of porous concrete.

DECOBI program was initiated at Royal Institute of Technology [20-21] with the objective to understand and model the processes of porosity formation and coolability observed in the COMET experimental program. A series of experiments was performed at medium (~ 600 ^{0}C) and at high temperature (~ 1100-1400 ^{0}C) conditions. The difference in cooling behaviour and porosity formation during solidification, between the molten metal and the binary oxide mixtures was established. The coolant used was water and the pool simulants were pure molten metal (Pb) and binary oxide mixtures (CaO-B_2O_3, CaO-WO_3 & MnO_2-TiO_2). Again, Widmann et al. [22] presented coolability with bottom injection in COMET tests with porous concrete concept. Cho et al. [23] carried out experiments to provide the fundamental understanding needed for melt–water interfacial transport phenomena during bottom injection. Recently, Lomperski and Farmer [24] presented engineered corium cooling systems modeled on the COMET concept involving nozzles, one filled with a porous concrete and the other injected both water and non-condensable gas which probably suppressed steam explosions.

All these experiments showed that with bottom flooding, coolability is substantially enhanced. Also, in both top and bottom flooding experiments a heat generating debris bed is formed with particle sizes ranging from 0.1 to 10 mm and porosities ranging from 20-50 % which needed to be cooled.

Several experimental and theoretical programmes on debris bed coolability have been performed, especially in the beginning of the 1980s. The objectives of most of these programmes had been to determine the maximum thermal power that can be removed from a heated particle filled column with a water reservoir on the top. The internal heating was produced by resistance heaters [25], by inductive heating [26] or by direct neutron irradiation in a reactor [27]. A local dryout was detected by the temperature rise at thermocouples inside the particle bed. Based on these data, correlations for friction laws of liquid and vapour were deduced. These correlations have then been used by Lipinski [28] in a model to calculate the heat flux that corresponds to the maximum bed power before reaching a local dryout anywhere in the bed. New experimental programmes to investigate the coolability of particulate corium have been started in recent years.

The SILFIDE experiments [29, 30] at EDF were aimed to study the coolability of a debris bed in multidimensional configurations. The experiments showed that bottom coolant injection was at least two times more efficient than top coolant injection and the major finding was that coolability is significantly better in terms of DHF i.e. the DHF values obtained were much higher than as predicted with the 1D formulation applied to the conditions. With increasing thermal power, steady temperature overheats up to 200 ◦C above saturation were observed, and the bed was still coolable.

Sehgal et al. [31] studied the quenching characteristics of homogenous particle beds and axially stratified particle beds in POMECO test facility with top- and bottom-flooding using downcomers of different size. They worked out that the quenching period is decided by the low porosity particle layers and their particle sizes. Also, the quenching period is significantly reduced with bottom-flooding. Jasiulevicius and Sehgal [32] investigated the quenching behaviour of homogenous particle beds with non-condensable gas addition from bottom. They found that the non-condensable gas affects the quenching period. Nayak et al. [33] studied the quenching characteristics of a volumetrically heated particulate bed composed of radially stratified sand layers with non-condensable gases injection from bottom. It was observed that, dryout occurred in high porosity region as compared to that in the low porosity region. This phenomenon was explained by the capillary forces moving water from the high porosity to the low porosity region to such an extent, that the cooling limit is reached in the high porous layer first [34].

A test facility called STYX [35] was constructed at Technical Research Centre of Finland (VTT) to simulate the ex-vessel corium particle bed in the conditions of Swedish BWRs. The STYX particle bed reproduces the anticipated depth of the bed and the size range of particles having irregular shape. The bed is immersed in water, creating top flooding conditions, and internally heated by an array of electrical resistance heating elements. Dryout tests were conducted at 0.1–0.7MPa pressure for both uniformly mixed and stratified bed geometries. In all the tests, including the stratified ones, the dry zone first formed near the bottom of the bed. The measured dryout heat fluxes increased with increasing pressure, from 232 kW/m^2 at near atmospheric pressure to 451 kW/m^2 at 0.7 MPa pressure.

A different attempt was made in the DEBRIS experiments performed at IKE [36] where the main focus of the experiment was understanding of the two-phase flow in porous media, determination of local pressure drops for steady state boiling for checking friction laws in two phase flow. In DEBRIS test facility, experiments were carried out on spherical steel balls to determine the dryout heat flux and pressure drop characteristics under atmospheric and elevated pressures.

1.4.2 Efforts on modeling of melt coolability

From the literature review, it is observed that there are very few efforts on modeling of water ingression phenomena in melt pool when flooded with water. Originally, the motivation behind modeling of water ingression phenomenon did not aim to study the quenching of molten corium pool during a postulated severe accident condition in a LWR. In fact, models were developed for simulation of cracking behaviour of hot rocks in geological reservoirs. In this context, Lister [37] did pioneering work in modeling the penetration of water into hot rocks by considering the simplest possible one dimensional model based on the concept of crack front propagation. Lister postulated that, in deep geological reservoirs, the solidified rock is subjected to intense pressure and high temperature from below and a colder temperature and water hydrostatic temperature at the top. As a result, the rock crust is subjected to transient creep and fails at a continuous rate and water ingression keeps on occurring continuously. Bjornsson et al. [38] found that penetration of water into hot rock is the primary reason for the intense heat release of the subglacial Grimsvötn geothermal area. Jagla et al. [39] presented a model to predict the statistical properties of columnar quasi-hexagonal crack patterns, as observed in the columnar jointing of basaltic lava flows. While Lister's model considered penetration of water into hot but initially solid rock under high pressure condition, recently, Epstein [40] used Lister's models of bulk permeability of cracked rock and developed a model for water penetration into initially molten, heat generating rock like material at low pressure which resembles the water ingression phenomena into molten corium pool. However, the applicability of the model on melt coolability in reactor condition has not been established previously.

On bottom flooding, Paladino et al. [41] attempted modeling of melt coolability in simulant material when flooded from bottom. Their model predicted the size of the eruption zone and the resulting porosity based on heat balance and some empirical correlations for calculation of eruption zone diameter. Widmann et al. [22], also modeled melt coolability under bottom flooding, but their focus of was to predict the porosity of the melts formed during bottom injection and its effect on coolability. Foit et al. [19] presented porosity formation as well as quenching and long-term coolability of different melt layers with resulting porosities using MEWA code. However, no attempt is yet made to model how the crust breaks under pressure.

For prediction of dryout and two phase pressure drop in heat generating debris beds, several models exist in literature. Most of the available dryout models use an extended version of the

Ergun-equation, which is adapted to two-phase flows by addition of terms called relative permeabilities and relative passabilities which are usually dependent on the gas phase void fraction. Models by Lipinski [42], Reed [43], and Hu and Theofanous [44] reflect the adjustment process to the experimental data based on top-flooding conditions. In contrast to the above mentioned models, the models of Schulenberg and Mueller [45] (1984) and Tung and Dhir [46] included a term which takes into account the influence of the interfacial drag. Schmidt [47] modified the Tung and Dhir model to take into account the revised flow pattern changes in the debris bed. Sinha and Nayak [48] developed models for Natural Convection heat transfer and dryout heat flux in a volumetrically heated porous debris bed flooded from top.

1.4.3 Insights taken from literature

- Under top flooding condition, water ingression in the melt pool is important phenomenon to establish melt coolability.
- From the experiments in literature, it was observed that, water ingression occurred upto a maximum depth of 10 cm.
- Only single model on water ingression was available in literature which is based on water ingression in deep geological reservoirs penetrating in rocks. The model is based on the coolability of molten lava rock when flooded from top due to creep.
- Experiments from COMET and DECOBI showed enhanced coolability under bottom flooding
- After the water was flooded from the bottom, a porous debris bed was formed with porosity ranging from 10-50 %
- The coolability of such heat generating debris bed depends upon bed characteristics such as particle size, porosity, axial and radial stratification and coolant thermal hydraulics like water temperature and containment pressure.

- In order to cool such bed, the surface heat flux of the bed should be less than the dryout heat flux as well as the pressure drop should be less than the available head. Hence, knowledge of dryout heat flux and pressure drop is very important.
- Various models exist to predict the dryout heat flux and two phase pressure drop in heat generating debris bed. The models can roughly be characterized as models with explicit interfacial drag term and without the drag term.

1. 5 Unresolved issues:

- Although it is known that, water ingression is very important aspect to enhance the melt coolability, however, the physics of water ingression is not yet fully understood. This is because the prior studies reveal that
    - In some cases water ingression occurred [9] whereas in some cases it did not [11]. In some cases, the water ingression occurred, but it stopped after some time [14]
- Hence further questions which arise are
    - Why water ingression stops below certain depth?
    - What parameters affect the water ingression?
    - What are the water ingression scaling parameters to simulate corium coolability under top flooding?
- The applicability of the only existing water ingression model on melt pool coolability has not been established priory.
- Only a few small scale experiments with lower melt depth showed evidence of better coolability under bottom flooding. However, there is lack of understanding of physics of coolability under bottom flooding. Most important issues are
    - What causes melt eruption and under what condition?
    - What is the particle size of the resulting debris formed

    - What parameters are responsible for the size of eruption, resulting porosity and ultimately, coolability of the debris.

- There are no mechanistic models in literature for predicting coolability under bottom flooding
- Most of the experiments on coolability of heat generating debris beds were carried out on spherical particles [25-27] whereas in actual core melt condition, particles of a variety of shapes and sizes can be found.
- Several models exist in literature for prediction of dryout heat flux and pressure drop. However, an assessment of applicability of these models for prediction of dryout heat flux and two phase pressure drop has not been carried out so far.

1.6 Objective

The main objective of this thesis is to understand and clarify the physics behind coolability of Top and Bottom Flooded Molten Corium Pool with Molten Core –Concrete Interaction and to resolve following issues

- Determining the mechanism of coolability under top and bottom flooding
    - Postulation of melt coolability under top and bottom flooding condition
    - Development of mathematical models
    - Carrying out experiment on melt coolability under top and bottom flooding
    - Validation of the models
- Determination of process parameters affecting the coolability
    - Identification of scaling parameters
    - Carrying out parametric analysis to study the effect of different parameters on coolability
- Predicting the coolability in reactor severe accident conditions.
    - Design of core catcher

- Performance assessment of core catcher under postulated severe accident

1.7 Organization of the thesis

The above objectives are addressed in the following chapters of the thesis

Chapter 1 of the thesis discusses the introduction of the thesis giving background of the topic, the need for research on this topic, the insights taken from literature and the motivation for this work

Chapter 2 presents a sequential study on melt coolability under top flooding which includes the comparison of the existing model on melt coolability under top flooding with experiments, assessment of the model to predict the experimental data, development of a new model on water ingression and its validation with experimental data, determination of scaling parameters of water ingression, effect of MCCI on melt coolability, experimental investigation on melt coolability under top flooding with different simulant material, revalidation of the developed model with experimental data and finally, a summary of research on top flooding.

Chapter 3 presents the melt coolability under bottom flooding. In this chapter, a new mechanistic model on melt coolability under bottom flooding and its validation with existing literature has been presented. In order to study the effect of different melt material and coolability of relatively deeper melt pool, experimental investigation on melt coolability has also been presented. The model has been validated against this experimental data also. Finally, a comparison of coolability under different strategies has been presented.

Chapter 4 discusses the coolability of molten simulant material under different cooling strategies such as top flooding, bottom flooding and indirect cooling. The depth of the melt pool, melt mass and melt initial temperature was almost kept the same in all the tests. The relative cooling behavior of the melt pool has been investigated.

Chapter 5 discusses the experiments carried out on dryout heat flux and two phase pressure drop in realistic debris beds. Also, assessment of capabilities of existing models on dryout heat flux and pressure drop has been carried out to select the most appropriate model for dryout heat flux and pressure drop.

After developing models for melt coolability, an integration of all these models has been carried out in In **Chapter 6,** a conceptual design of a core catcher for an LWR has also been presented. The integrated model was used to evaluate the coolability of melt pool relocated in the core catcher.

Chapter 7 presents the conclusions of the entire study.

2. Melt coolability under top flooding condition

2.1 Introduction

Top flooding is the simplest strategy to tackle the core melt situation where ample amount of water is flooded on the top of the melt pool. The coolability of molten pool under top flooding strongly depends upon the water ingression into the crust. However, the question that arises is to what extent the water can ingress in the corium melt pool to quench and cool it? In the MACE experimental program [9], it was found that a tough crust is formed on the upper surface of the melt pool during top flooding situation, which was found to limit the access of the water overlayer to the melt pool below the crust. Test results from COTELS project [10] indicated that water ingression through cracks/defects in core material interacting with concrete can contribute to melt coolability. SWISS experiments [11] highlighted that crust separation from the melt and subsequent anchoring can severely affect the water ingression. COMECO tests [14] indicated that water could hardly ingress up to a depth of 10 cm beneath the top of the pool thereby limiting further coolability. The purpose of this work is to investigate the water ingression behaviour when the melt pool is flooded from the top in an ex-vessel situation. From these experiments, it was observed that, in some cases water ingression occurred, in some cases it did not occur and in some cases it stopped midway. However, the reason behind this is not unclear.

Besides, it is observed that there are very few efforts on modeling of water ingression phenomena in melt pool when flooded with water. Originally, the motivation behind modeling of water ingression phenomenon did not aim to study the quenching of molten corium pool during a postulated severe accident condition in a LWR. In fact, models were developed for simulation of cracking behaviour of hot rocks in geological reservoirs. In this context, Lister [37] did pioneering work in modeling the penetration of water into hot rocks by considering the simplest possible one dimensional model based on the concept of crack front propagation. Epstein [40] used Lister's models of bulk permeability of cracked rock and developed a model for water penetration into initially molten, heat generating rock like material at low pressure which resembles the water ingression phenomena into molten corium pool. However, the applicability of the model on melt coolability in reactor condition has not been established previously.

The purpose of this work is to investigate and clarify the water ingression and melt coolability behaviour when the melt pool is flooded from the top in an ex-vessel situation. Towards this purpose, initially the only existing model in literature was assessed for its capability to predict the water ingression and coolability of an experiment from literature. It was observed that the model was unable to predict the behaviour. Hence, considering the need of development of new model, postulation of melt coolability phenomena was carried out. A new mechanistic model based on the governing equations was developed considering above postulations. The model was tested with the same experimental data and was found to not only simulate the data in good agreement but also explain the physics satisfactorily. In order to quantify property changes during the molten core concrete interaction and uncertainties in determination of properties of corium, simulations have been carried out by varying thermo-physical properties of corium. An experiment was also carried out wherein molten sodium borosilicate glass simulating the glassy corium concrete mixture at 1200 ^{o}C was poured in a test section and flooded from top with water. It was observed that water could ingress only upto 10 mm depth and it took a lot of time to cool the melt. Analysis with our model showed that the crust break parameter was very low and the stresses never exceeded the fracture stress which did not cause any water ingression and the water ingression was only due to surface interaction with the melt. The model was able to predict the temperature history quite well.

2.2 Assessment of applicability of existing models for prediction of melt coolability

As a first exercise, the existing models in literature were assessed for their capability to predict the melt coolability behaviour. Originally the motivation for prediction of water ingression came from simulating water penetration in hot rocks in geological reservoirs [37]. Lister, in his pioneering work, presented a 1 –D steady state model based on creep for water ingression into hot rocks beneath the sea. Epstein [40] used Lister's model based on creep to simulate water ingression in a melt pool with 1-D geometry. This is probably the only model on water ingression available in literature. However, the applicability of this model on molten pool coolability has not been established priory. In the present work, Epstein's model was first applied on experiment carried out in COMECO [14] test facility. The reason behind the application on COMECO facility is that, this is a very simple test with detailed experimental data available in open literature. The COMECO facility consists of a test section (200 x 200 mm cross section) with a maximum pool height of 300 mm. Figure 2.1 shows a schematic of the facility. The test section walls are made of carbon steel plates with thickness of 25 mm. The test section was connected to an upper tank whose height is about 1000 mm and its cross-section is same as that of the test section. The upper tank was used for the purpose of water flooding on the melt pool to the desired height. For this, water was preheated to a suitable temperature in the water storage tank before it was delivered to the upper tank via the water line. The level of the water in the upper tank was kept at around 700 mm during the tests. The melt pool was heated by heaters, located outside the test section on the four sidewalls. The heaters were made of Molybdenum silicide ($MoSi_2$) alloy that can be operated to a temperature of about 1700^0C. The four heaters could deliver the maximum power of 16 kW to the melt pool which corresponds to a heat generation rate of nearly 1.33 MW/m^3.

The most important measurement in this experiment is the transient melt pool temperature during the water flooding and quenching. The temperature in the melt pool was measured at different radial and axial positions. For this, a total of 24 K-type thermocouples were employed at 3 radial planes (8 numbers in one radial plane) to record the transient temperature. The distributions of the thermocouples are shown in Figure 2.2. The steam flow rate was measured using a vortex type steam flow meter before it was condensed in the condenser.

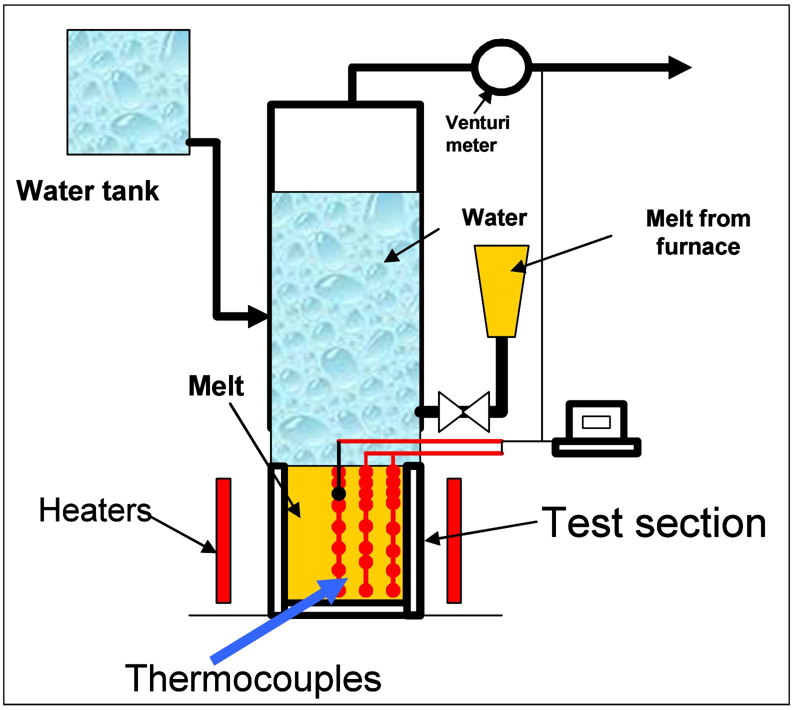

Figure 2.1 Schematic of COMECO test facility

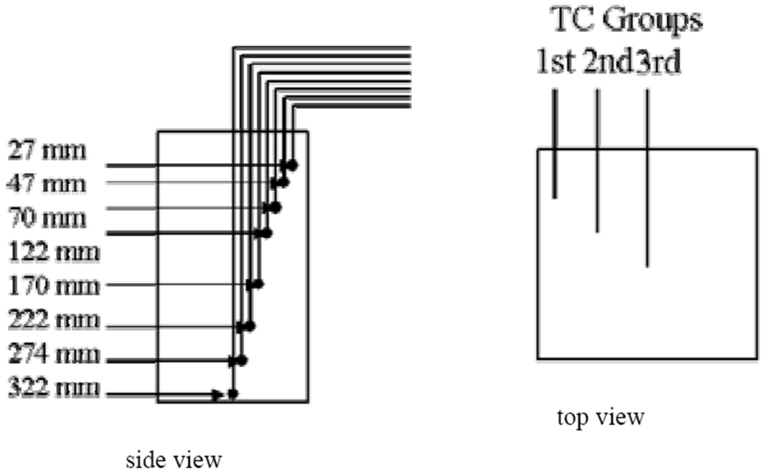

Figure 2.2 Thermocouple arrangement in COMECO tests

The COMECO experiments correspond to the later stages of the MCCI [14]. Figure 2.3 shows the temperature of the melt at various locations during the experiment. As we can see, the temperatures of the melt in the first three locations from the top reduce to almost the saturation temperature of water quite quickly. It is possible due to water touching the surface at the corresponding locations by ingression. The temperature at the fourth location from the top (which is about 122 mm) is found to drop significantly from the initial temperature due to heat conduction from the melt to the region. Water did not ingress to this location.

Temperatures at locations below 122 mm. also decreased due to similar heat conduction. The temperature decrease, however, was not large due to the large distance from the quenched zone and the low conductivity of the melt mixture.

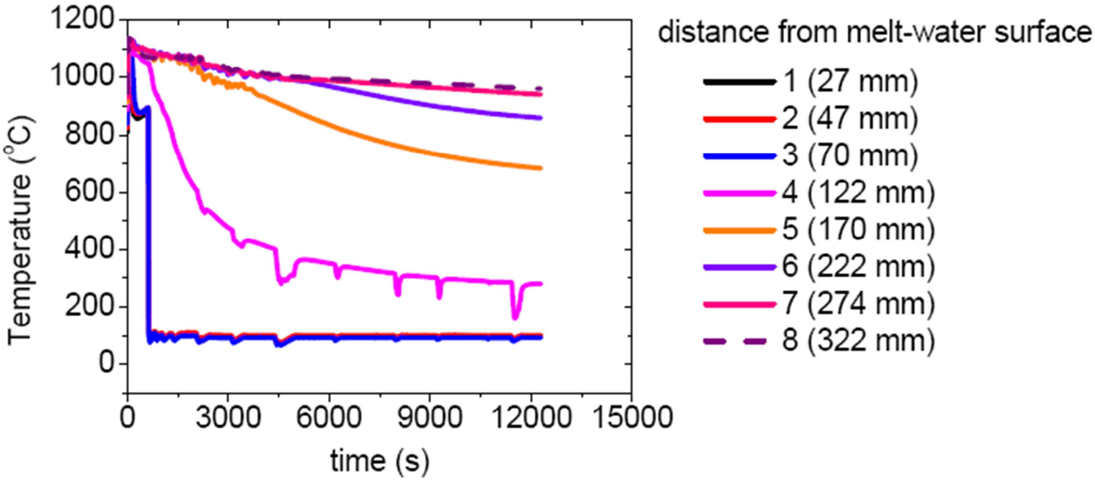

Figure 2.3 Temperature history during quenching of the melt pool

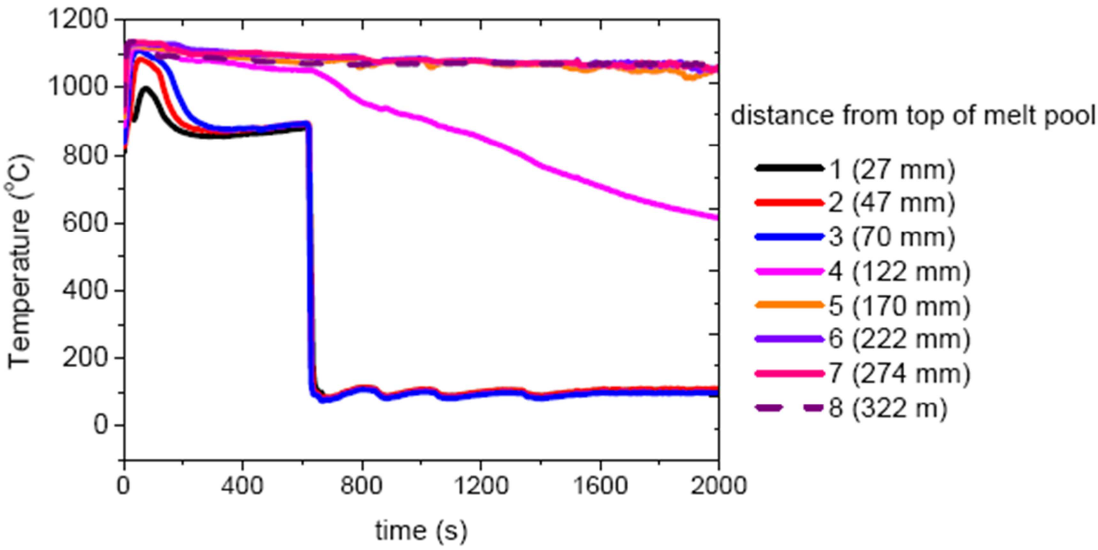

Figure 2.4 Temperature history during the initial period of quenching

Epstein's model was tested on COMECO experimental data. The crust predicted by Epstein model was 35 cm (Figure 2.5), whereas actual crust was only 10 cm thick. Epstein's , model showed that water could ingress into the melt pool completely whereas the tests showed only 10 cm thick crust.

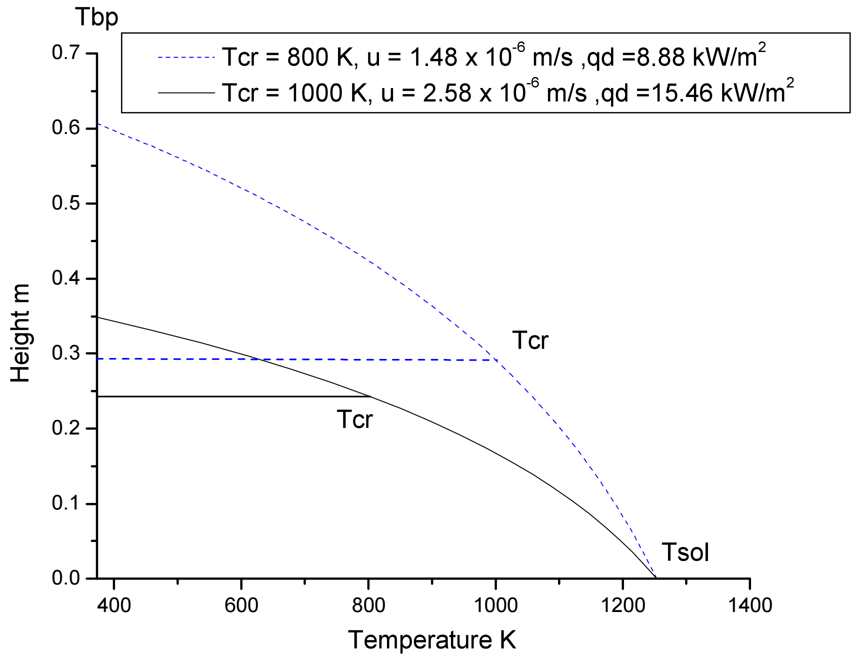

Figure 2.5. Comparison of Epstein Model with experiment

Epstein's model uses a parameter called critical temperature (Tcr) below which the water ingression in insignificant. This temperature is near to the solidus temperature. Since this temperature (Tcr) is not available for the test material, a parametric analysis with different temperatures was carried out. Even by assuming the critical temperature as high as 1000 ^{0}C, complete coolability is observed as seen in Figure 2.5. Lowering this temperature increases the crust thickness (Zone of solidification) further ensuring better coolability.

Hence, it can be concluded that, Epstein's model was unable to predict the water ingression phenomena. The reasons could be that,

- Epstein's model was based on Lister's Model of Transient Creep which primarily depends upon strain rate and is definitely appropriate for the large scale and long time frame events like geological phenomena. However, the phenomena in corium coolability are catastrophic and time scales are much smaller than that in geological phenomena

- In Lister's model, crack front moves progressively over prolonged period whereas, in present system, we believe that, crack occurs only when thermal stresses exceed fracture strength. The thermal stresses develop because of large temp gradient along the height of the crust. Since the crust thickness increases with time, thermal stresses increase with time. At the point of time when the thermal stresses exceed the fracture strength of the material, which, at ex-vessel condition is glass type which is brittle in nature, cracks are formed and propagate catastrophically causing breaking of the crust into small debris. Water ingresses into this by gravity. Hence, in our opinion, crack in the crust occur not because of creep but by thermal stresses.
- The corium at ex-vessel situation is a mixture of UO_2, ZrO_2, structural materials such as steel, concrete, etc. The composition is really complex and definitely it cannot be considered as a rock.

Hence, there is a strong need of development of better models to understand physics behind water ingression phenomena in a melt pool flooded from top

2.3 Model development of melt coolability studies under top flooding

2.3.1 Postulation of melt coolability phenomena:

In view of lack of a concrete model for prediction of water ingression phenomenon, postulations were made for phenomena taking place during melt pool coolability as follows:

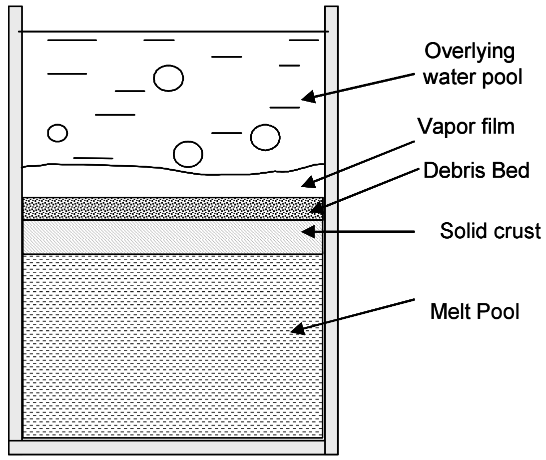

Figure 2.6. Domain of postulation for melt coolability under top flooding

- As soon as water is introduced in the pool, a vapor film is formed over the melt surface. The heat transfer from melt pool to water overlayer is by convection and radiation.
- Heat conduction is dominant mode of heat transfer. This is because at ex-vessel core melt condition, the melt is near to its solidus temperature having very high viscosity.
- As the melt is cooled at the top, a solid crust is formed at the top of molten surface due to cooling. The crust sees low temperature at water side and high temperature at the melt side resulting in thermal stress development.
- When the thermal stresses exceed the fracture stress, the crust becomes mechanically unstable, it disintegrates into debris.
- Water ingresses into the debris by gravity. It takes the heat away by convection. During this heat transfer, there is a counter current flow of steam and water into the debris bed. At high heat flux, the upward steam flow may limit the water downflow leading to counter current flooding limit (CCFL). This would ultimately cause dryout.
- Once the dryout condition is occurred, water would not ingress into the debris.

2.3.2 Development of New model based on postulations:

A new mechanistic model based on the governing equations was developed considering the above postulations for water ingression behaviour in the top flooded molten pool

The model considers

- Heat transfer in melt pool and solid crust;
- crust generation and its growth
- Thermal stress development in the crust
- Fracture in crust, debris formation
- Mass, momentum and energy transfer from debris to coolant
- Dryout flux of the debris bed
- Water ingression into the debris

2.3.3 Governing equations

(i) Governing equations for molten pool

In ex vessel situations, the viscosity of corium is around 0.1 Pa.s which is around 100 times that of water. Hence, in molten pool, it is considered that the dominant mode of heat transfer is due to conduction only. With this, the transient 2-D heat conduction equation can be written as

$$\rho C_p \frac{\partial T}{\partial t} = \frac{1}{r}\frac{\partial}{\partial r} r(k\frac{\partial T}{\partial r}) + k\frac{\partial^2 T}{\partial z^2} + q''' \qquad (2.1)$$

where q” is the volumetric heat generation rate due to decay heat.

The major boundary conditions are:

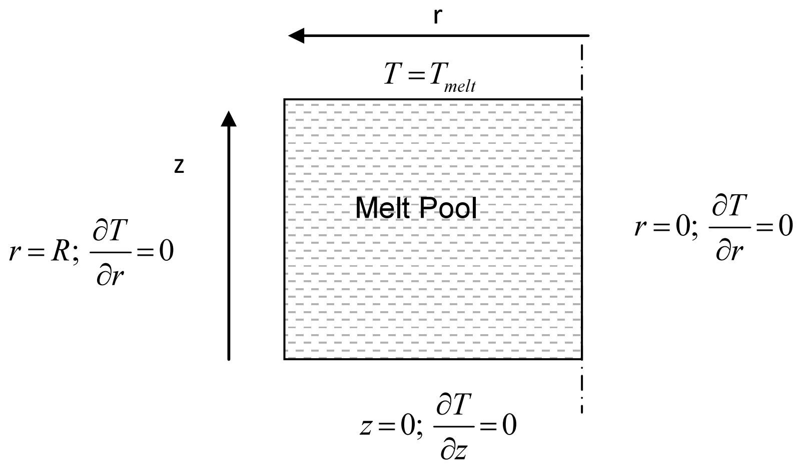

Figure 2.7 Boundary conditions for melt pool region

(ii) Governing equations in solid crust:

Heat transfer in solid crust is due to conduction only. The energy equation can be written as

$$\rho C_p \frac{\partial T}{\partial t} = \frac{1}{r}\frac{\partial}{\partial r} r(k\frac{\partial T}{\partial r}) + k\frac{\partial^2 T}{\partial z^2} + q''' \tag{2.2}$$

The boundary conditions for this region are:

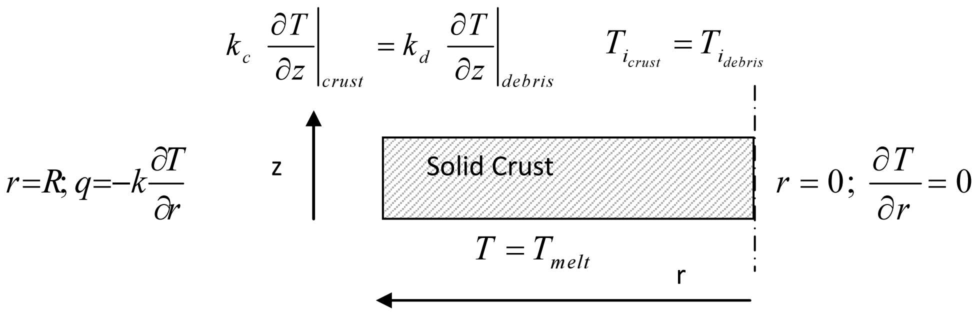

Figure 2.8 Boundary conditions for crust region

(iii) Governing equations in debris region:

Mass balance equation

$$\nabla \cdot v = 0 \tag{2.3}$$

Momentum balance equation

$$v = \frac{\kappa}{\mu}(-\nabla \cdot p + \rho g) \tag{2.4}$$

Energy balance equation:

$$\gamma_1 \frac{\partial \mathrm{T}}{\partial t} + v \cdot \nabla T = \alpha \nabla^2 T + \frac{q''}{(\rho C_p)_f} \tag{2.5}$$

Here q'' is heat generation term in debris region. (In debris region water or steam is present between particles so here heat generation can be different from crust.)

and,

$$\gamma_1 = \varepsilon + (1-\varepsilon)\frac{\left(\rho C_p\right)_s}{\left(\rho C_p\right)_f} \tag{2.6}$$

Boundary conditions:

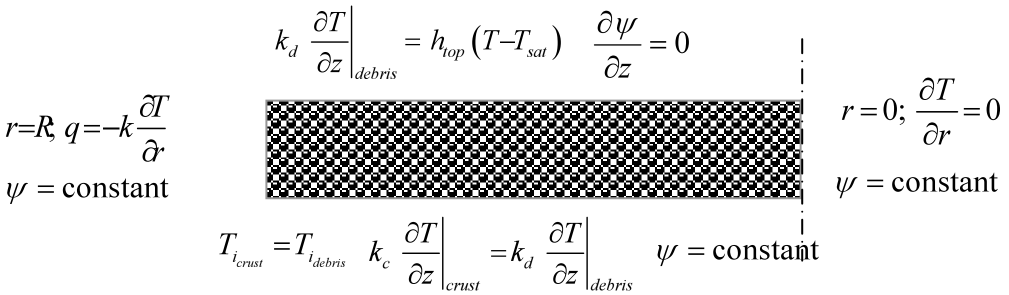

Figure 2.9 Boundary conditions for debris region

Here ψ is the stream function defined as

$$v_r = \frac{1}{r}\frac{\partial \psi}{\partial z};\ v_z = -\frac{1}{r}\frac{\partial \psi}{\partial r} \tag{2.7}$$

Calculation of surface heat transfer coefficient:

For calculation of heat transfer from top of the debris to the pool of water, appropriate heat transfer correlations are used as given below.

If surface heat flux is greater then the debris bed dry out flux, combination of radiation and film boiling heat transfer is used, i.e.

$$q''_{surface} > q''_{d} \qquad h = h_{fb} + h_{rad} \tag{2.8}$$

The film boiling heat transfer coefficient is calculated using the Berenson's [49] film boiling model as

$$h_{fb} = 0.425 \left(\frac{h_{fg} \cdot \rho_v \cdot g \cdot (\rho_l - \rho_v) \cdot k_v^3}{\mu_v \cdot \sqrt{\dfrac{\sigma_{ST}}{g \cdot (\rho_l - \rho_v)}} \cdot \Delta T} \right)^{1/4} \tag{2.9}$$

The radiation heat transfer coefficient correlations is calculated as

$$h_{rad} = \sigma_{stefan} \cdot \varepsilon_s \cdot (T^2 + T_{sat}^2)(T + T_{sat}) \tag{2.10}$$

When the surface heat flux falls below the dryout flux, i.e.

$$q''_{surface} < q''_{d} \qquad h = h_{nb} \tag{2.11}$$

Nucleate boiling correlation by Rohsenow [50] is used

$$h_{nb} = \frac{1.25 \times 10^5 \mu_l h_{lv} \left[\dfrac{C_{Pl}}{h_{lv}} \right]^3 (\Delta T_{\sup})^2}{\left[\dfrac{C_{Pl} \times \mu_l}{K_l} \right]^{5.1} \sqrt{\dfrac{\sigma_{ST}}{g(\rho_l - \rho_v)}}} \tag{2.12}$$

The dryout heat flux was calculated using the following relationship based on counter current flooding limitations (CCFL) as given by Sinha and Nayak [45]

$$q_d = 0.539 h_{lv} \frac{\left[(\rho_l - \rho_v) \rho_v g d \varepsilon^3 / (1 - \varepsilon) \right]^{1/2}}{\left[1 + \left(\rho_v / \rho_l \right)^{1/4} \right]^2} \tag{2.13}$$

Solid crust generation rate:

Crust generation rate is calculated from energy balance.

$$\iint \left(-k_m \left. \frac{\partial T}{\partial z} \right|_{pool} + k_c \left. \frac{\partial T}{\partial z} \right|_{crust} \right) dA \cdot \Delta t = A \cdot \Delta z_{crust} \cdot \rho_s \cdot C_{p_s} \cdot \Delta T + A \cdot \Delta z_{crust} \cdot \rho_s \cdot h_{fus} + q''' \cdot A \cdot \Delta z_{crust} \tag{2.14}$$

There is no heat flux continuity at crust - melt interface. This heat flux discontinuity is responsible for the crust growth. If the left hand side of the above equation is negative, it implies that crust is dissolving in molten pool. This will occur due to high heat generation rate in pool which leads to increase in pool temperature whereas top flooding is unable to take the heat away.

Stresses in solid crust:

As cooling initiates, there will be a temperature distribution in the crust. Initially, the crust will be formed only at the melting temperature of the material. At the top of the crust, the crust gets cooled and is at water saturation temperature. At the bottom, there is melting temperature. Hence, thermal stresses are induced inside the crust.

The 2-D axi-symmetric equations for stress developed in solid crust are:

$$\frac{\partial}{\partial r}\left(r \cdot \tau_{rz}\right)+\frac{\partial \sigma_z}{\partial z}=0 \tag{2.15}$$

$$\frac{\partial}{\partial r}\left(r \cdot \sigma_r\right)+r\frac{\partial \tau_{rz}}{\partial z}=\sigma_\theta \tag{2.16}$$

These equations straightway come from force balance in differential element. The boundary conditions are given as follows:

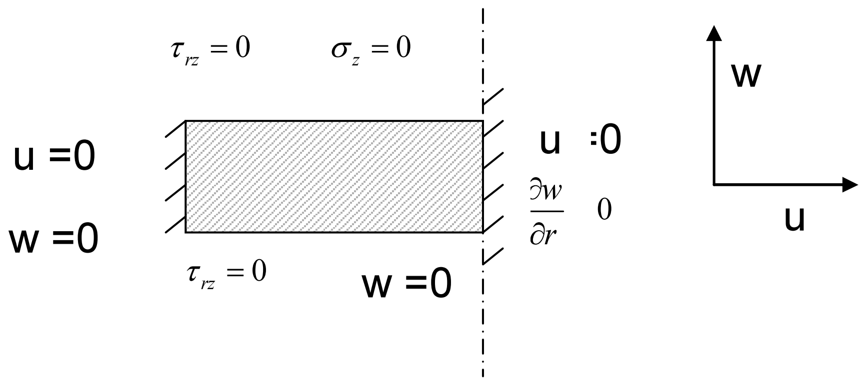

Figure 2.10 Stresses in the crust and boundary condition

Where u is radial and w is the axial displacement.

Stress strain relationship is given as

$$\begin{pmatrix} \sigma_r \\ \sigma_\theta \\ \sigma_z \\ \tau_{rz} \end{pmatrix} = \frac{E}{(1+\nu)(1-2\nu)} \begin{pmatrix} 1-\nu & \nu & \nu & 0 \\ \nu & 1-\nu & \nu & 0 \\ \nu & \nu & 1-\nu & 0 \\ 0 & 0 & 0 & \frac{1-2\nu}{2} \end{pmatrix} \begin{pmatrix} \varepsilon_r \\ \varepsilon_\theta \\ \varepsilon_z \\ \gamma_{rz} \end{pmatrix} \tag{2.17}$$

So we can write

$$\begin{pmatrix} \varepsilon_r \\ \varepsilon_\theta \\ \varepsilon_z \\ \gamma_{rz} \end{pmatrix} = \begin{pmatrix} \frac{\partial u}{\partial r} - \alpha_l \Delta T \\ \frac{u}{r} - \alpha_l \Delta T \\ \frac{\partial w}{\partial z} - \alpha_l \Delta T \\ \frac{\partial u}{\partial r} + \frac{\partial w}{\partial z} \end{pmatrix} \tag{2.18}$$

From these equations, ultimately two equations in u and w are obtained. At the top of the crust there will be no shear stress and the axial stress due to self-weight of the debris is considered to be negligible. These equations were discretized in implicit manner and solved with boundary conditions as shown in Figure 2.10, to obtain stresses distribution in crust.

Criteria for fracture of the solid crust:

The solid crust, being a ceramic mixture of the oxides, behaves like brittle material. Brittle materials have no yield limit and they fracture catastrophically at the a peak stress which is termed as fracture stress. For fracture initiation, the Ritchie's model, [51] was used. In this model, fracture initiation occurs only when thermal stress exceeds critical stress in some region. This region is taken generally order of eight-grain sizes. So fracture initiation occurs only when stresses are above critical limits in more than eight-grain size area. Since this requires detail knowledge of dimension of critical region (like eight-grain size), it may not be known for some materials. Hence, an alternative model is used to simulate fracture initiation, which is known as the Beremin's [52] model. In this model, the critical stress σ_c required for the separation of cleavage facets, which can be related to the length 'l_0' of a micro crack by the equation.

$$\sigma_c = \sqrt{\frac{2E\gamma_s}{\pi(1-\nu^2)l_0}} \tag{2.19}$$

Where E is Young's modulus of elasticity, ν is the poison's ratio, and γ is the surface energy. The length 'l_0' is maximum size of micro crack present in some volume. This is a probabilistic model and distribution of micro cracks is required for the longer ones.

In each volume, the probability of finding a crack of length between l_0 and $l_0 + dl_0$ can be written as:

$$P(l_0)dl_0 = \frac{\alpha_1}{l_0^{\beta_1}} dl_0 \tag{2.20}$$

Where α and β are material constants for a particular value of V_0. Hence, in a given volume for a stress level σ, the probability of failure is

$$P(\sigma) = \int_{l_0^c}^{\infty} P(l_0)dl_0 = \frac{\alpha_1}{\beta_1 - 1} \frac{1}{(l_0^c)^{\beta_1 - 1}} \tag{2.21}$$

So from some stress level σ, the critical length of micro crack needed is obtained from equation (2.19) and the probability of failure of the concerned grid is calculated using equation (2.21) .

The total probability of failure is

$$P_R = 1 - \exp(-\left(\frac{\sigma_w}{\sigma_u}\right)) \tag{2.22}$$

Where σ_u is material constant and is given as

$$\sigma_w = \sqrt[m]{\sum_{i=1}^{n} (\sigma_1^i)^m \frac{V_i}{V_0}} \tag{2.23}$$

In equation (2.23) V_i is the volume of the i_{th} element experiencing the maximum stress σ_i .

In brittle materials when fracture occurs it moves catastrophically. In lower points of crust, temperatures are as high as melting point; so crack may be arrested. To model this, the R6 model is used as given by

R6 model:

$$K_r = \begin{cases} \left(1-0.14L_r^2\right)\left[0.3+0.7\exp\left(-0.65L_r^6\right)\right] & for\ \ L_r \le L_r^{\max} \\ 0 & for\ \ L_r > L_r^{\max} \end{cases} \tag{2.24}$$

where

$$Lr = \frac{\text{Applied load}}{\text{Limit load based on yeild stress}}$$

$$Kr = \frac{\text{Stress intensity factor}}{\text{Fracture toughness}}$$

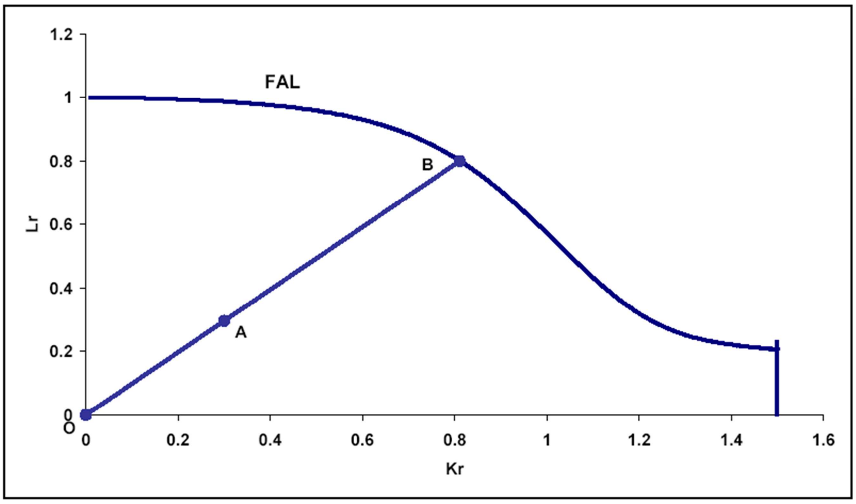

Figure 2.11. R6 model curve

If at some time Lr and Kr lie under curve shown (FAL). It indicates that crack is arrested.

2.3.4 Solution strategy:

The algorithm is given in Figure 2.12. The governing equations in melt pool and solid crust region are discretized using finite difference method and solved implicitly using Gauss elimination method to obtain temperature distribution in the melt pool. After evaluating the temperatures, the crust growth rate is calculated and subsequently the thickness of the solid crust region is updated. After the temperature distribution has been obtained, the stress equations are solved implicitly by finite difference technique. With the stresses, the fracture conditions are evaluated. If the criteria for fracture is satisfied, the fractured grids are merged into debris region.

For solving the equations in debris region, stream function approach is used which eliminates the pressure term. Then applying Boussinesq approximation, momentum equation in ψ and T are obtained. Energy equation is also reduced in terms of ψ and T. Then both the equations are solved implicitly. The detailed equations are given in Appendix – 1.

The calculation procedure for debris surface heat transfer coefficient has already been discussed in equations (2.8)-(2.13). When the surface heat flux falls below the dry out flux, water ingresses into the debris.

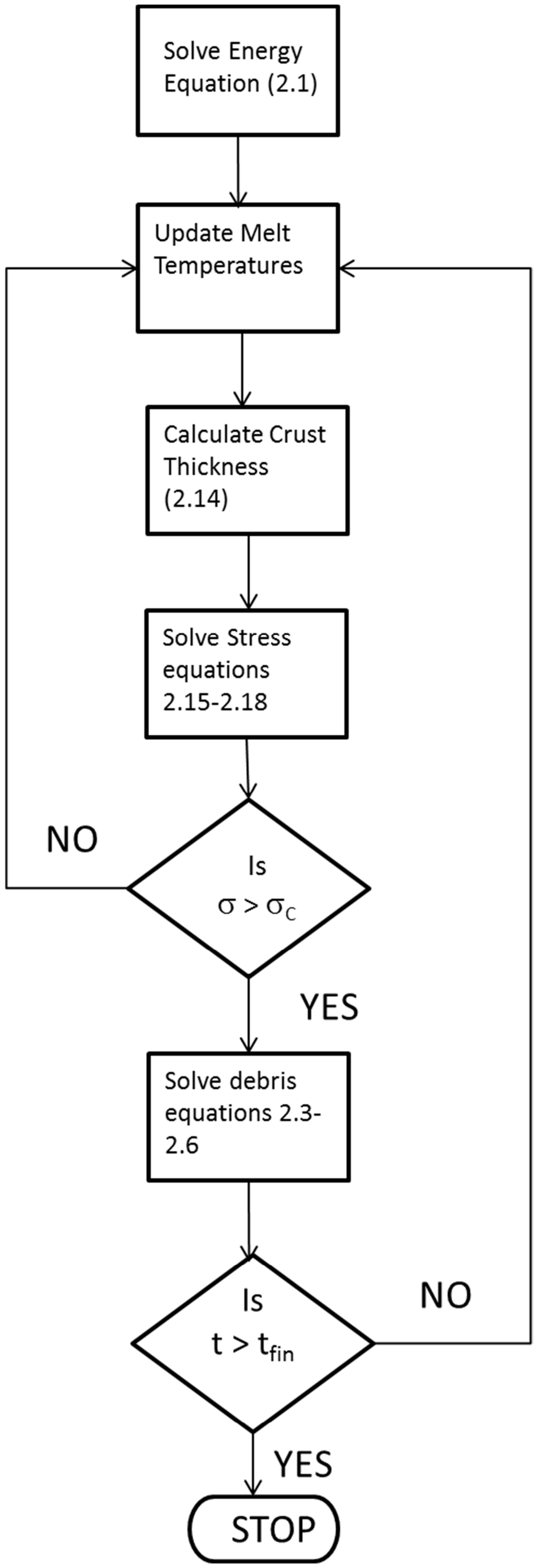

Figure 2.12. Solution Algorithm

2.3.5 Model validation with COMECO experiments

For validation of the model, experimental data from COMECO [14] was taken. Figure 2.13 shows transient temperature history of the molten pool during quenching, as predicted by our model. Theoretical results also show that temperature of top layer falls suddenly in 500 seconds which is closer to measured value. The transient temperature history due to quenching is similar at all the depths as in the experiments (Figure 2.4). Model predicts water ingression of 0.11 meters, as shown in Figure 2.14. It is very close to experimental result which was around 100 mm.

In Figure 2.14 and Figure 2.15, the total depth of water ingression, crust height and dry debris have been plotted with respect to time. It can be seen that water ingression rate is faster initially. During this time, the crust height is found to be fluctuating. This is due to the fact that initially whatever crust forms, disintegrates into debris and the debris gets quenched due to water ingression into it. Since brittle fracture is the mode of crust disintegration as assumed in the model, the debris formation occurs in steps, i.e. when crust disintegration stops, depth of crust increases again periodically.

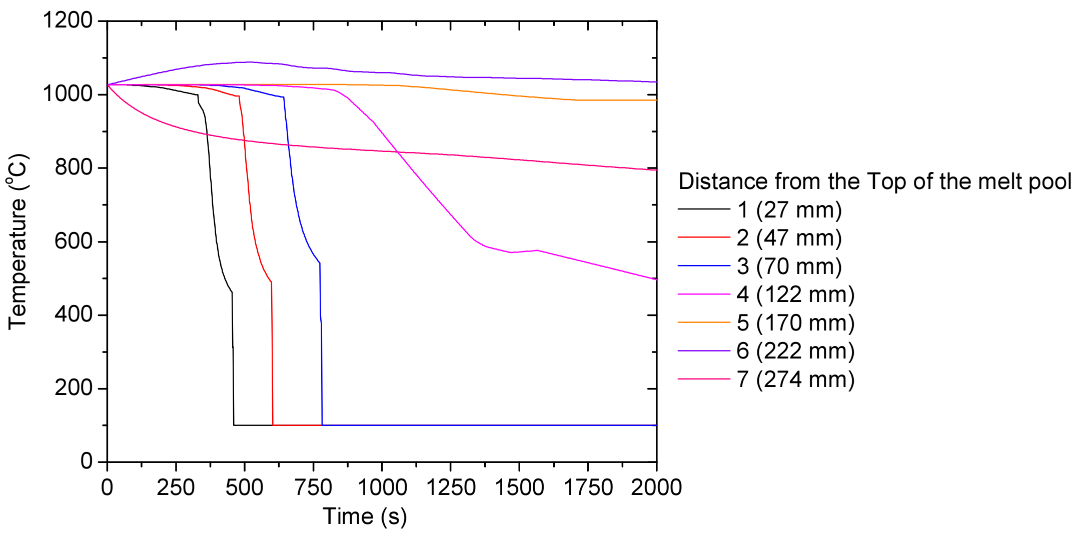

Figure 2.13 Model predictions

There arises a big question 'why water ingression stops after some depth?' As depth of water ingression increases, it means depth of debris flooded with water increases. This water takes the heat produced i.e. volumetric heat generation due to decay heat. However, due to increased debris depth as disintegration of crust proceeds, the path resistance increases for water to ingress down and down to cool the top of the crust which is at the bottom of debris. So the crust top surface temperature progressively increases as time proceeds. Since bottom part of crust is always at liquidus temperature, the thermal gradient inside the crust becomes lower and lower with time, which reduces the thermal stresses inside the crust. After some time, the stresses become so low to disintegrate the crust further. That is why water ingression stops after some depth. In addition, with reduction in thermal gradient across the crust, the heat absorption rate from molten part also slows down, which reduces the solidification rate.

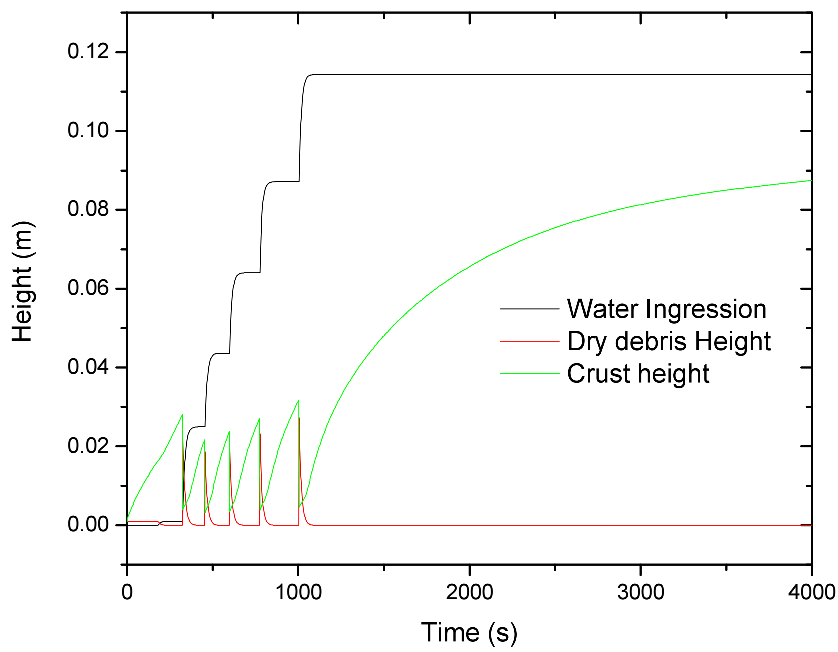

Figure 2.14 depth of water in ingression and crust height predicted by model

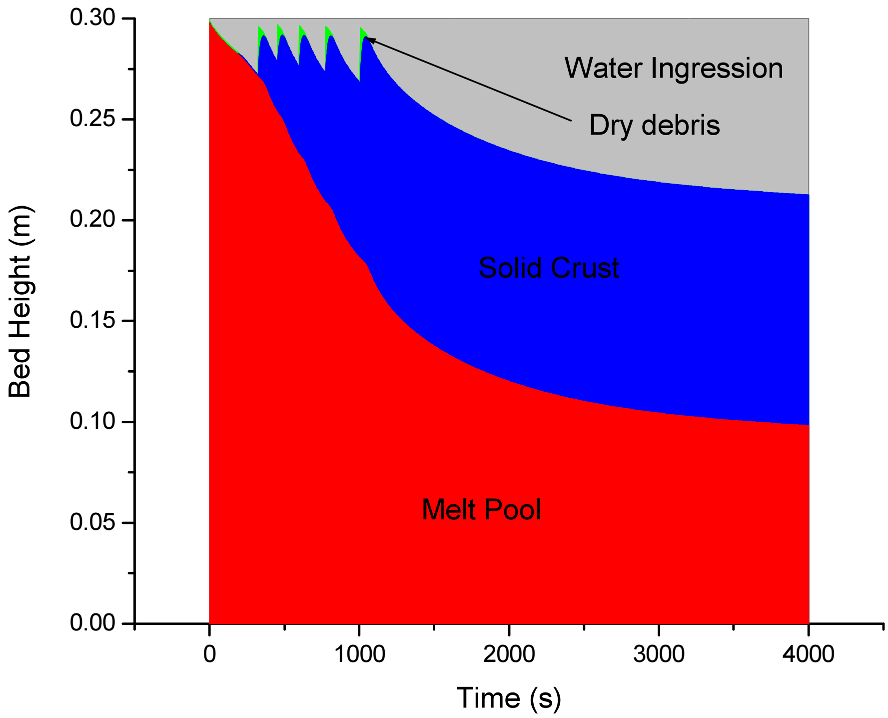

Figure 2.15 various regions in pool vs time

After water ingression stops, crust depth increases slowly. Increasing depth of crust having low conductivity material, act as a blanket for molten material filled below. So heat transfer from molten part decreases. It leads to very low crust formation rate. After some time, when net heat produced in molten pool equals to heat taken away by the overlaying water, crust formation stops. And these lead to an eventual steady state.

2.4 Influence of variation of thermophysical properties of the melt on coolability

During the accident progression, the properties of corium such as the viscosity, the melt solidus and liquidus temperatures and thermal conductivity can change drastically due to its interactions with the in-vessel and ex-vessel structures and also with the concrete basement. Similarly, the Modulus of Elasticity, tensile strength and linear thermal expansion coefficient, which are some of the key parameters that determine the crack formation during melt quenching, can change depending on the amount of structural and concrete materials mixing with corium as shown in Figure 2.16. Besides, there are a lot of uncertainties in measurement of the parameters like strength of the corium [53] as shown in Figure 2.17. Concrete addition results in increase in strength as well as decrease in the linear thermal expansion coefficient.

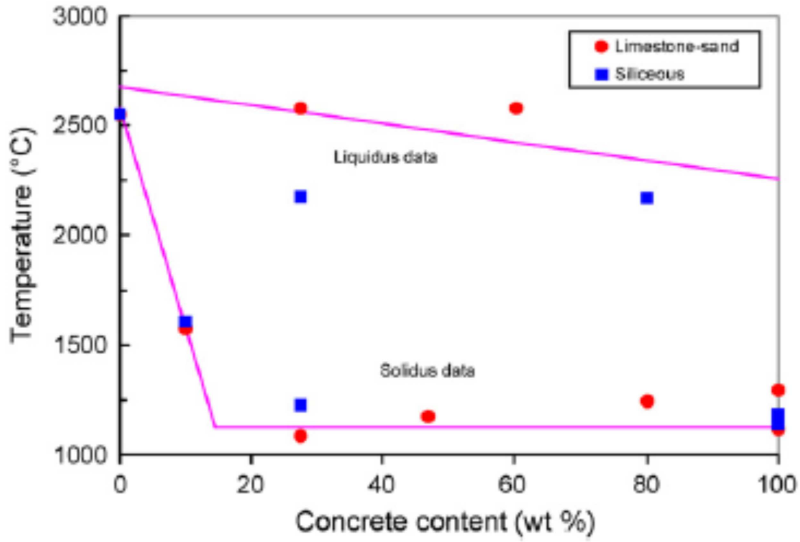

Figure 2.16. Variation of solidus and liquidus temperature of corium with concrete addition

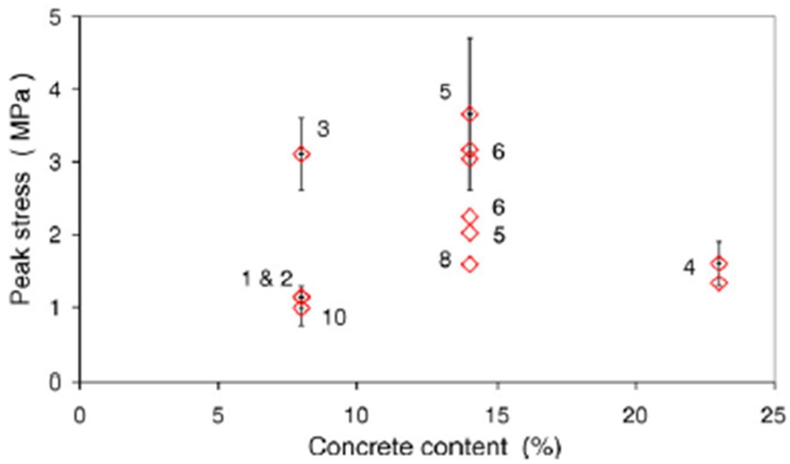

Figure 2.17 Uncertainty in measurement of corium crust

In order to study how the coolability is affected as a result of change in these parameters, a parametric analysis was carried out. The effect of change in thermal expansion coefficient on coolability is given in Figure 2.18a and b. Figure 2.18a shows the water ingression predicted during corium quenching. It can be seen that water is able to ingress completely into the melt pool. Figure 2.18b shows that, because of concrete addition, the thermal expansion coefficient is reduced which no longer causes water ingression and coolability is limited as shown in Figure 2.19a and b. this can be attributed to the fact that, because of decreased thermal expansion coefficient, there are less thermal stresses generated in the corium, which prevents it from fracturing thus limiting water ingression.

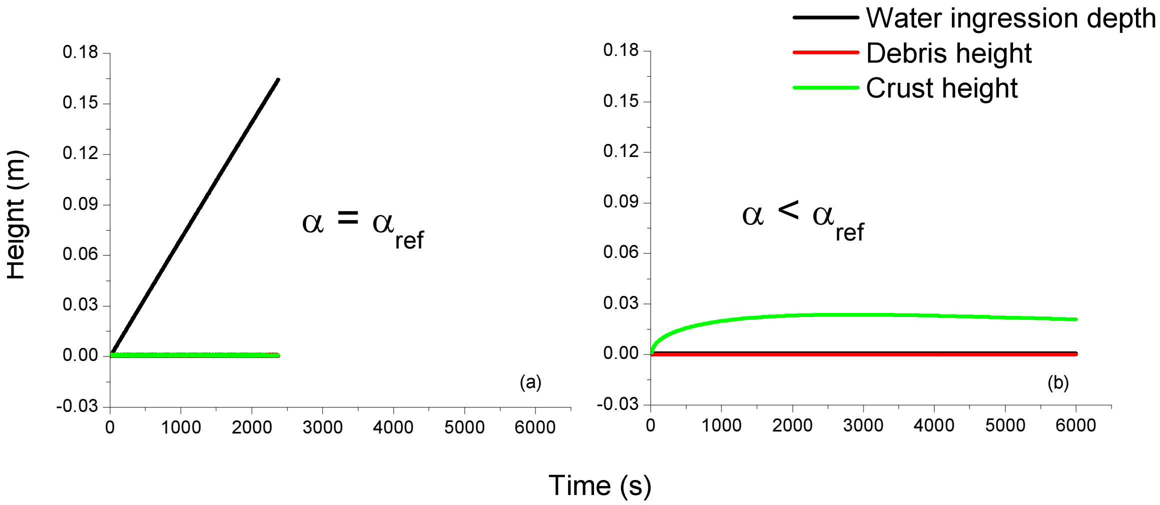

Figure 2.18 Effect of concrete addition on thermal expansion coefficient of corium

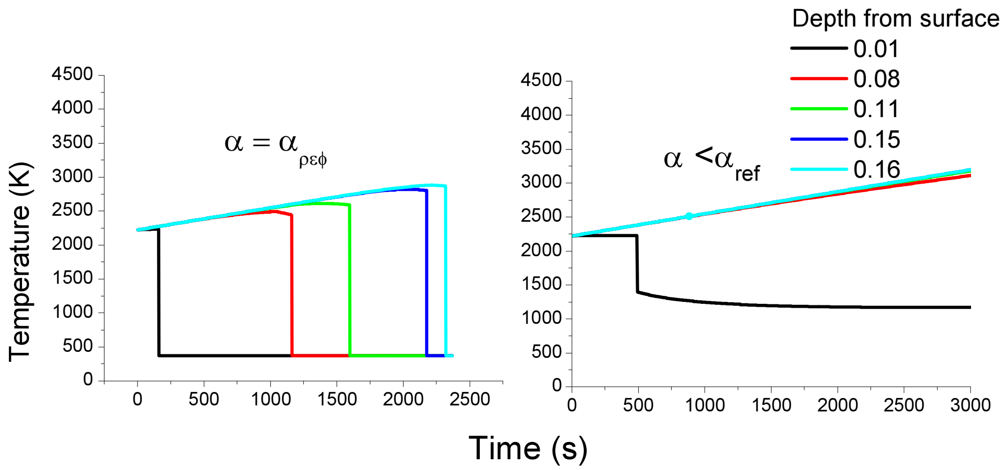

Figure 2.19 Temperature history of corium before and after changing the thermal expansion coefficient

Similar effect is seen when there is increase in corium strength as shown in Figure 2.20a and b. As the strength of corium increases, it is difficult to fracture it and it stops the water ingression. The corresponding temperature history is given in Figure 2.21 a-b

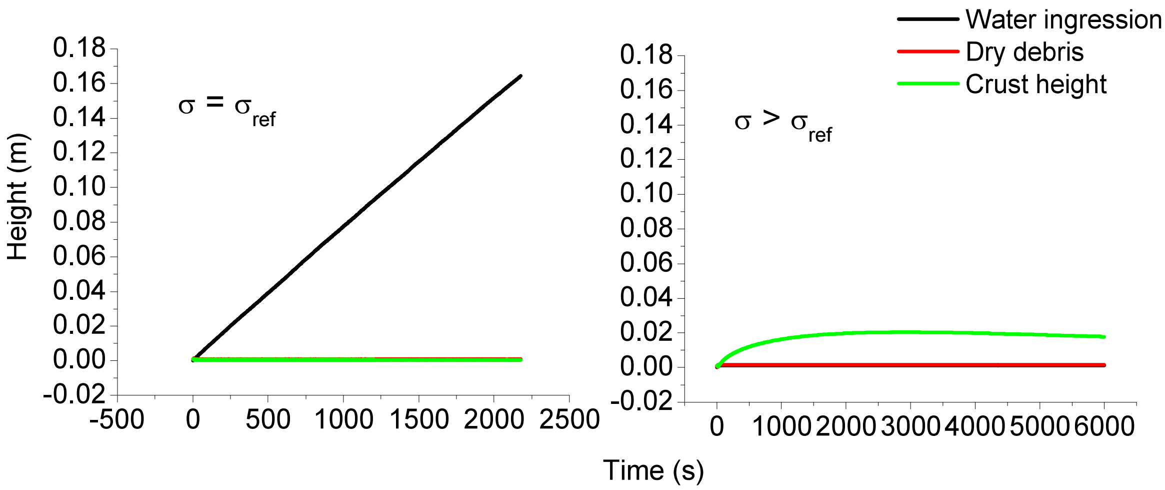

Figure 2.20 Effect of change in strength of corium on water ingression

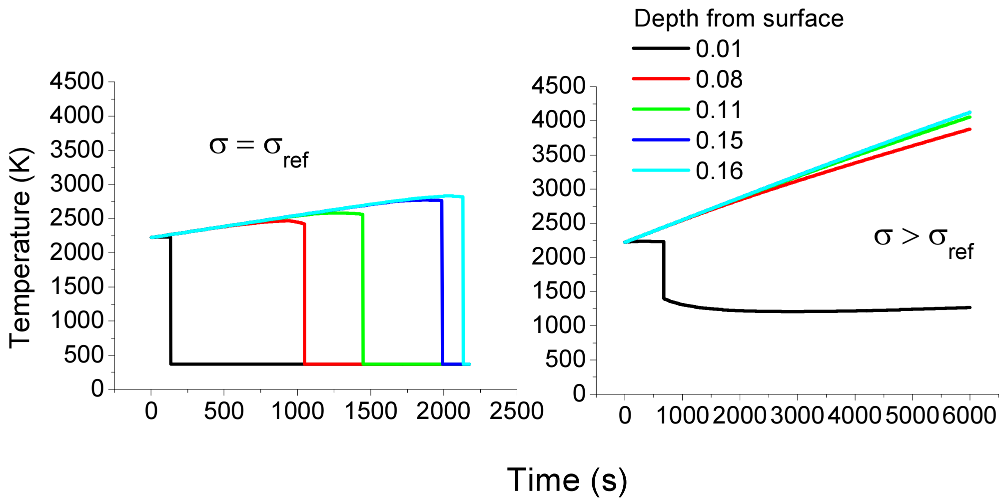

Figure 2.21 Temperature history of corium before and after changing the corium strength

2.5 Scaling criteria for simulation of coolabilty of molten corium.

It was observed that when the strength of the corium concrete mixture decreased, water ingression was enhanced. Similarly, when thermal expansion coefficient and Young's modulus increase the stresses in the crust increase which results in crust break and ultimately causes water ingression. Thus, we can conclude that, the factors which make the corium difficult to break hinder the coolability. It was conceived that, coolability and water ingression can be simulated by a dimensionless parameter. A new non dimensional parameter is defined as a "crust break parameter" given as $E\alpha/\sigma$ where E is Young's modulus, α is thermal expansion coefficient and σ is strength of corium. The Numerator denotes the stresses induced inside the crust as a result of the thermal stresses and denominator denotes the endurance of the material to the stress. Naturally, if the crust has to fail, the parameter must have value greater than 1. Analysis was carried out by varying individual parameters but keeping the crust break parameter the same i.e., the individual parameters were adjusted such that $E\alpha/\sigma$ remains the same. The results are shown in Figure 2.22 and Figure 2.23. Figure 2.22a shows that for a reference value of $E\alpha/\sigma$, complete water ingression takes place into the melt upto a depth of 0.16 m. The temperatures at different heights are given in Figure 2.23a which also show complete coolability. If we make E and α half of the original and make σ four times higher such that crust break parameter remains same, the coolability is found to be same as given by Figure 2.22b. Similarly the temperature distribution also remains same as before as shown in Figure 2.23b.

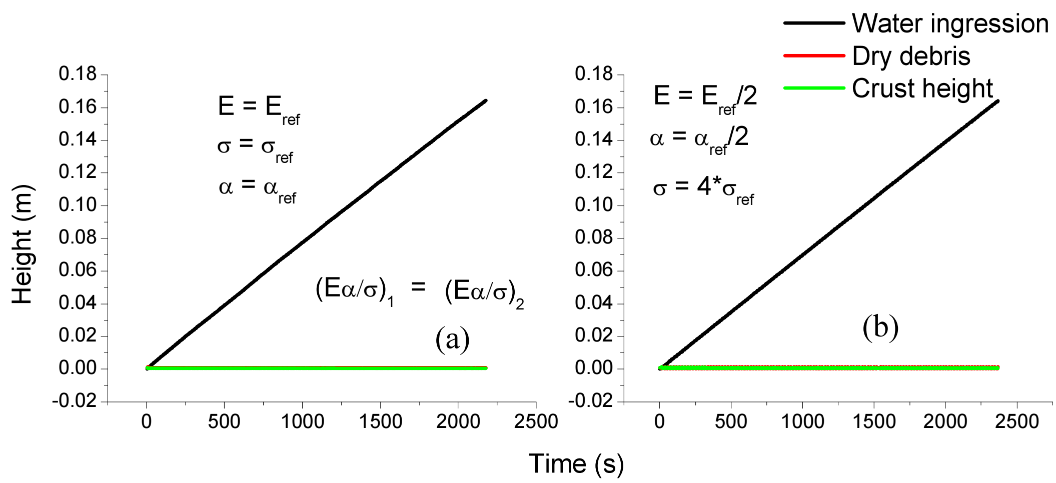

Figure 2.22 Effect of keeping dimensionless parameter constant on water ingression

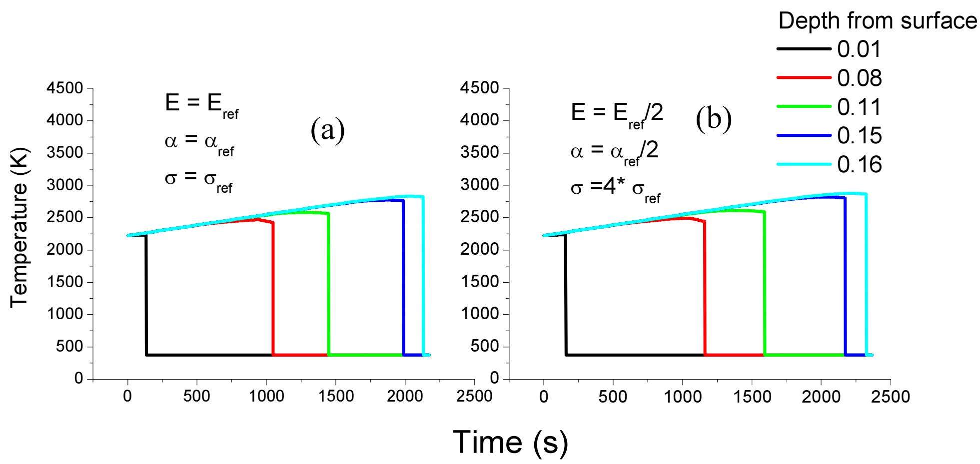

Figure 2.23 Temperature history of corium with varying individual parameters

It has been demonstrated that, the coolability is influenced by a dimensionless parameter $E\alpha/\sigma$ which we call it as a "crust break parameter". Higher is the parameter, better is the coolability.

2.6 Further validation of model on water ingression in top flooding in glass melt pool.

In actual reactor conditions, corium mixes with concrete which has high silica content. The resulting mixture contains metal silicates which acts as a brittle glassy material with solidus temperature as low as to 1200 ^{0}C. Difference between solidus and liquidus temperature is as high as 200 deg C. Besides, the temperature dependant properties of the mixture material ($CaO + B_2O_3$) are not fully known.

The properties of glass are well known. Hence, it was decided to use glass as a simulant material and perform experiments.

2.6.1 Objective of the experiment

- To study the effect of water ingression in glass type material
- To generate sufficient experimental data for validation of top flooding model with more precision using simulant material of which the thermo-mechanical properties are well known

2.6.2 Experimental Setup

The experiment was carried out as per the setup shown in Figure 2.24. The test section consists of a 300 mm OD carbon steel pipe with 600 mm height. The capacity of test section is about 25 litres corresponding to melt height of 500 mm. The upper part of test section can contain water pool up to 700 mm height. Steam outlet and water inlet have been provided in the upper part of the test section. Temperature inside the melt pool was measured at different locations. Thermocouples were inserted in the test section through a 10 mm inconel tube. A total of 21 K type thermocouples arranged in 7 axial and 3 radial positions as shown in Figure 2.25 were used. In addition, inlet water temperatures, temperatures of water pool as well as outgoing steam were also measured by thermocouples in the upper part of test section. The accuracy of the measurement of the instruments is as given in Table 2.1. The test section was insulated in lower part using ceramic wool. The assembled test setup is shown in Figure 2.26

Table 2.1. Accuracy of measurement

Parameter	Accuracy	Range
Temperature	$\pm$ 0.75% of measured value	0-1200 ^{O}C
Pressure	$\pm$ 0.35% of measured value	0-100 bar
Water level	$\pm$ 0.2% of the measured value	0-1000 mm

2.6.3 Experimental Procedure

Sodium borosilicate glass was first melted in a cold crucible induction furnace. The properties of the glass are shown in Table 2.2. On account of relatively poor electrical conductivity, induction melting of glass requires high frequency for efficient heating. For this, a 200 kHz, 350 kW induction furnace was chosen. The glass was melted and the melt temperature was raised up to 1200 ^{o}C. The experimental setup was placed below the furnace and the melt was delivered in the test section by opening a solenoid valve below the furnace. About 20 litres of melt at 1200 ^{o}C was poured in the test section. After pouring was completed, the top flap of the test section was remotely closed which contained automatic sealing arrangement. After the flap was closed, water supply at the rate of 1 lpm was started using a peristaltic pump from a storage tank. Water supply was kept on till the level gauge showed 100 % (450 mmWC). The transient temperature history inside the melt was recorded till the entire melt reached room temperature.

Table 2.2. Properties of glass

Type	Sodium borosilicate
Melting temperature	600 deg C
Density	2200 kg/m3
Thermal conductivity	1.1 W/mK
Specific heat capacity	750 J/kg K

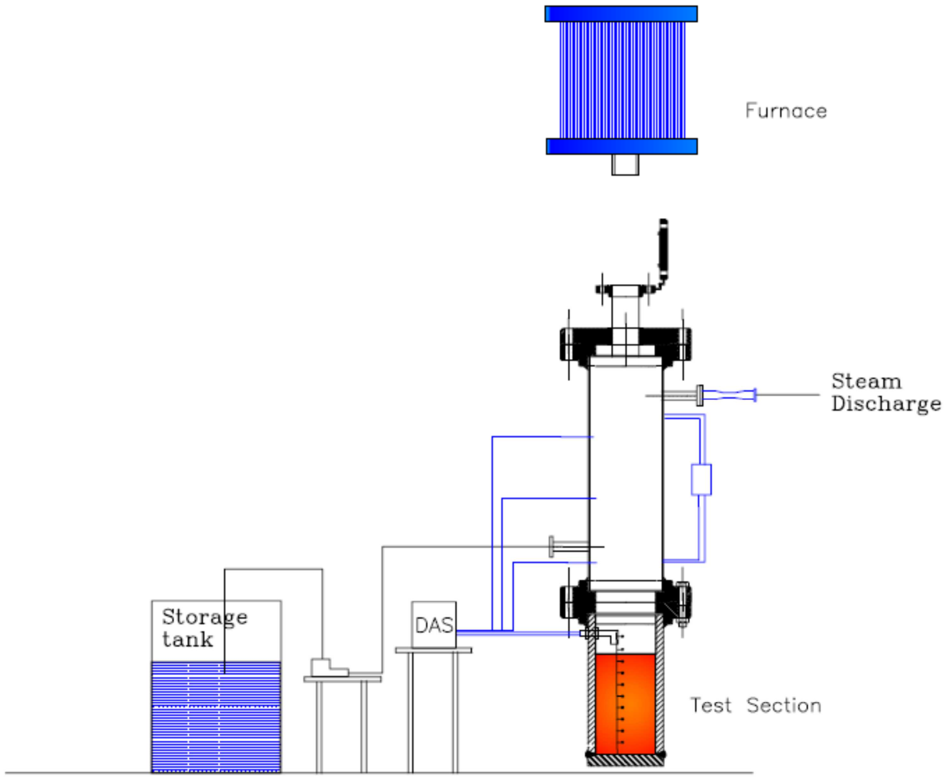

Figure 2.24 Schematic of the experimental setup

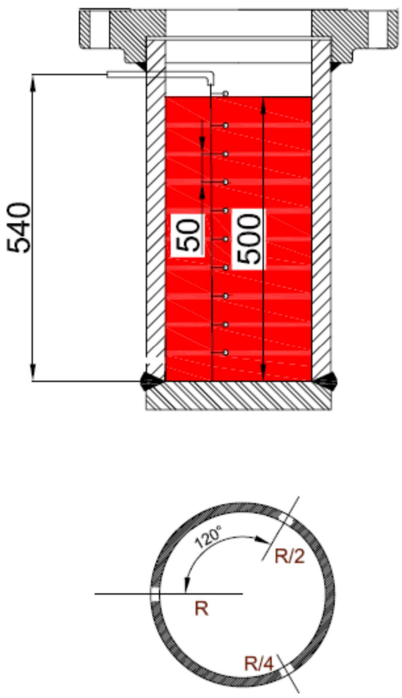

Figure 2.25 Thermocouple arrangement inside the test section

Figure 2.26 Assembled test section

2.6.4 Results and discussions:

In this experiment, decay heat was not simulated. Pouring was started at after 8 minutes from the start of the experiment. It took about 5 minutes to pour the entire melt. After pouring was finished, immediately water supply was started. The melt height was about 390 mm. As soon as the water touched the melt, it formed steam and a steam jet was observed. Thermocouples near surface showed dip in the temperature. However, within a short span of time, steam formation was suppressed (Figure 2.27).

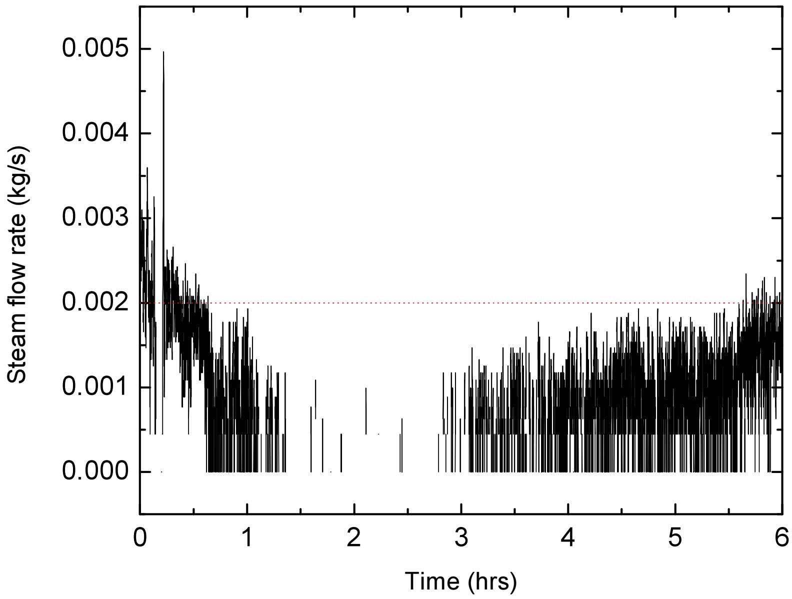

Figure 2.27 Measured steam flow rate

The level gauge showed continuous rise of water (Figure 2.28). Within half an hour, the level reached 450 mm mark. The water supply was stopped at the time and the melt was allowed to cool to room temperature.

The measured temperatures near wall are given in Figure 2.29 and Figure 2.30. From Figure 2.30, it can be observed that, as soon as water supply was started, top thermocouples T1 and T2 immediately reached water saturation temperature indicating onset of flooding. Thermocouples T3-T7 were inside the melt and showed very slow decrease in temperature indicating conduction dominated region. Although, the decrease in temperature indicated by thermocouple T3 show different slope and is cooled relatively fast which indicted that water ingression has taken place at the top of the crust. It took almost six hours to cool the melt even though the melt was flooded with water pool of about half a meter height. Figure 2.31 and Figure 2.32 show temperatures in the central and half radius. Two thermocouples in the half radius and one in the central regions were damaged during experiment hence, the data is not obtained. However, the remaining thermocouples show similar trend as near wall region

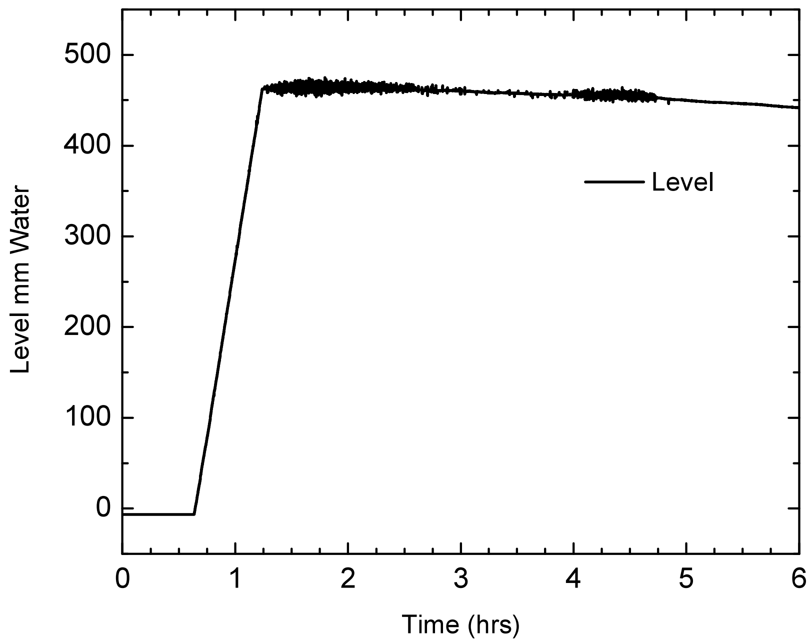

Figure 2.28 Level of water pool

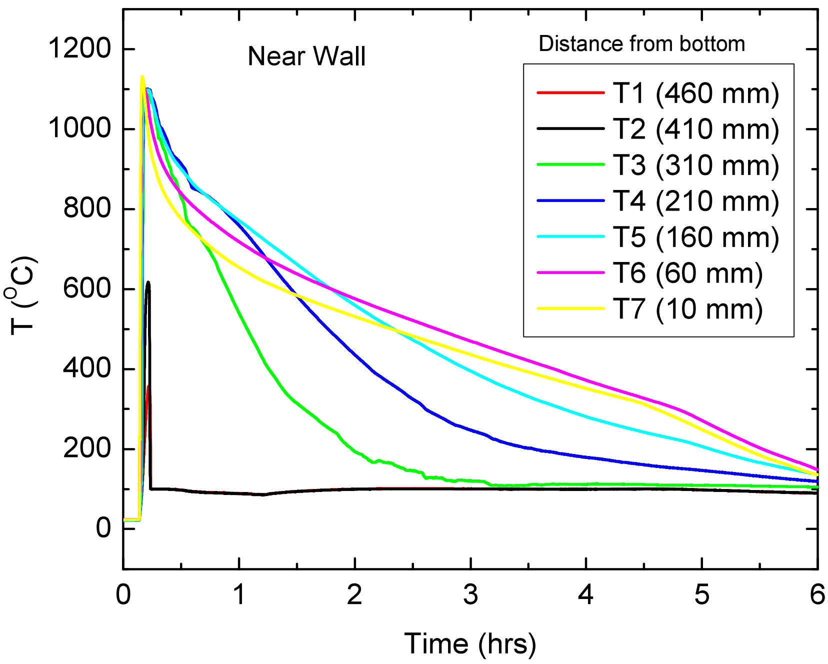

Figure 2.29 Measured temperature near wall

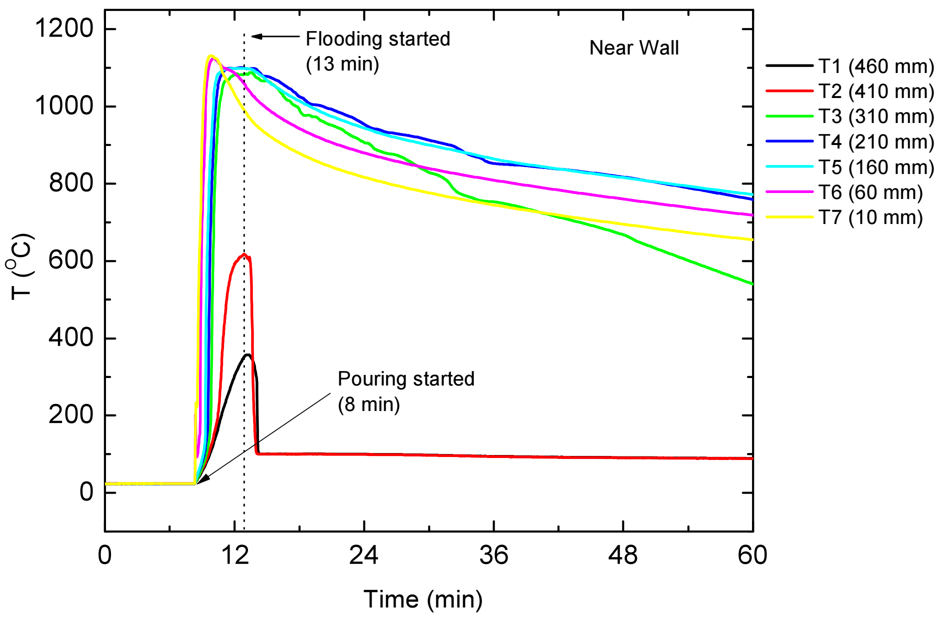

Figure 2.30 Temperature history within one hour

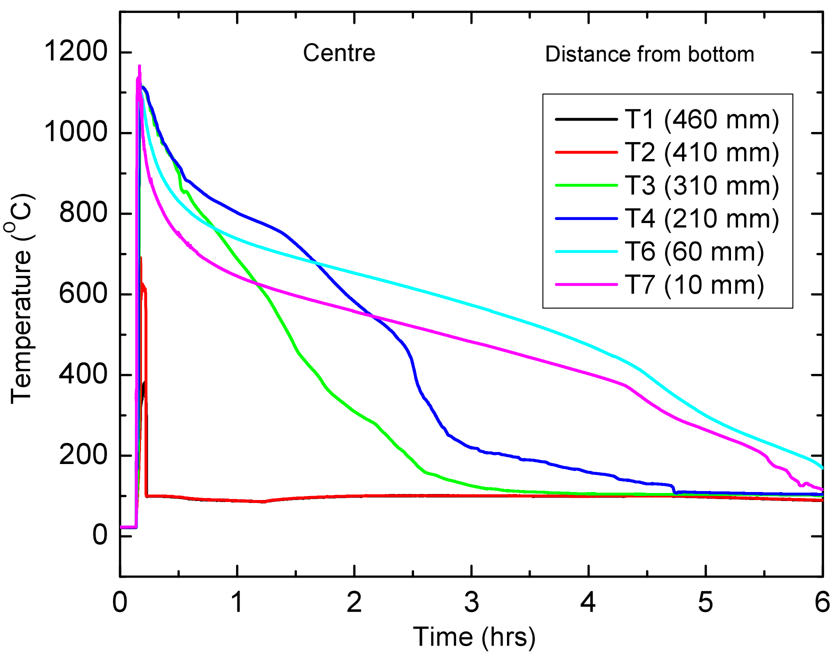

Figure 2.31 Temperature in central region

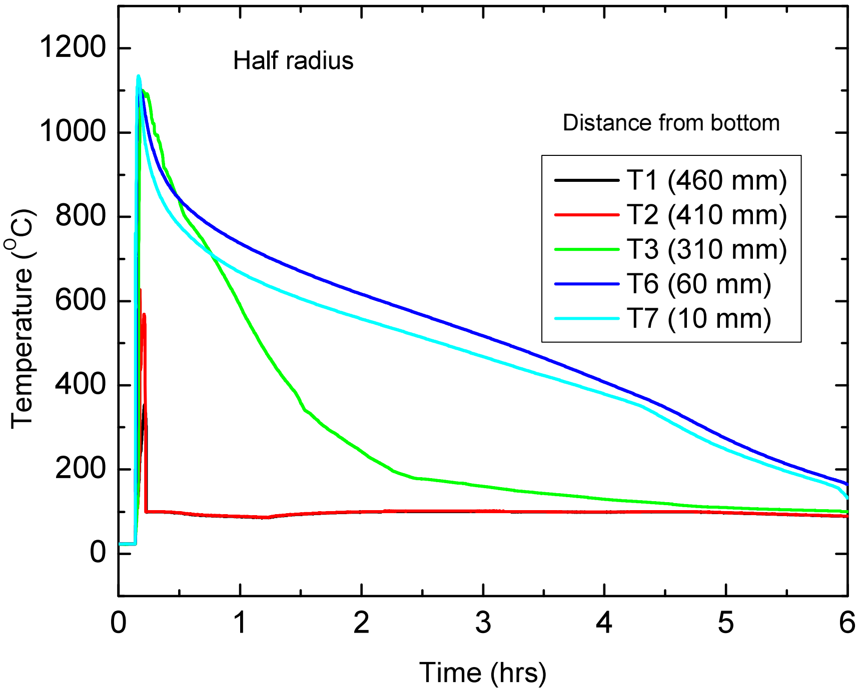

Figure 2.32 Temperatures in half radius region

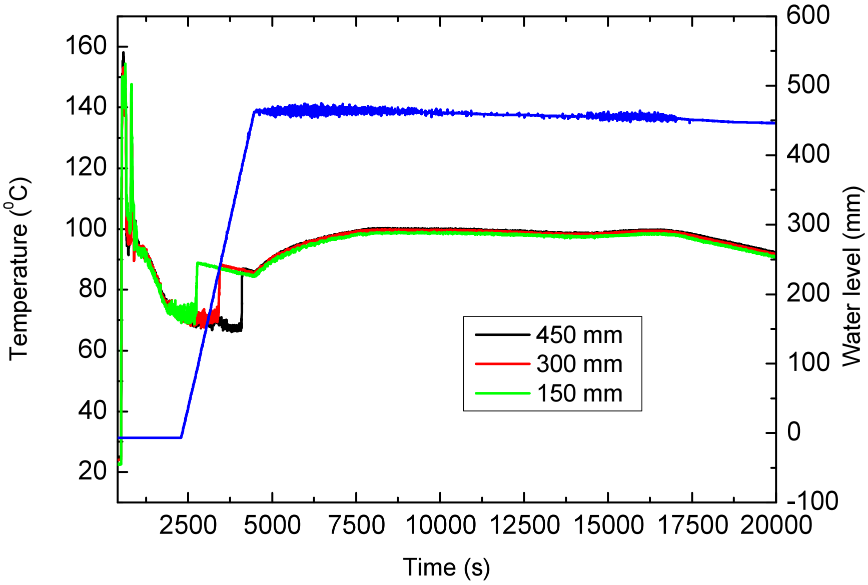

Figure 2.33. Water pool temperature

Figure 2.33 shows the temperature at different heights in the upper part of the test section along with the water level. It is observed that, the moment water is introduced, it gets evaporated and superheated steam at temperature of around 160 ^{0}C is formed. After the initial steam ejection, there is fall in temperature. This indicates that a crust has formed at the top and water is now filling up the test section. At t = 2500 s, the level in the upper part of the test section starts rising. As the water level rises, the thermocouples in the upper part of the test section start recording the water pool temperatures. It is observed that, initially the temperatures are below water saturation temperature. Water supply was stopped when the level reached ~470 mm. Now the heat was taken away from the melt top surface to the water pool by convection only. It is observed that, water starts boiling after long time (~ 7500 s) indicating diminished heat transfer from top surface of the crust. After the boiling was initiated, the level started dropping. However, the rate of level drop was very low and after 10000 s (at 17500 s), only 20 mm water was lost. After this, boiling stopped and the water temperature started decreasing.

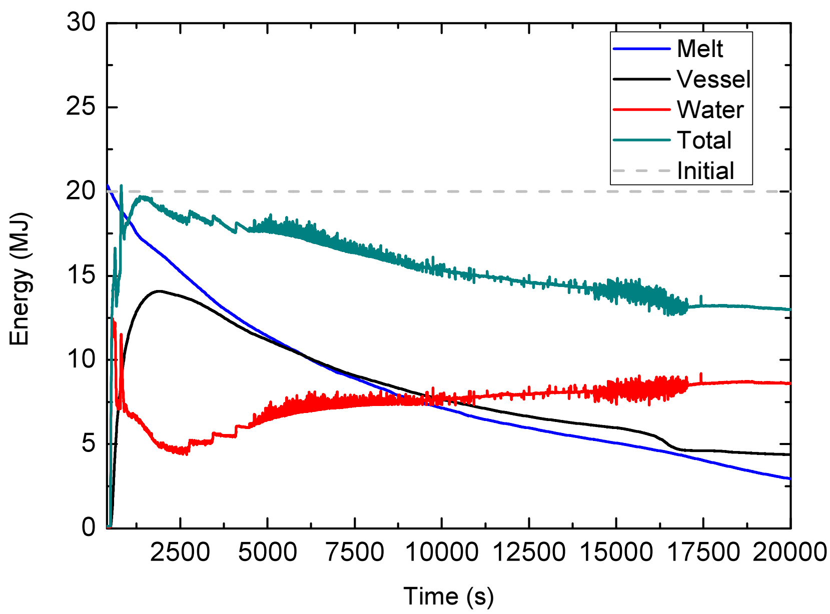

Figure 2.34 Heat balance.

Figure 2.34 shows the energy balance of the experiment. Initially, as soon as the melt is poured in the vessel, heat is transferred to the vessel as the vessel has large thermal capacity. Subsequently, when water is introduced, initially there is substantial heat is taken away by steam generated through interaction of hot melt surface and water marked by peaks in the above figure. After that, a stable crust is formed at the top of the melt. At this condition, the heat is transferred to water by conduction through the crust marked by steady increase in water temperature. There was a substantial heat loss from vessel upper containing the water pool as it was not insulated.

The temperature history in central region and half radius region is given in Figure 2.31 and Figure 2.32. It was observed that, temperatures in both these regions showed similar trend and there was very little stratification in the radial direction. Using these temperatures, contours of temperatures were plotted in 2-D axi-symmetrical geometry. Figure 2.35 shows the experimental contours at different times (after completion of pouring)

The melt surface is clearly indicated by yellow coloured contour which is at 390 mm level. Water is added after 60 s. It can be seen that, when water is added, within 60 s (at 120 s), the yellow contour drops down by about 10 mm as a result of water ingression. Thereafter, cooling takes place slowly because of conduction. Heat loss was taking place from one side at the bottom right corner as well as from entire bottom showing faster temperature drop as compared to the centre portion of the test section.

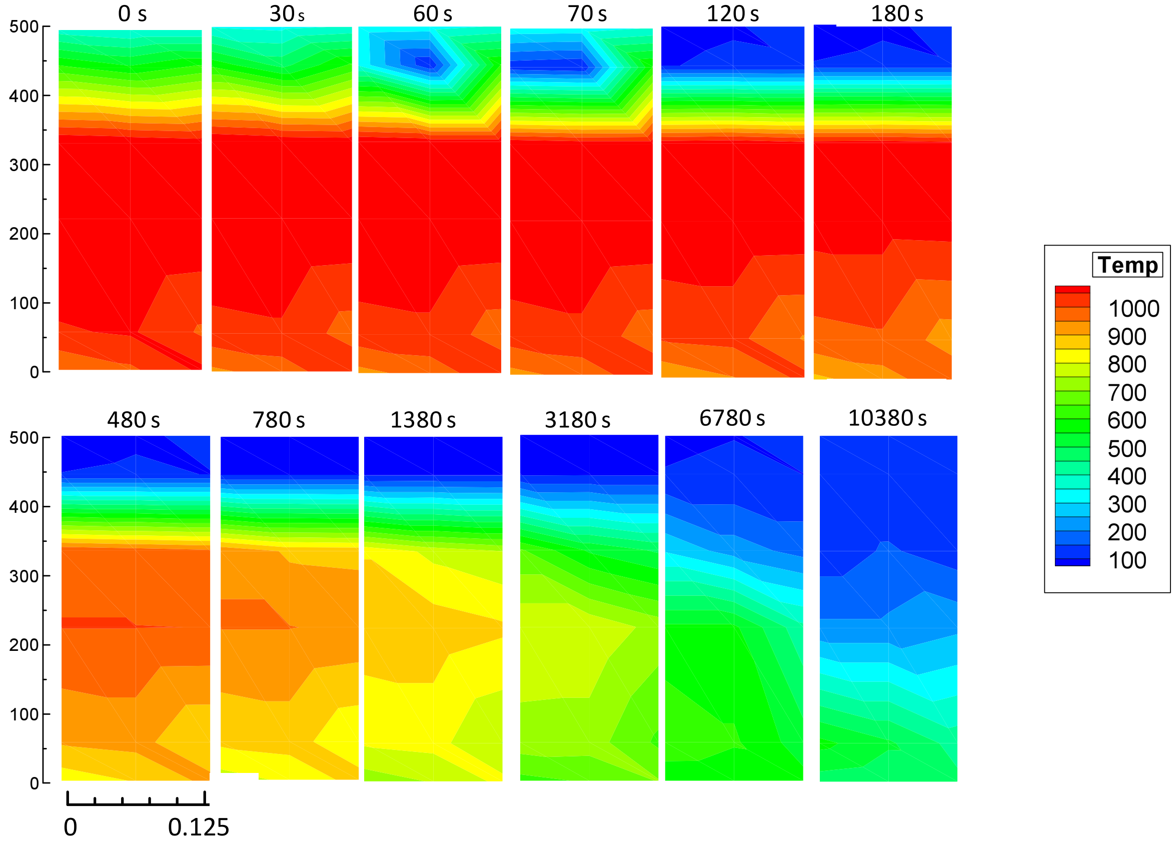

Figure 2.35 Temperature contours at different times inside the melt

2.6.5 Post-test examination

After the experiment was completed, the upper part of the setup was removed and the solidified glass was inspected. Figure 2.36 shows the fractured surface of the glass and the size distribution of the debris material. From Figure 2.36, it can be seen that, the top surface of the crust has fractured and formed a debris bed. The encircled part shows the site where water ingression has occurred. It was observed that, water ingression has occurred up to a depth of 10 mm from surface. The size of debris particles ranged from 0.5 mm to 10 mm.

Figure 2.36 Fractured surface of the glass and size of the particles forming debris

2.7 Validation of model with experimental data:

Our model was used to simulate the experimental data using glass. The glass thermophysical properties were updated in the code. The experimental and predicted temperatures at different locations inside the pool are shown in Figure 2.38 -Figure 2.40

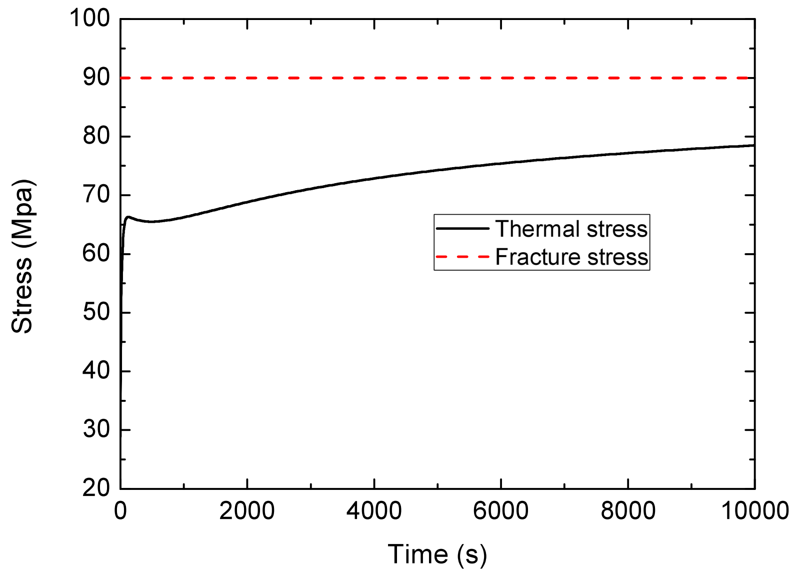

Figure 2.37. Stresses in the glass crust

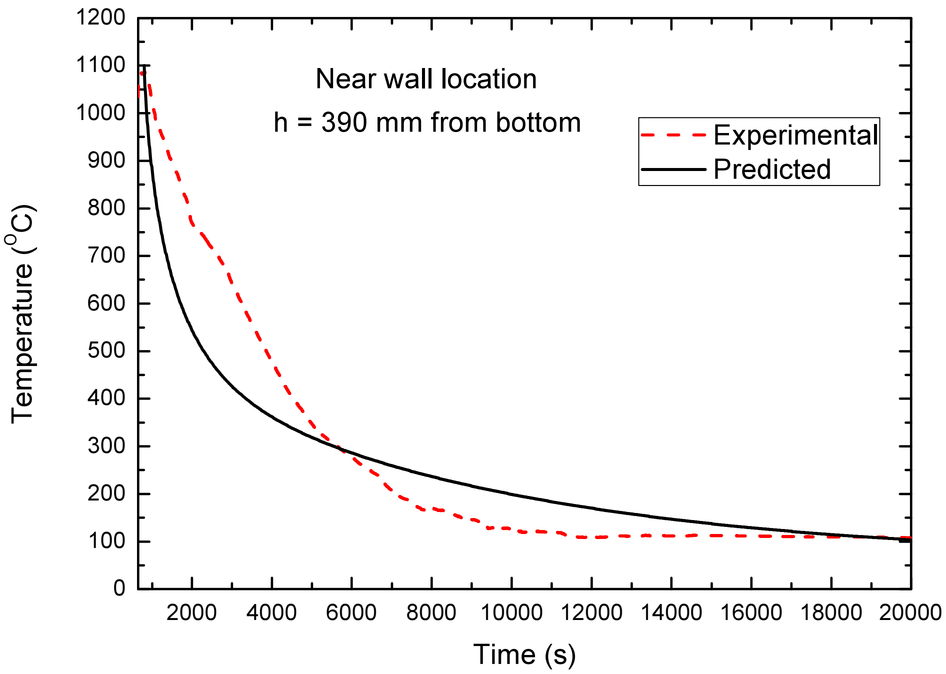

Figure 2.38 Experimental Temperatures in the top region

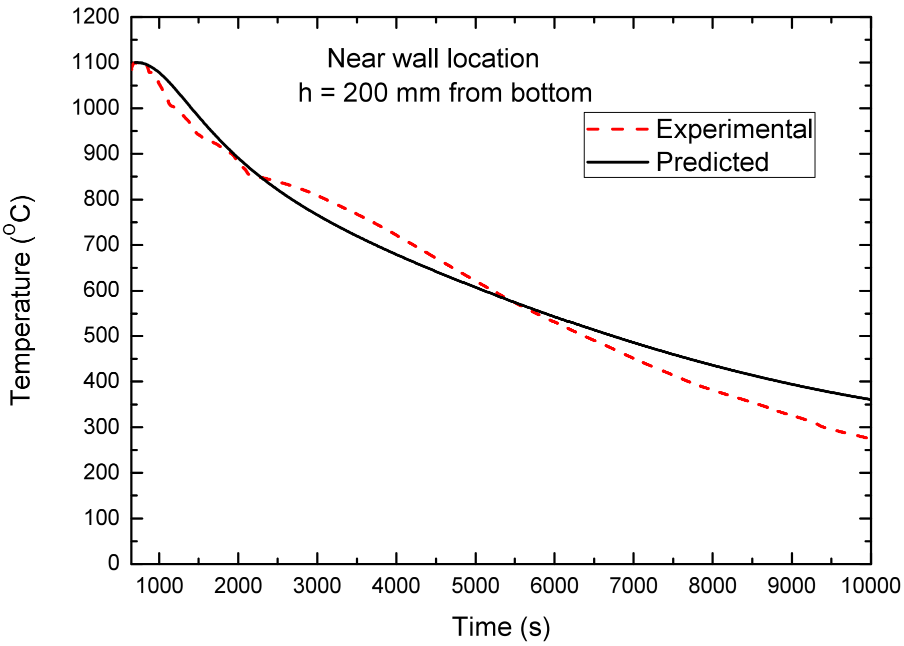

Figure 2.39 Predicted temperatures in the centre of the pool

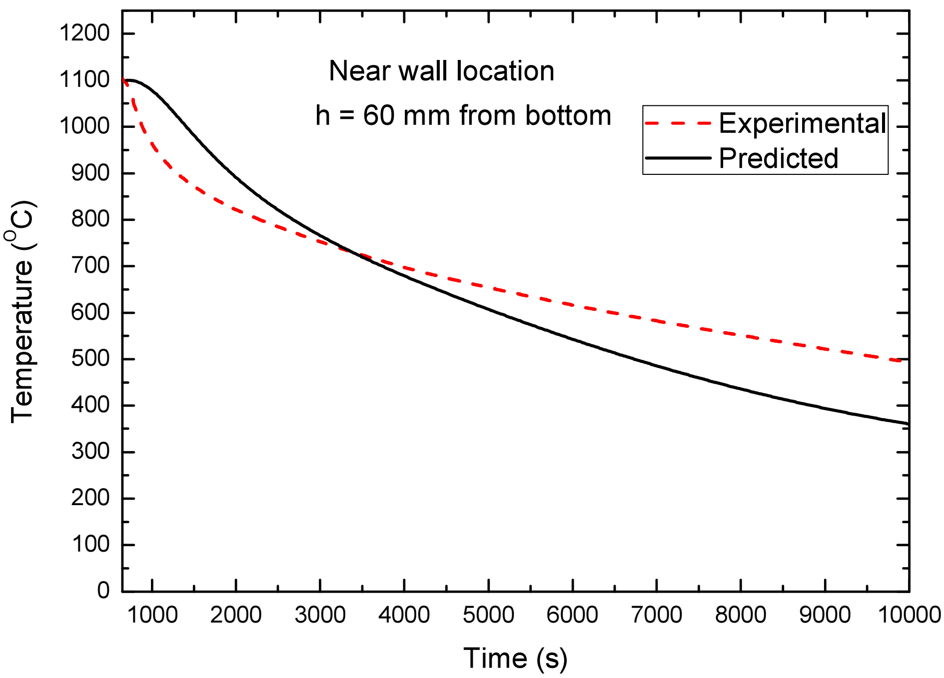

Figure 2.40 Experimental Temperatures at the bottom of the pool

It was observed that, the thermal stresses never exceed the strength of the glass as shown in Figure 2.37. Hence the model does not predict any water ingression inside the glass. In experiment, only 10 mm water ingression was observed. This could also be due to vigorous thermal interaction at the glass surface causing the melt to splash at the top and form debris. It can be seen that the model is able to predict the temperatures quite accurately. The maximum error is 33 % and average RMS error is 6 %. The difference arises because there may be variation in the actual heat transfer coefficient as well as the properties variation with temperature than what was considered in the model. Nonetheless the physics has been captures by the model. Also, the model is able to predict the temperatures with different materials also.

2.8 Summary

In this chapter, studies were carried out to investigate the water ingression phenomena in melt pool coolability. Postulations of melt pool coolability were carried out and a numerical model for melt coolability under top flooding was developed. The model considers the heat transfer behaviour in axial and radial directions from the molten pool to the overlaying water, crust generation and growth, thermal stresses built-in the crust, disintegration of crust into debris, natural convection heat transfer in debris and water ingression into the debris bed. The model was first validated with experimental data from COMECO experiments. The model was found to simulate the quenching behaviour and depth of water ingression in good agreement.

Later on, effect of MCCI on the change in properties of corium and subsequently on the coolability of the corium was explored. It has been found that, the coolability is influenced by a dimensionless parameter $E\alpha/\sigma$ called as "Crust Break Parameter". Higher is the parameter, better is the coolability.

In order to gain better understanding of coolability of molten pool under top flooding condition and to generate sufficient experimental data for validation of top flooding model using simulant material of which the thermo-mechanical properties are well known, experiment on melt coolability under top flooding was carried out. A simulant material (sodium borosilicate glass) of about 20 litres at a temperature 1200 ^{o}C was poured into the test section and it was flooded from top with water. The experiment highlighted that, under adiabatic conditions also, water ingression occurred only upto 10 mm depth, below which a stable solid crust was formed which limited the heat transfer. Also, it was observed that, no gap between crust and vessel was formed which could assist the ingression of water from sideways to the bottom of the melt to enhance coolability. It took very long time to cool the melt which highlights that; top flooding is insufficient to quench the molten pool in case of severe accidents.

3. Melt coolability under bottom flooding condition

3.1 Introduction

Experimental as well as theoretical investigation on top flooding corroborated the fact that, top flooding is not a reliable strategy to achieve complete coolability in case of core melt accidents. The question still remains is, whether there exists any better core cooling strategy which can effectively quench the melt completely in stipulated time?

Very few small scale experiments like COMET [14] and DECOBI [20-21] hinted at much better coolability under bottom flooding. In the COMET scheme, molten corium material spreads onto a layer of sacrificial concrete material located in the containment cavity, erodes this layer and finally reaches a matrix of plastic water injectors buried in this layer. Upon contact with the molten core material, the plastic plugs melt and water is injected into the molten corium. The driving water pressure is due to the location of the water reservoir above the containment cavity. In the COMET experiments, the melt was found to quench in a relatively short time, to a porous, easily penetrable debris, with continued access of water to the regions of the solidified debris. The DECOBI program addressed the issue of the ex-vessel debris coolability by bottom injection, with the objective to understand and model the processes of porosity formation and coolability observed in the COMET experimental program. However, the observations could not explain how the bottom flooding has better potential to cool the melt. Also in DECOBI, the melt depth was too small to conclude that bottom flooding is more effective than in top flooding. Paladino et al [41] and Widmann et al [22] attempted modeling of melt coolability under bottom flooding, but their focus was to predict the porosity of the melts formed during bottom injection and its effect on coolability. To our knowledge, no attempt is made yet to model entire phenomenology of bottom flooding, which is very essential in order to carry out design, validation and optimization of core catchers for nuclear reactors.

A more detailed model on melt coolability under bottom flooding has been presented in this chapter. The model has been tested with the data on DECOBI and found to predict reasonably well. Subsequently, experiments were carried out under bottom flooding condition with borosilicate glass as the melt at a temperature of 1200 ^{O}C. About 20 liters of melt having a depth of 300 mm was flooded with water from bottom. The amount of melt and the depth was more or less same as that compared to top flooding case presented in earlier chapter so that comparison can be made. The model was used to compare the test data for the melt temperatures during the bottom flooding test.

3.2 Model development on melt coolability under bottom flooding

3.2.1 Postulation of melt coolability under bottom flooding

In bottom flooding, the melt is allowed to fall on a porous surface so as to allow the water to be fed from bottom through some nozzles. Mostly, passive means are used to allow water flooding [24] where water is fed from gravity driven water tank. At the melt water interface, a sacrificial material is placed. When the melt falls on the sacrificial surface, it gets ablated and the water is then forced upwards by gravity. In some cases like COMET [14], the melt falls on the porous material itself and then water is fed through the porous material. In the present model, this situation is considered where the melt falls on the porous material and then water is fed from bottom at fixed rate. We postulate that, when melt falls on the porous material, it starts getting cooled and a thin crust starts getting formed. When water supply is continued, water reaches the melt from below and starts further cooling the melt and the crust starts growing. As a result of heat transfer from melt to the water, steam starts getting formed and it expands in volume which exerts back-pressure to water. As a result, steam pressure builds up in the area below the melt crust. Hence, the crust is subjected to stresses mainly because of the water and steam pressure on one side, hydrostatic head of melt pool on the other side and thermal stresses as a result of temperature gradient across the thickness. When the stresses in the crust exceed the fracture stress, the crust breaks resulting in debris formation. The steam passes through the debris continuously pressurizing it, which ultimately causes eruption at selected sites. As a result of eruption, the steam escapes through the melt cooling it instantly and forming porous passage. The erupted melt forms debris like structure on the top of the melt. The eruption sites act as passage for water and steam which brings about a multi-dimensional coolability.

Based on this phenomenology, an integrated model has been developed for each phenomenon taking place as postulated above. Figure 3.1a-d show the phenomenology of the melt coolability under bottom flooding. Figure 3.1a shows the scheme for bottom flooding. In Figure 3.1b, thin crust generation and steam pressure built-up is depicted. When the pressure exceeds the fracture stress, the crust breaks and porous zone is formed and ultimately, melt eruption occurs (Figure 3.1c). As a result of melt eruption, the coolability is enhanced as shown in Figure 3.1d. Based on these phenomena, models are developed for each phenomenon.

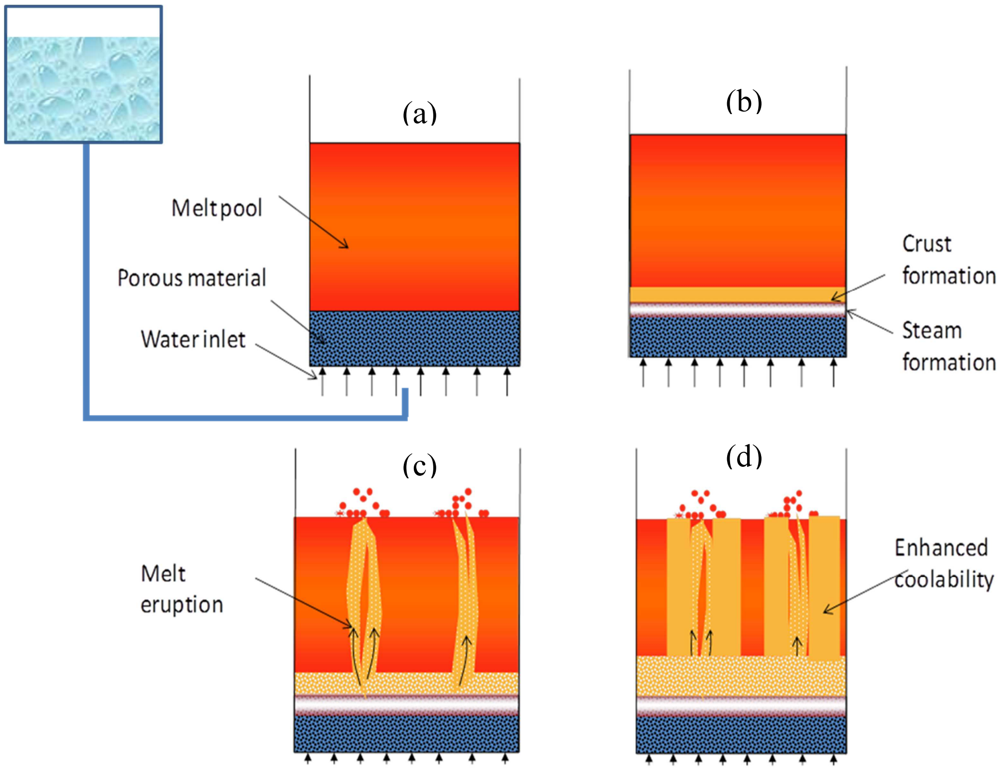

Figure 3.1Phenomenology of melt coolability under bottom flooding

3.2.2 Governing equations

(i) Governing equations for molten pool

In molten pool, it is assumed that the dominant mode of heat transfer is due to conduction only. With this, the transient 2-D axi-symmetric heat conduction equation can be written as

$$\rho C_p \frac{\partial T}{\partial t} = \frac{1}{r}\frac{\partial}{\partial r} r(k\frac{\partial T}{\partial r}) + k\frac{\partial^2 T}{\partial z^2} + q''' \qquad (3.1)$$

Similarly, the in crust layer, conduction equation is given as

$$\rho C_p \frac{\partial T}{\partial t} = \frac{1}{r}\frac{\partial}{\partial r} r(k\frac{\partial T}{\partial r}) + k\frac{\partial^2 T}{\partial z^2} + q''' \qquad (3.2)$$

The boundary conditions for the above equations are given in Figure 3.2. At the top, heat loss from radiation is considered. The Emissivity of corium is 0.87 as reported in IAEA TECDOC 1496.

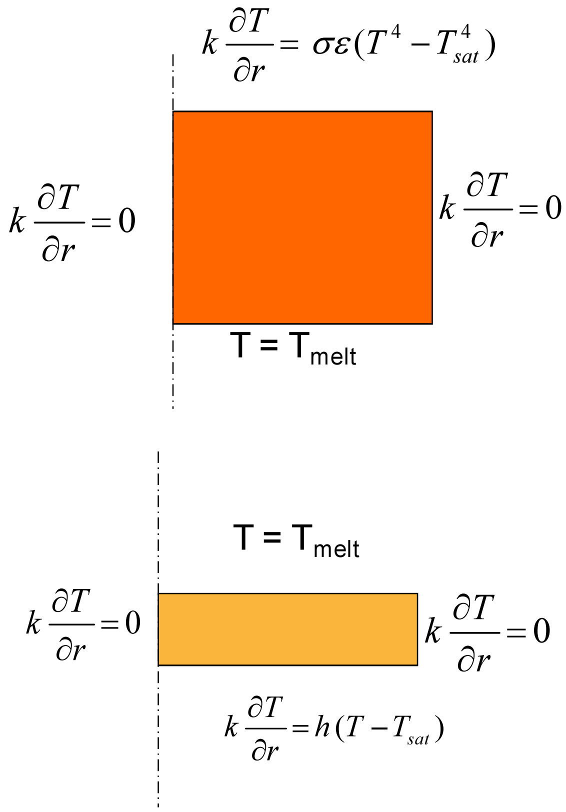

Figure 3.2 Boundary conditions for melt and crust layer

(ii) Equation in porous zone:

– Velocity is predicted by Darcy equation

$$v = -\frac{dp}{dz}\frac{\kappa}{\mu} \tag{3.3}$$

Rate of vaporization is given as

$$\Gamma = \frac{V \cdot A \cdot \rho \cdot (h_{in} - h_{fs}) + h \cdot A \cdot (T_{melt} - T_{sat})}{h_{fg}} \tag{3.4}$$

Steam generated in a given time

$$M_{st} = \Gamma \cdot dt \tag{3.5}$$

Specific volume of the steam ϑ

$$\vartheta = M_{st} / V_p \tag{3.6}$$

From equation of state, the pressure developed is calculated as

$$p = f(\vartheta) \tag{3.7}$$

(iii) Stresses in the crust:

The crust is subjected to stresses as shown in Figure 3.3.

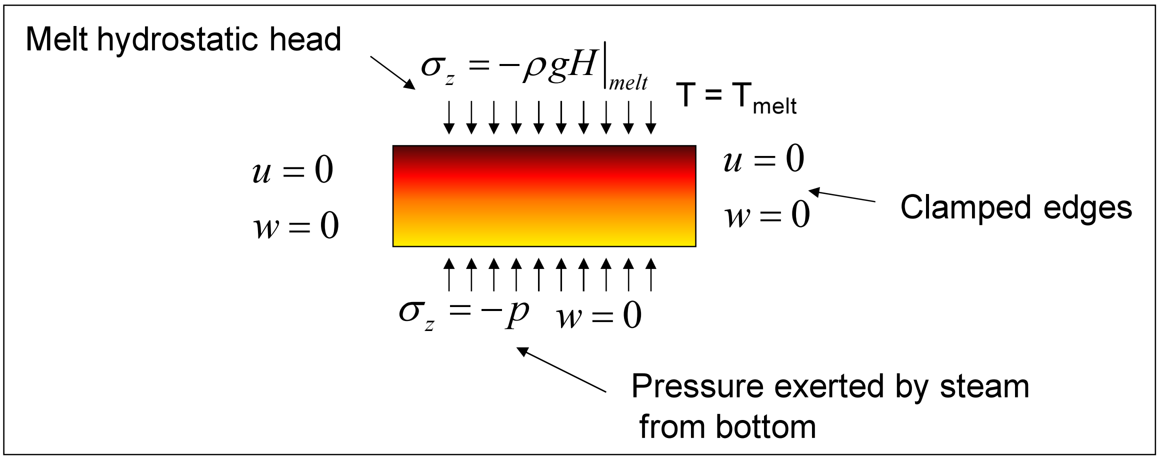

Figure 3.3 Stresses in the crust

At the top of the melt, there is hydrostatic head and at the bottom, the pressure exerted by the steam. In addition to this, the top edge of the crust is at melting temperature whereas, the bottom end is at much lower temperature. This exerts thermal as well as mechanical stresses. The bending stresses on the circular plate type crust as a result of clamped edges are given as [54]

$$\sigma_b = 0.75 \cdot \frac{(\Delta p \cdot r^2)}{t_{cr}^2} \tag{3.8}$$

The thermal stresses as a result of temperature gradient are given as

$$\sigma_{th} = \frac{\alpha \cdot \Delta T \cdot E}{2(1-\nu)} \tag{3.9}$$

Since the total strain is additive and the material, being brittle, remains in elastic region. Hence, we can add the individual stresses to obtain the total maximum stress acting on the crust as

$$\sigma_{tot} = \sigma_{th} + \sigma_b \tag{3.10}$$

The crust will break if the total stress exceeds the strength of the crust i.e.

$$\sigma_{tot} > \sigma_{\max} \tag{3.11}$$

After the crust is broken, melt eruption takes place at certain locations. The location of melt eruption sites is random in nature and it is involves certain empiricism to predict the exact location of eruption sites. However we can estimate the distribution of the sites in the entire area. Paladino et al [36] has developed an empirical model for density of the openings and their diameter. The average number of channels is given as

$$\Psi = \frac{\Gamma[Cp_w.\Delta T_{sub} + h_{fg} + Cp_{st}.\Delta T_{\sup}]_c}{h_{pool} \cdot A_{ch} \cdot N_n \cdot \overline{\Delta T_{m,w}}} \tag{3.12}$$

Where, $\overline{\Delta T_{m,w}}$ is average temperature drop between melt and water

The above parameter is a measure of heat transfer enhancement due to formation of small porous openings which enhance the area available for heat transfer.

The average density of channels per unit area can be given as

$$\gamma = \frac{1}{\xi^2} \tag{3.13}$$

Where ξ is the spacing between the channels given by Zubers' [55] modified Critical Taylor Wavelength formula as

$$\xi = 2\pi\sqrt{\frac{\sigma_{mc}}{(\rho_m - \rho_{st})g}} \tag{3.14}$$

The diameter of the eruption area is given as

$$d = 2\sqrt{\frac{\psi}{\gamma\pi}} \tag{3.15}$$

The resulting porosity is given as:

$$\varepsilon = \frac{\Psi \cdot \pi \cdot D_n^2 \cdot h_{pool}}{\pi \cdot L_b^2 \cdot h_{pool}} \tag{3.16}$$

Once the crust is broken, the melt layer is considered to be made of 2 zones, mainly porous zone and non porous zone. We know the diameter, porosity and the number of openings. We can predict the coolability by modifying the initial domain and governing equations. The equation for porous medium is modified as

$$\rho_{eff} C_{p,eff} \frac{\partial T}{\partial t} + v \frac{\partial T}{\partial y} = \frac{1}{r}\frac{\partial}{\partial r} r(k_{eff} \frac{\partial T}{\partial r}) + k_{eff} \frac{\partial^2 T}{\partial z^2} + q''' \tag{3.17}$$

Where v is the velocity of steam flowing through the bed calculated using equation (3.3) and the flow rate which is kept fixed during bottom injection. The effective properties are volume averaged over the void fraction in bed with boundary conditions as

$$k_{eff} \frac{\partial T}{\partial z} = h(T - T_{\infty}) \tag{3.18}$$

where, h is evaluated from surface temperature based on heat transfer regime i.e. film boiling or nucleate boiling. For film boiling, Berenson's [49] model is used and for nucleate boiling, Rohsenow [50] correlation is used.

For the solid zone, the boundary conditions are modified as shown in Figure 3.4. In addition to top and bottom, now the span of the solid zone has reduced and additional convective boundary condition at one side has been introduced which makes it coolable from two dimensions.

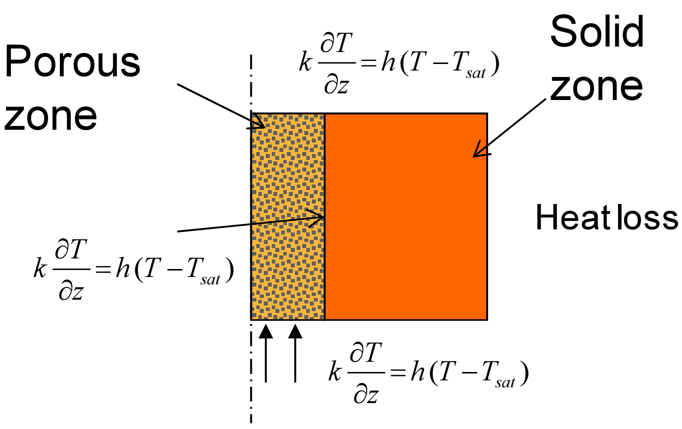

Figure 3.4 Modified boundary conditions for the domain

3.2.3 Solution procedure:

The governing equations in melt pool and solid crust region are discretized using finite difference method and solved implicitly using Gauss-Siedel iterative method to obtain temperature distribution in the melt pool. After evaluating the temperatures, the crust growth rate is calculated and subsequently the thickness of the solid crust region is updated. After the temperature distribution has been obtained, the stresses are calculated. With the stresses, the fracture conditions are evaluated. When the crust breaks, it is considered to be a porous zone with calculated porosity and number of eruption sites and diameter of eruption sites are calculated. After that, the domain is modified and the equations for porous zone and solid zones are recalculated using modified governing equations using similar technique.

3.3 Validation of the model:

To validate the model, experimental data from DECOBI tests was used [41]. The details of the tests are as given in
Table 3.1.

Table 3.1. Details of DECOBI CB14 tests

Simulant Material	$CaO\text{-}B_2O_3$
Volume	6 lit
Melt height	14.2 cm
Melt Temperature	1400 K
Water injection rate	0.014 kg/s
Inlet temperature	27 deg C
Decay heat	Not simulated

The temperature history in the porous zone above the nozzle and in the solid zone was reported. Figure 3.5 shows the experimental and predicted temperature history. The predicted and actual pressure history is given in Figure 3.6.Table 3.2 gives the other predicted parameters.

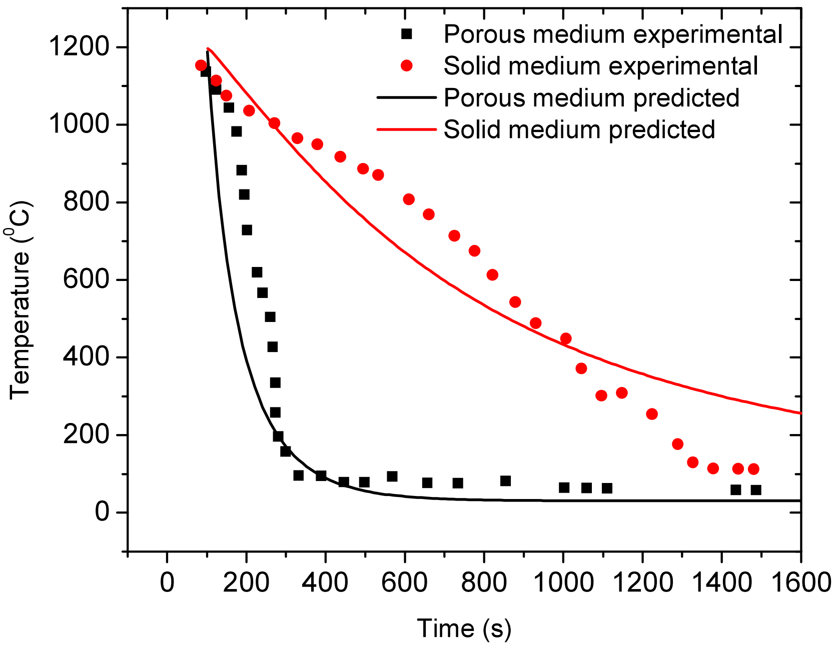

Figure 3.5 Validation of bottom flooding model

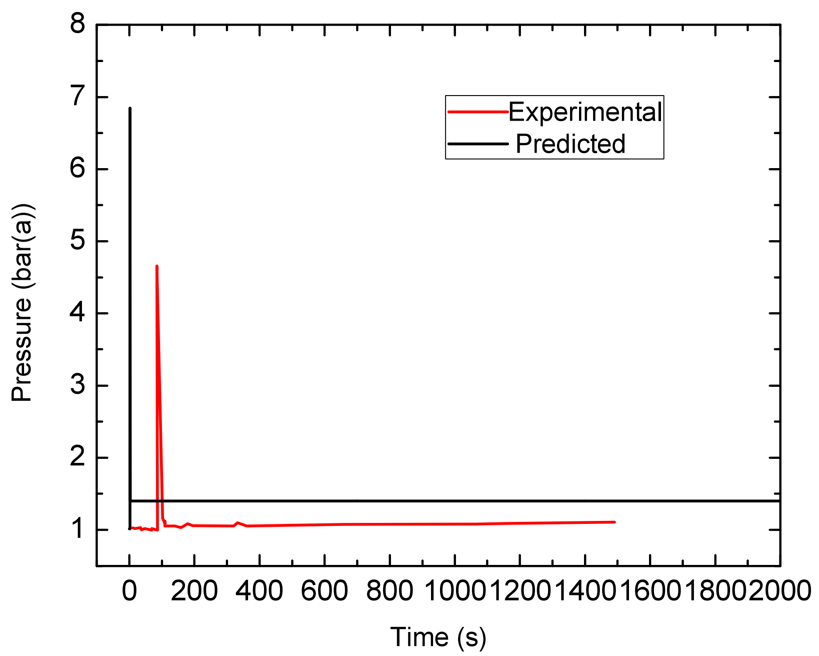

Figure 3.6 Experimental and predicted pressure

Table 3.2. Predicted parameters

Parameter	Experimental	Predicted
Diameter of eruption zone	6 cm	7.2 cm
Maximum pressure pulse	3.7 bar(g)	5.8 bar(g)

It is observed that, the model predicts the temperature history quite well. The diameter of opening is also closer to actual. The trend of pressurization is also captured well. The mismatch in maximum pressure is due to lack of availability of free volume of experimental system.

3.4 Top flooding vis-à-vis bottom flooding.

Since we have a model that can predict the coolability under bottom flooding, it would be very interesting to compare coolability under bottom flooding with top flooding for same melt conditions. For this, a numerical exercise was carried out on COMECO experiments [14]. The experiment was carried out for top flooding and the experimental data was available. Using the similar melt condition, its coolability was predicted under bottom flooding. The details of the test are given in Table 3.3.

Table 3.3 Details of COMECO experiment.

Simulant Material	$CaO\text{-}B_2O_3$
Volume	14 lit

Melt height	30 cm
Melt Temperature	1250 deg C
Decay heat	1 MW/m^3

Similar conditions were considered for bottom flooding and rate of injection of 0.01 kg/s was arbitrarily selected. The experimental and predicted results are shown in Figure 3.7 -Figure 3.9

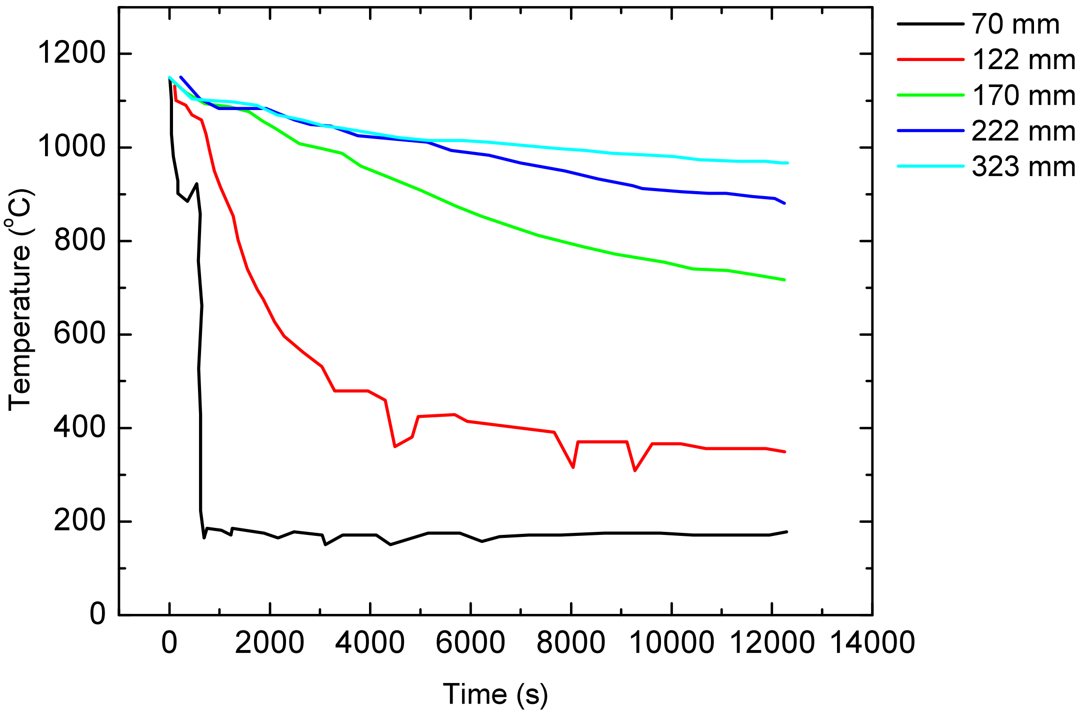

Figure 3.7 Experimental temperature history of COMECO test under top flooding

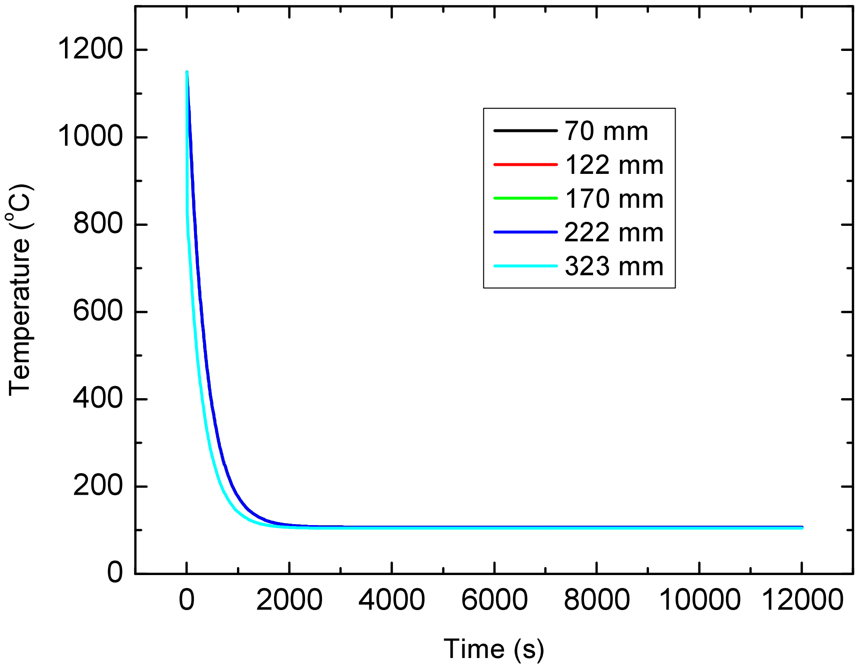

Figure 3.8 Predicted temperatures with bottom flooding in porous zone

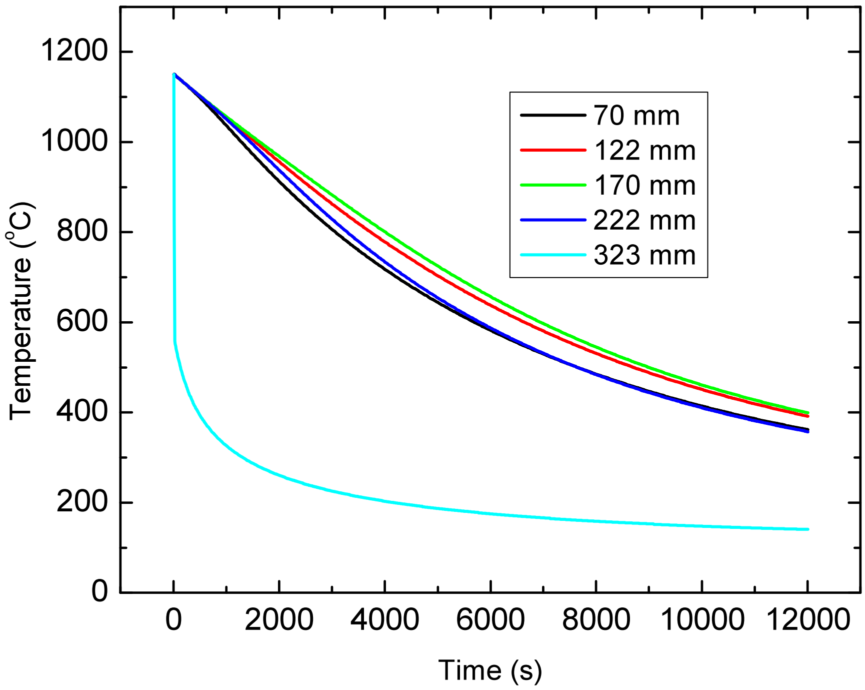

Figure 3.9 Predicted temperatures in solid zone under bottom flooding

As described earlier, after the melt eruption takes place, there are two zones formed in the pool, namely porous zone and solid zone. The porous zone gets quenched within 2000 s.

Hence, as compared top flooding, the coolability is much more enhanced under bottom flooding because of formation of porous zone. In remaining solid zone also, as seen in Figure 3.9, the bottom part gets quenched immediately (323 mm from surface) and temperatures at other locations are quite lower than that of top flooding as seen in Figure 3.7, where, below 170 mm from surface, there was no coolability due to high decay heat and low conductivity. If, we could achieve maximum size of porous zone, the extent of coolability will be much higher.

3.5 Prediction of coolability under bottom flooding condition

Figure 3.10 shows the contours of temperature in the pool to depict the progression of coolability with time for the bottom flooding. It is seen that, within few seconds crust is formed (Figure 3.10a). After 5 s the crust breaks forming two opening in the melt pool (Figure 3.10b). This results in formation of porous zone in between the openings as the water and steam erupt through the melt (Figure 3.10c). The porous zone gets cooled very fast (Figure 3.10d). In solid zones, the coolability progresses slowly (Figure 3.10e-f) but overall coolability is enhanced substantially as compared to top flooding.

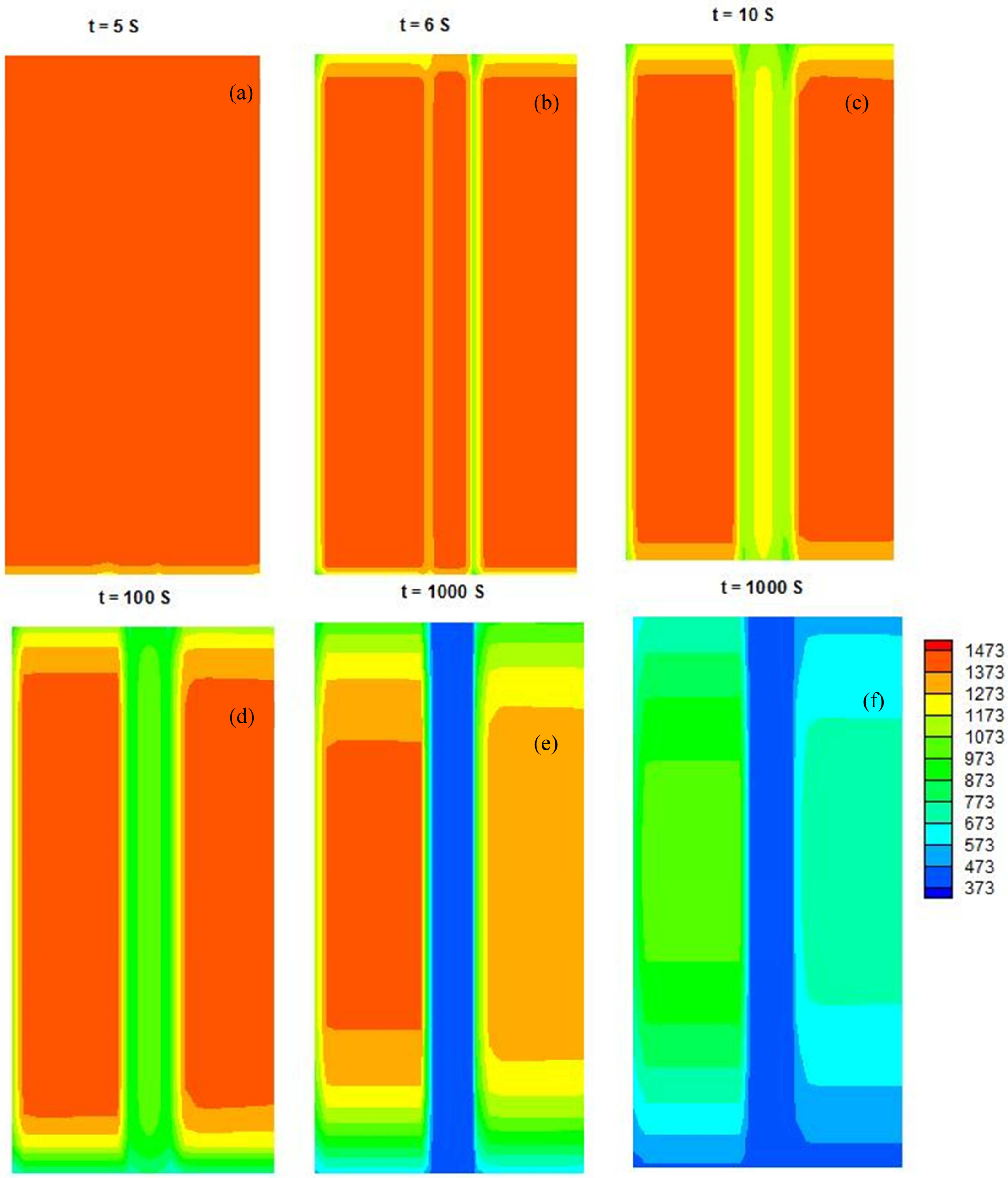

Figure 3.10 Progression of coolability under bottom flooding

3.6 Melt coolability experiment under bottom flooding

In comparison of model prediction with DECOBI experimental data, there were some differences in parameters like pressure generated at the bottom, porosity formed etc. This was because the properties of the simulant material and the exact geometrical data of the test section were not reported. In addition, the depth of melt was very small.

As explained earlier, the core melt forms a glassy mixture at the ex-vessel condition [4]. In order to validate the bottom flooding model with more precision, an experiment on melt coolability under bottom flooding was carried out using sodium borosilicate glass whose properties are well known.

3.6.1 Experimental Setup

The experiment was carried out in the test setup similar to that of top flooding with some modifications (Figure 3.11). The test section consists of a 300 mm OD carbon steel pipe with 600 mm height. The capacity of test section is about 25 liters corresponding to melt height of 500 mm. The upper part of test section can contain water pool up to 700 mm height. Steam outlet and water inlet have been provided in the upper part of the test section. At the bottom, an inlet nozzle having water distributor was provided. The water distributer was covered with 100 mm height sand bed. On the top of the bed, a plate having six nozzles of different heights was placed (Figure 3.12Figure 3.13). Each nozzle was a 12 mm OD SS tube with 0.6 mm wall thickness. The nozzles had an Aluminium strip at the top and were filled with porous medium so that when melt falls on the nozzle, the Aluminium strip will take some time to melt and the melt will not penetrate the nozzle till entire amount of the melt has been poured. Water was fed through an overhead tank under gravity flow. An additional safety steam line was provided at the bottom to relieve the overpressure. Total 24 K type Inconel sheathed 1 mm thermocouples were inserted in the test 8 axial and 3 radial positions. In addition, inlet water temperatures and temperature of outgoing steam were also measured by thermocouples in the upper part of test section. The test section was insulated in lower part using ceramic wool. Water was drawn from gravity tank at 1.2 bar head. A 2 ½" steam line was provided in the upper part of the test section which was released to atmosphere. In addition to the main steam line, a safety steam line was provided at the bottom of the test section in order to avoid over-pressurization of the test section. A relief valve and a rupture disc were provided in parallel in safety steam line

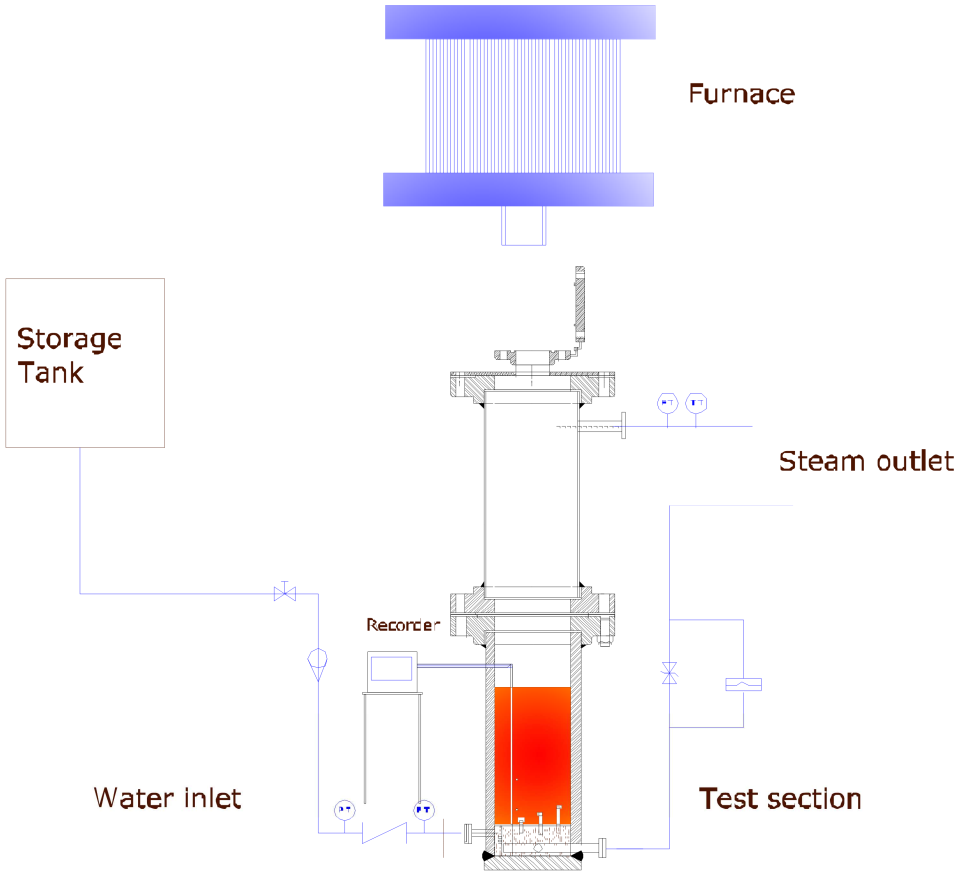

Figure 3.11 Schematic of the bottom flooding experimental setup

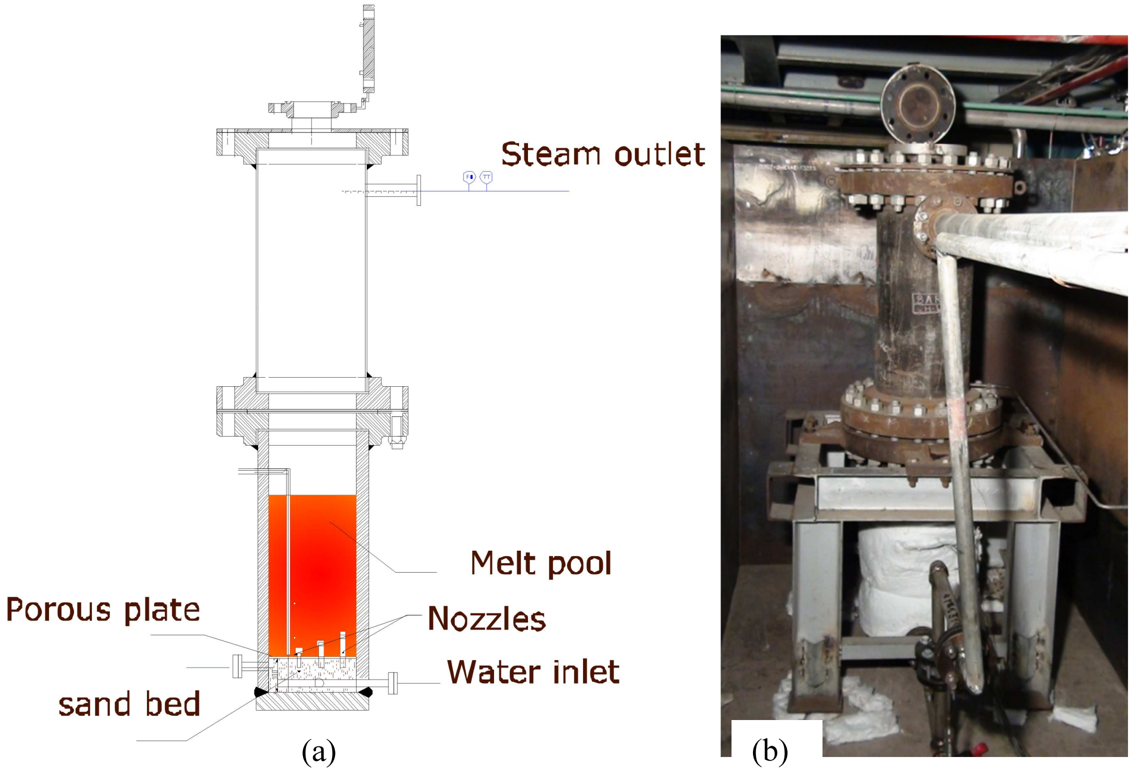

Figure 3.12 Bottom flooding test section (schematic and actual)

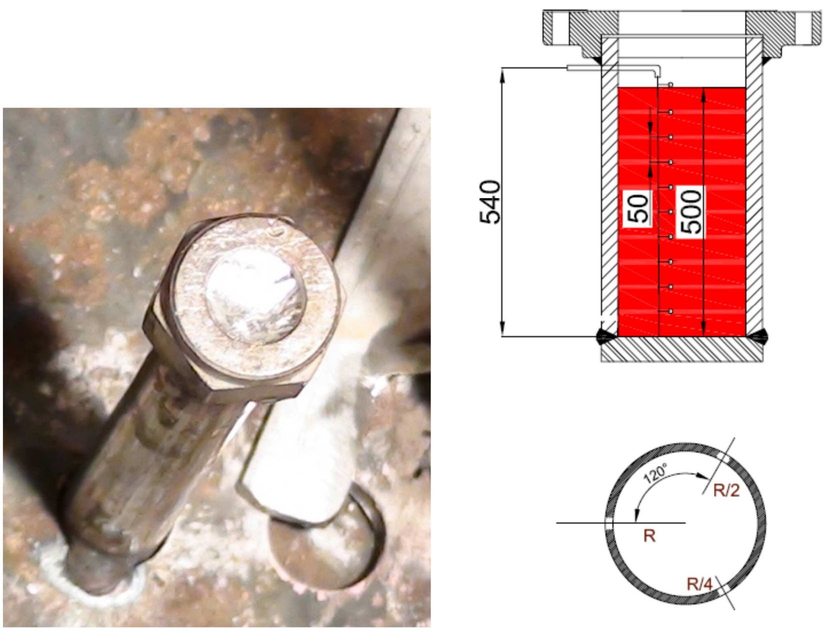

Figure 3.13 Nozzle used in the experiment and location of thermocouples

Table 3.4 Accuracy of measurement

Parameter	Accuracy	Range
Temperature	$\pm$ 0.75% of measured value	0-1200 ^{O}C
Pressure	$\pm$ 0.35% of measured value	0-100 bar
Differential Pressure	$\pm$ 0.2 % of the measured value	0-1500 mmWC
Water level	$\pm$ 0.2% of the measured value	0-1000 mm

3.6.2 Experimental procedure.

In this experiment, the melt was generated in the furnace in similar fashion. Once the desired temperature was reached, molten glass was poured in the test section and after pouring, the top flange was closed and water at 1.2 bar head was fed from bottom by opening the inlet valve, through the nozzles which injected water inside the melt at different heights of 20, 50 and 100 mm from bottom.

3.6.3 Results and discussion

After the water supply was started, within few seconds, large amount of steam was seen coming out of the discharge line. Within few minutes, most of the thermocouples showed saturation temperature indicating complete quenching. Water supply was stopped when the level in the upper part of the test section showed 100 % mark. Figure 3.14Figure 3.15 show the temperatures in the central region, and Figure 3.16Figure 3.17 show temperatures near wall and Figure 3.18Figure 3.19 show temperatures in half radius region.

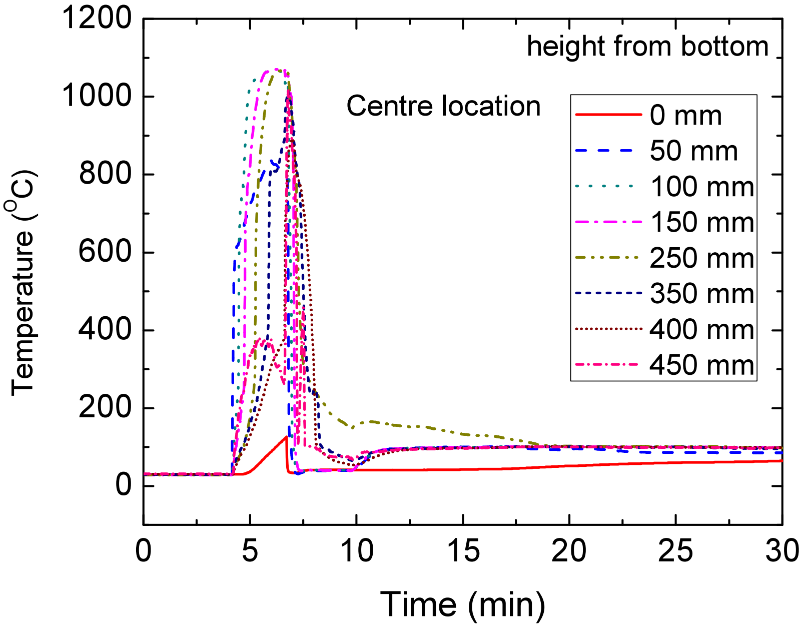

Figure 3.14. Temperatures at the center of the pool

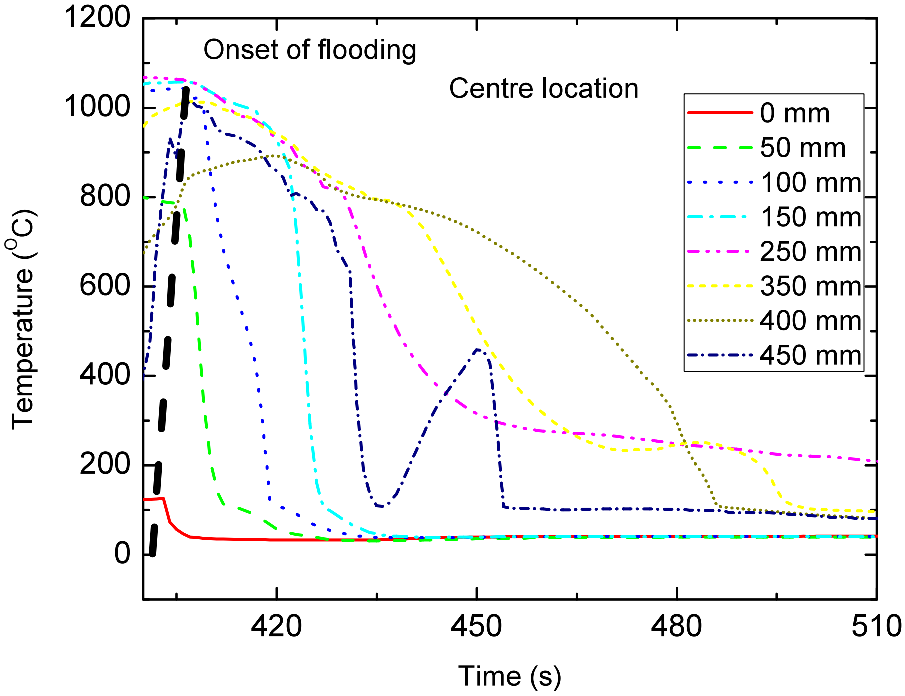

Figure 3.15. Temperatures just after flooding

The dotted line in Figure 3.15 represents the onset of flooding at each elevation which indicates the time at which the flooding takes place at each location. For example, flooding is first observed in thermocouple at 0 mm from bottom at around 400 s. This thermocouple is located inside the debris below the melt. Hence, the temperature at that location is low and as soon as water supply was started, this thermocouple shows ambient temperature. However, the next thermocouple at 50 mm from bottom is located inside melt and shows flooding after a delay of about 10 s (at 410 s). This time delay may be attributed to the time taken for steam formation, pressurization, crust formation and crust breakage. After eruption takes place, thermocouples at location 50, 100 and 150 mm get quenched rapidly. The thermocouple at 350, 400 and 450 mm location from bottom are above the melt. Hence, they show increase in temperature after the eruption has taken place and melt rises to the height of the thermocouples due to formation of porosity. The thermocouple at 450 mm location even shows a momentary dip before showing another outburst of melt indicating multiple eruptions. But after 90 s, all the thermocouple show ambient temperature indicating complete quenching.

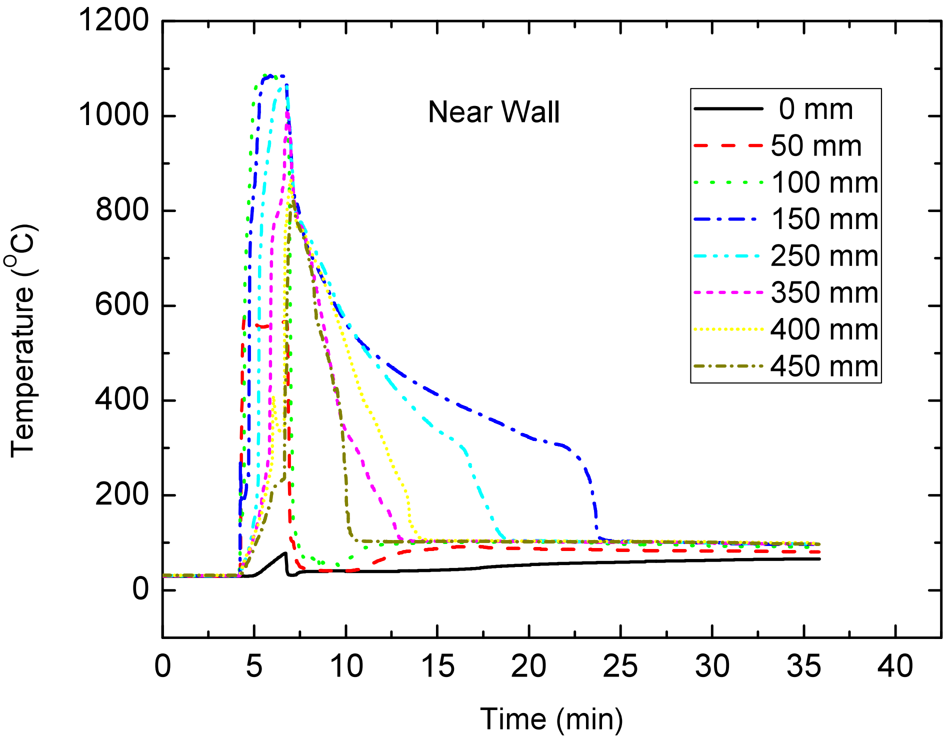

Figure 3.16. Temperatures near wall region

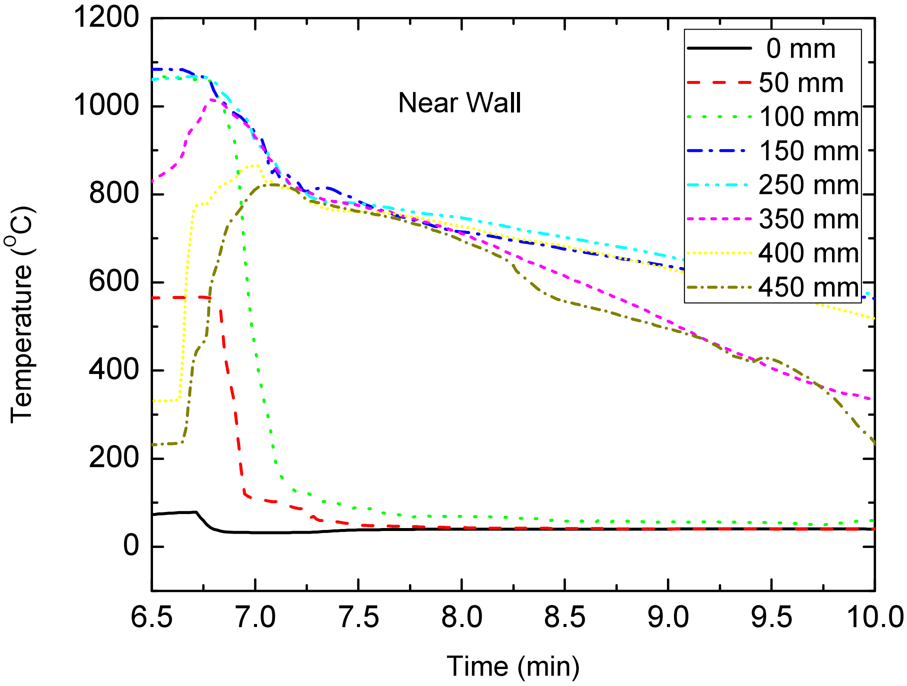

Figure 3.17 Temperatures just after flooding

Figure 3.17 shows temperature at near wall location. It can be seen that, thermocouples at 50 and 100 mm show complete quenching at the onset of flooding. However, at 150 and 250 mm location, coolability is a bit slow indicating eruption has taken place at center and a solid non porous zone is remaining at the wall with conduction dominated zone. Again, temperatures at 350, 400 and 450 mm location show faster coolability indicating that the melt has risen up with uniform porosity all along the diameter of the vessel and got quenched within short time.

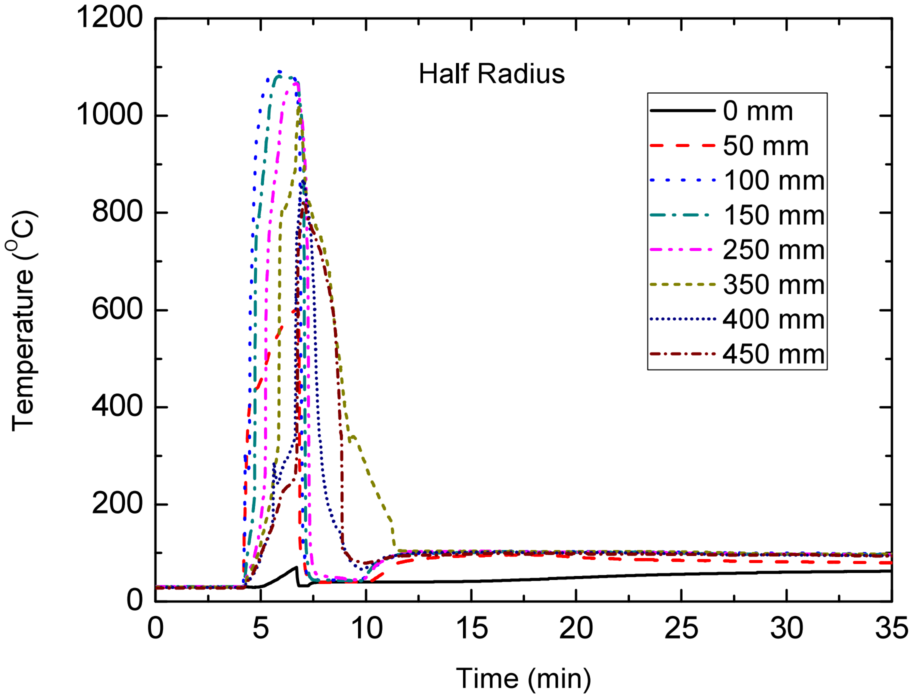

Figure 3.18. Temperature in half radius distance

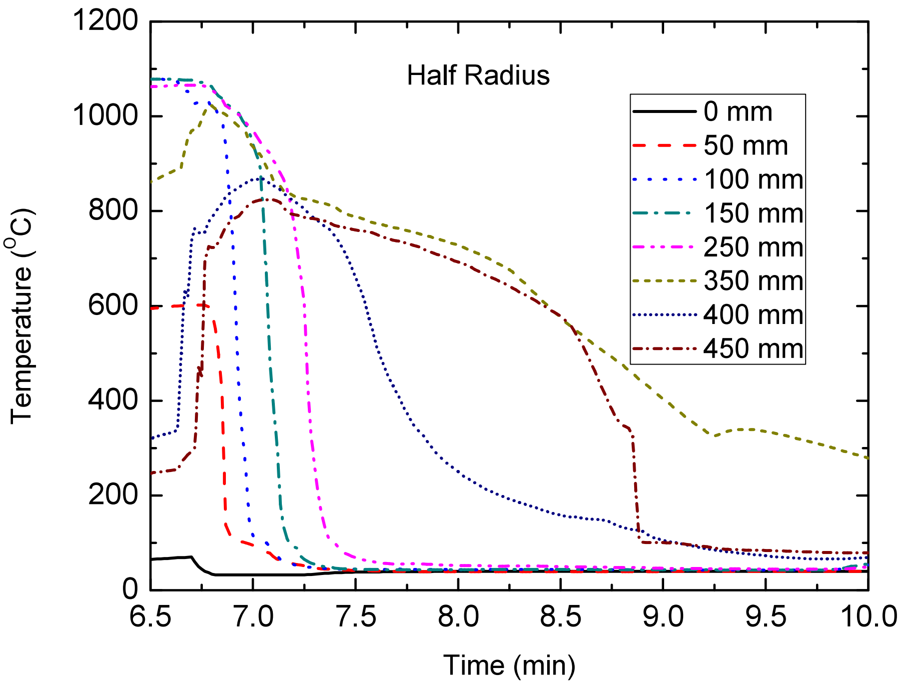

Figure 3.19. Temperatures just after flooding

The steam outlet temperature is shown in Figure 3.20. It can be seen that, the temperature has rose to as high as 750 ^{O}C indicating the superheated steam going out. There may also be possibility of entrainment of molten glass particles into the steam line which might have caused such high temperature. Figure 3.21 shows the pressure at the bottom of the test section. Just before the eruption, a peak pressure of 0.37 bar(g) was observed which led to steam eruption through the melt. Subsequent to the eruption, the pressure reduced to the ambient indicating that the water passed through the melt continuously. After that, there was a gradual increase in pressure indicating the continuous increase of water level inside the vessel. When the level reached the mark and water supply was stopped, the pressure also showed steady reading corresponding to the hydrostatic head of the water inside the vessel.

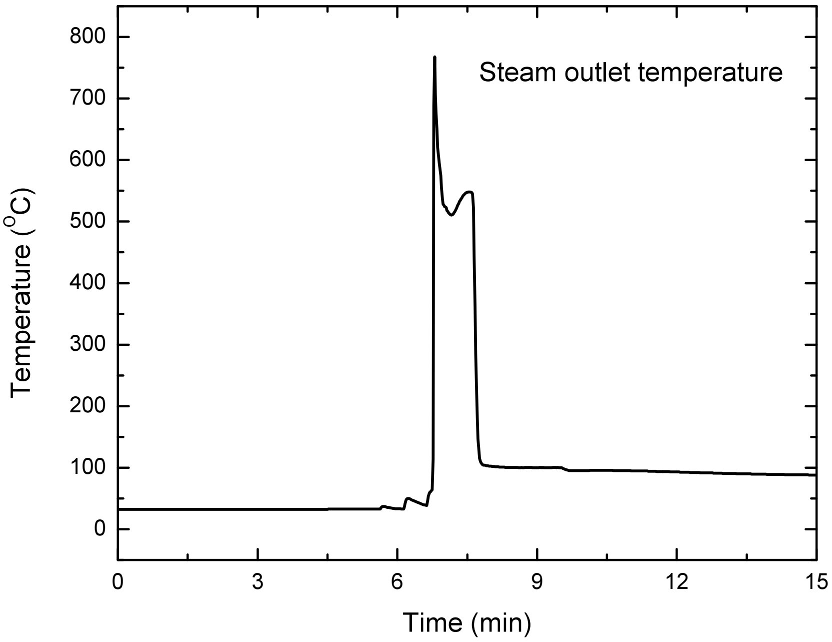

Figure 3.20 Steam outlet temperature

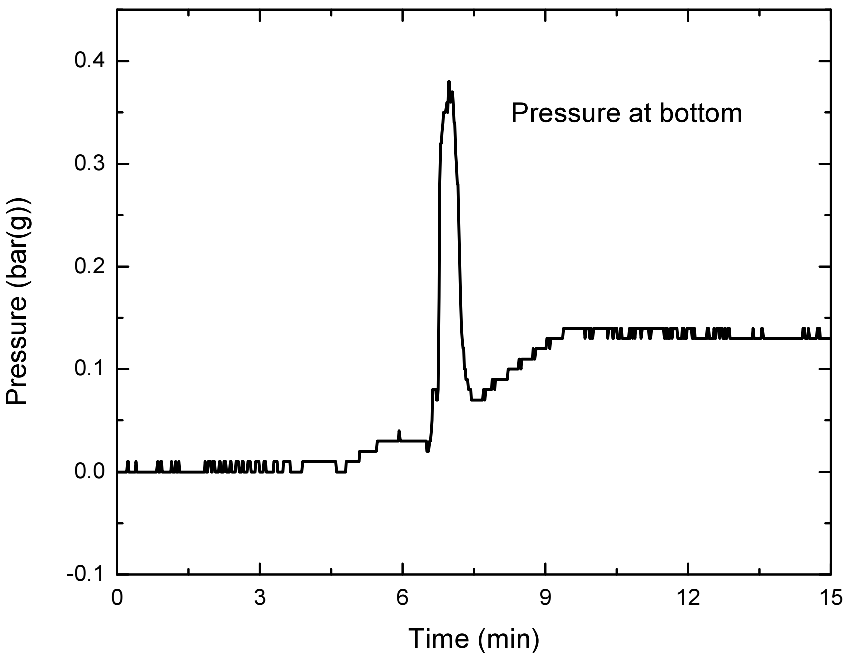

Figure 3.21 Pressure at the bottom of the test section

After the experiment was completed, the test section was opened. It was observed that, the melt was converted into a large porous mass as shown in Figure 3.22, which has risen to double its height. When water was poured onto this mass, it disappeared immediately into the porous mass indicating high porosity. The formed debris consisted of particle sizes ranging from very fine particles to 10 mm size chunks. The measured average porosity was 51 %.

Figure 3.22 Debris formed after the bottom flooding

3.7 Further validation of the model with bottom flooding experiment

The model for bottom flooding was applied for this experiment. Figure 3.23 shows the experimental and predicted temperature in the central region of the pool and Figure 3.24 gives the pressure predicted by the model. It can be seen that the pressure and temperature are predicted by the model are in very good agreement with the experimental data.

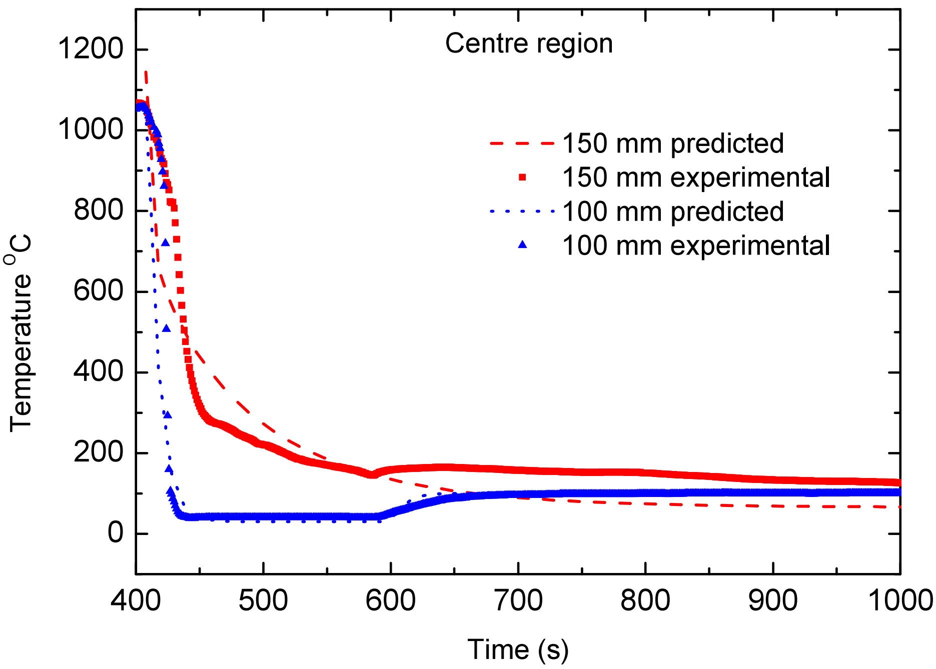

Figure 3.23. Comparison of predicted temperature with experiment

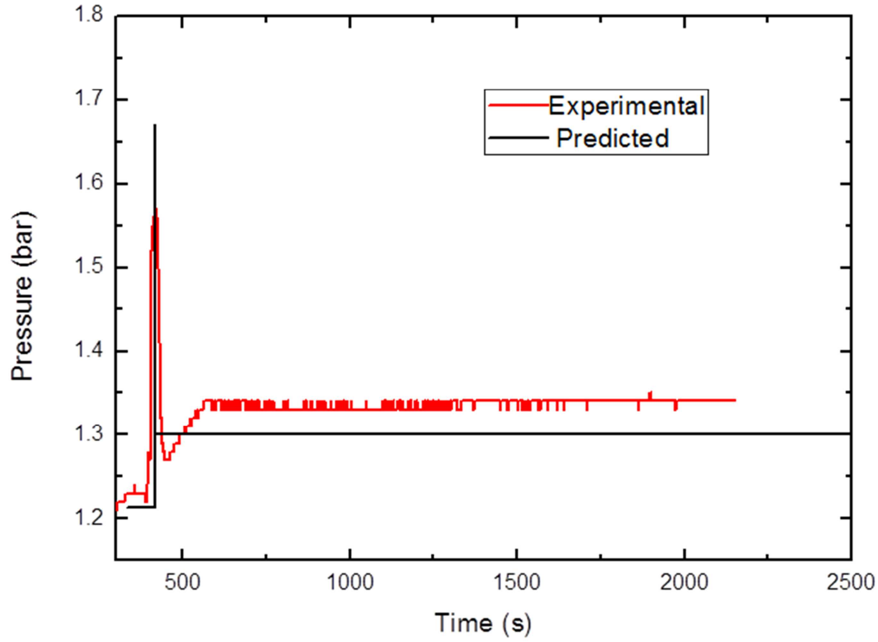

Figure 3.24. Predicted pressure history

Table 3.5 shows the predicted diameter of the eruption zone and peak pressure. The model was able to predict the diameter of eruption zone with good precision.

Table 3.5 Predicted parameters

Parameter	Experimental	Predicted	Error
Diameter of eruption zone	130 mm	126 mm	3.1 %
Maximum pressure pulse	1.57 bar	1.67	5.7 %

3.8 Summary

In this chapter, a model for melt coolability has been presented based on the postulations on melt coolability under bottom flooding. The model was first validated with experiments in literature. Subsequently, an experiment was carried out to study the melt coolability under bottom flooding using glass as a simulant whose properties are well known. The experiment showed that, by flooding the melt pool from bottom, because of steam formation at the bottom, steam and water erupt through the melt creating porous mass making it a coolable geometry by increasing heat transfer area and providing paths for passage of water enhancing the heat transfer greatly. The model was further validated with the experiment. It is observed that, unlike in top flooding, where coolability depends strongly upon properties of melt, coolability in bottom flooding is a thermal phenomenon depending upon the coolant mass flow rate, inlet pressure and subcooling, Nozzle diameter, melt pool height and melt superheat.

4. Melt coolability under different strategies

4.1 Introduction

Several strategies have been contemplated for quenching and stabilization of core melt accidents like top flooding, bottom flooding, indirect cooling [56-58] etc. Several experiments have been performed for coolability of molten pool under top flooding condition [9-11]. A few experiments have been performed for study of coolability of melt pool under bottom flooding as well as by indirect cooling [20-24]. However, these tests are very scattered because they involve different simulant materials, initial temperatures and masses of melt, which makes it very difficult to judge the relative effectiveness of a particular technique and advantage over the other. In this section, a comparison of different cooling techniques wherein a single simulant material with same depth of the melt was cooled with top flooding, bottom flooding and indirect cooling, starting from the same initial temperature has been presented.

4.2 Melt coolability under indirect cooling

In indirect cooling techniques, the core melt is often collected in an external vessel containing sacrificial material or contained inside the RPV and the vessel is then cooled externally by water. This scheme is employed by VVER [56], AP1000 [57] and PHWRs [58]. ESBWR [59] also to some extent uses this scheme where melt is cooled indirectly from below the core catcher and directly from the above. In the EC-FOREVER program, Sehgal et al., [60] studied the creep behavior of the lower head of the PWRs under in vessel cooling. Coolability of an in-vessel melt pool has been investigated experimentally by Henry and Dube, [61] and Henry [62]. However, most of the experiment targeted the vessel failure or gap cooling mechanism. The experiment LIVE [63] was performed to investigate the in vessel melt pool behavior and cooling strategies for in-vessel corium retention. RASPLAV [64] experiment was carried out to study the behavior of molten core materials on the RPV lower head and to assess the possible physicochemical interactions between molten corium and the vessel wall. Effectiveness of in-vessel cooling was also studied in ACOPO [65], COPO [66] and BALI [67]. LHF [68] and OLHF [69] tests were conducted to examine the lower vessel rapture behavior due to corium relocation and pool formation. SIMECO [70] experiments were carried out to study the variation of heat flux inside the vessel head due to stratification of the melt. Very few experiments have been carried out towards heat transfer from melt to water at high temperatures. The issues in this type of cooling are the formation of crust at the melt – vessel interface which limits the heat removed by the water by natural convection and hence on the dryout heat flux.

In the previous chapters, melt coolability experiments under top and bottom flooding with sodium borosilicate glass as s simulant were presented. It was observed that under top flooding, it took several hours to cool the melt and water ingression did not occur. Whereas, in bottom flooding experiment, the melt got quenched in few minutes. In order to judge the performance of indirect cooling with respect to and bottom flooding, an experiment on melt coolability under indirect cooling was carried out using same simulant material of about same melt depth and initial temperature.

4.2.1 Experimental Setup

For melt coolability with indirect cooling, a slightly different test section was used which consists of a 300 NB Sch 120 SS 304 pipe of 460 mm height supported horizontally inside a tank and submerged in the water pool (Figure 4.1). Temperatures were measured inside the melt pool, on the inner surface and the outer surface of the vessel and in the water pool. The thermocouple locations are shown in Figure 4.2. The accuracy of measurement is shown in Table 4.1

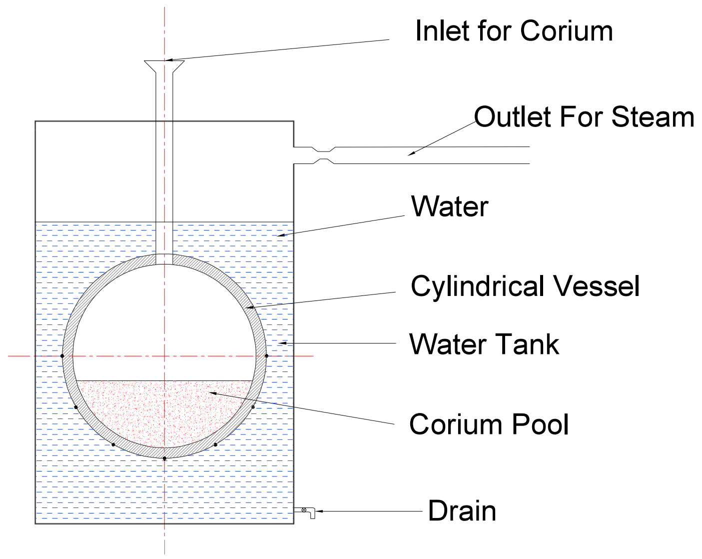

Figure 4.1 Schematic of the experimental setup for indirect cooling

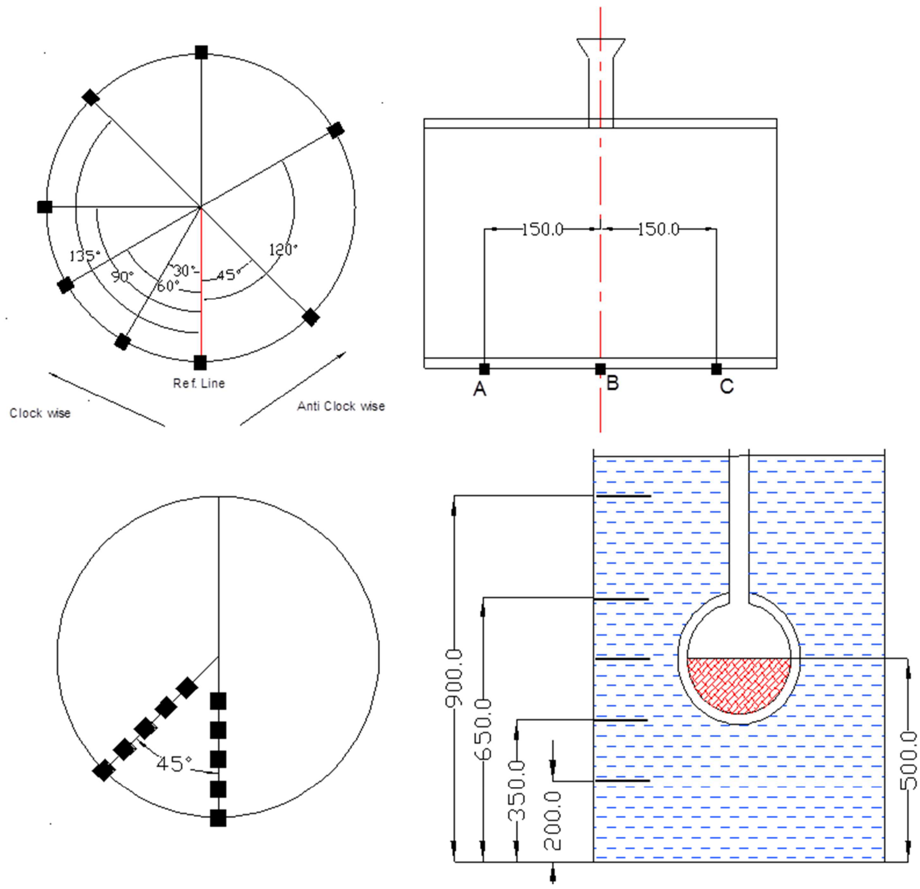

Figure 4.2 Thermocouple arrangements for indirect cooling experiment

Table 4.1 Accuracy of measurement

Parameter	Accuracy	Range
Temperature	$\pm$ 0.75% of measured value	0-1200 ^{O}C
Water level	$\pm$ 0.2% of the measured value	0-1000 mm

4.2.2 Experimental Procedure

The melt was generated in the furnace similar to earlier experiment. In order to maintain 300 mm depth inside the test section, about 60 kg melt at 1200 ^{o}C was poured in the vessel. In this experiment, there was no water addition in melt. After the melt was poured in the test section, the heat was transferred to water through the vessel wall to the surrounding water pool.

4.2.3 Results and Discussion

Figure 4.3 shows the molten pool cooling temperature radial distribution at 0° location. From the figure, it can be observed that temperature in molten pool is increases from bottom towards the center. At 20 mm from bottom of the vessel, maximum temperature of 550ºC is obtained, whereas at 120 mm from bottom of vessel maximum temperature of melt of 1125ºC is obtained. After about 240 minutes, the maximum temperature at the center had dropped down 450 ^{o}C. At that time, at 20 mm from bottom, it was around 120 ^{o}C. The melt pool temperature reaches to 100°C in 14 hours with a cooling rate of 1.2 ºC per min. Figure 4.4 shows the circumferential temperature variation of inner surface of cylindrical test section. Initially there is a temperature rise as the melt comes in contact with the thermocouples. Subsequently, the heat is transferred to water and the temperature drop occurred. It was also observed that there was slight variation in temperatures from circumferential location 0°

(225°C) to 180° (325°C). Figure 4.5 shows the temperature variations at the outer surface of cylindrical test section. It is observed that the outer temperature did not even reach to water saturation temperature. Figure 4.6 shows the temperature of water pool. It was observed that, water did not even reach boiling temperature. The thermocouples located at the bottom of the pool below the test section showed constant stagnation temperature of ambient water. It is also observed that, heat transfer is mainly due to natural convection.

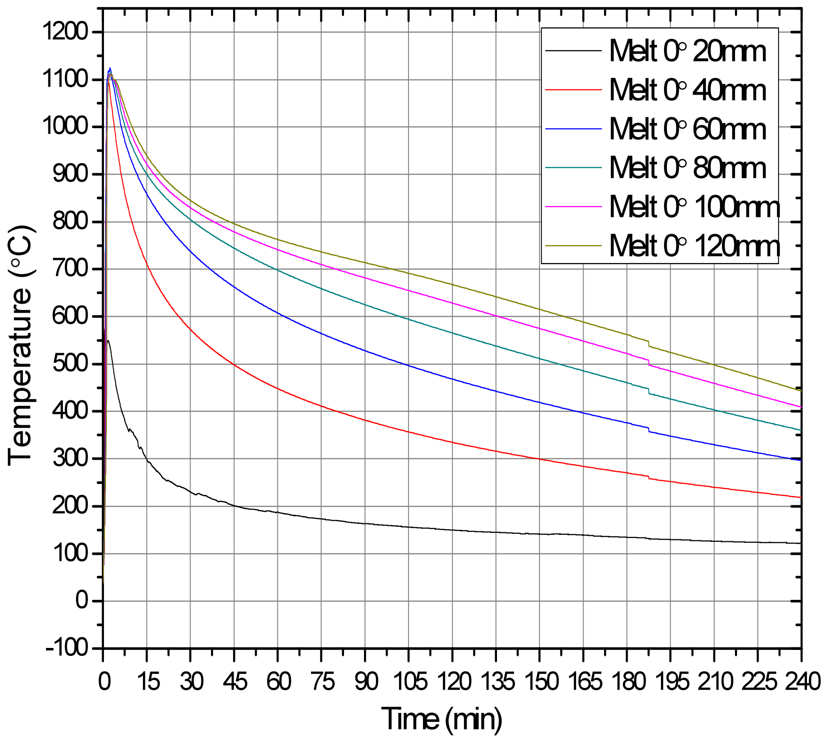

Figure 4.3 Measured temperatures inside the pool

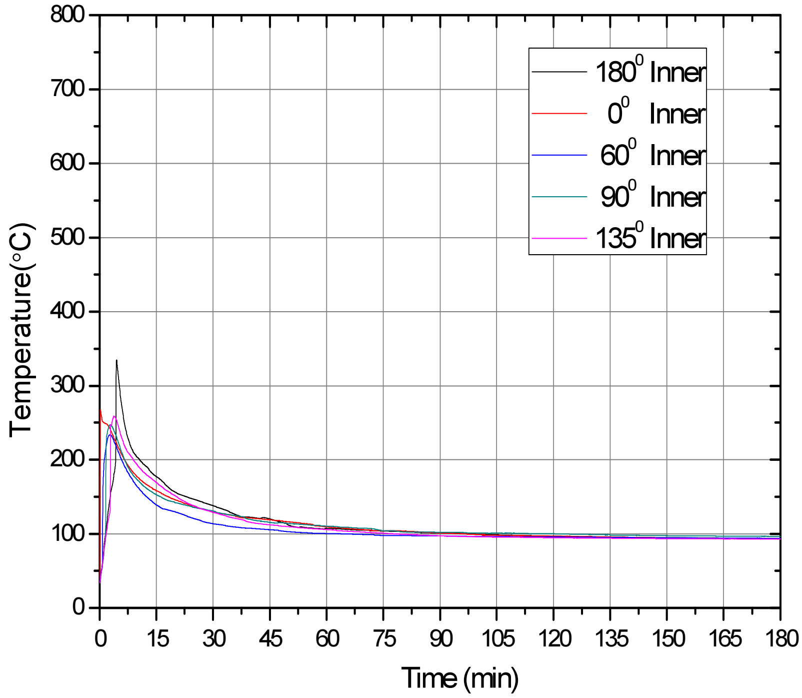

Figure 4.4 Melt temperature at the inner surface of the vessel

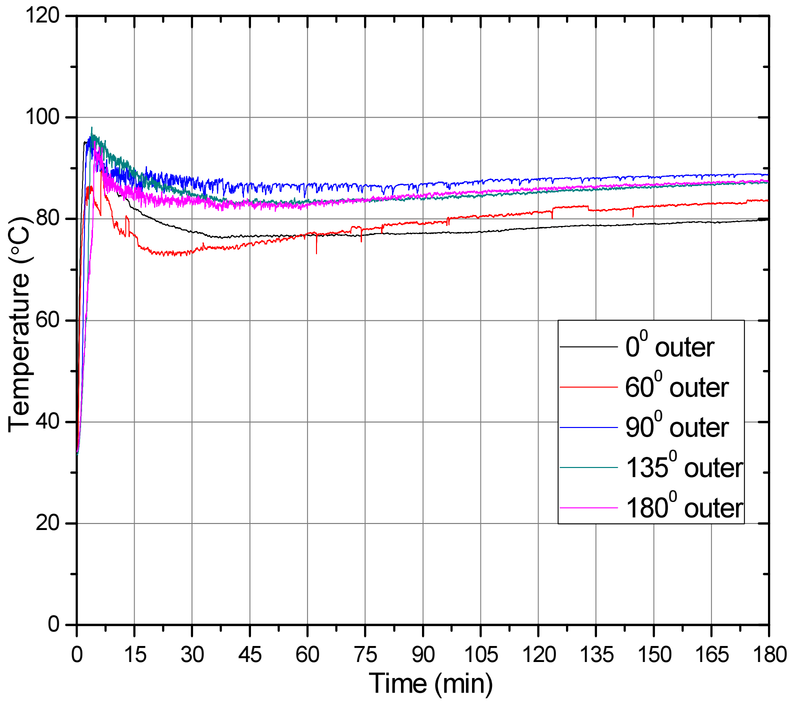

Figure 4.5 Temperatures at outer surface of calandria vessel

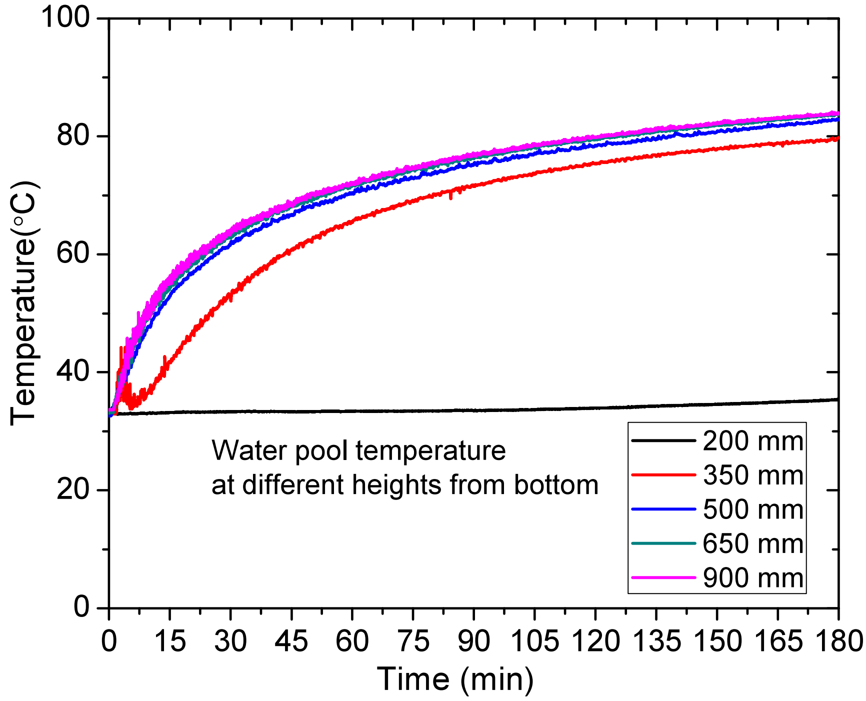

Figure 4.6 Temperatures inside the water pool

It was observed that, as soon as the melt falls on the cold vessel surface, a crust is formed at the interface which acts as insulation, leading to high temperature gradient in molten pool along radial direction. The solidus temperature of melt is around 600°C and the temperature below this indicates the formation of crust at that position. Figure 4.7 shows the crust growth with time. It is seen that within few minutes of the pouring, a 20 mm thick crust is formed. As a result, the heat transfer is poor taking long time to cool the melt.

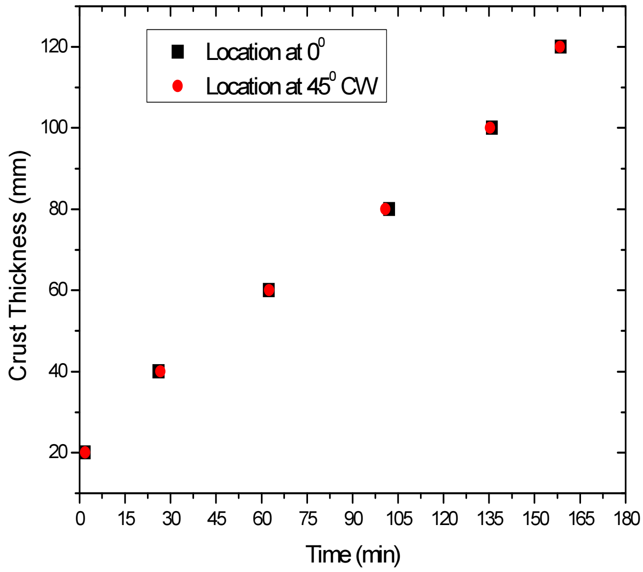

Figure 4.7 Crust thickness with time

4.3 Comparison of melt coolability with different strategies

Top flooding

Indirect Cooling

Bottom flooding

Figure 4.8 Test sections used for different tests

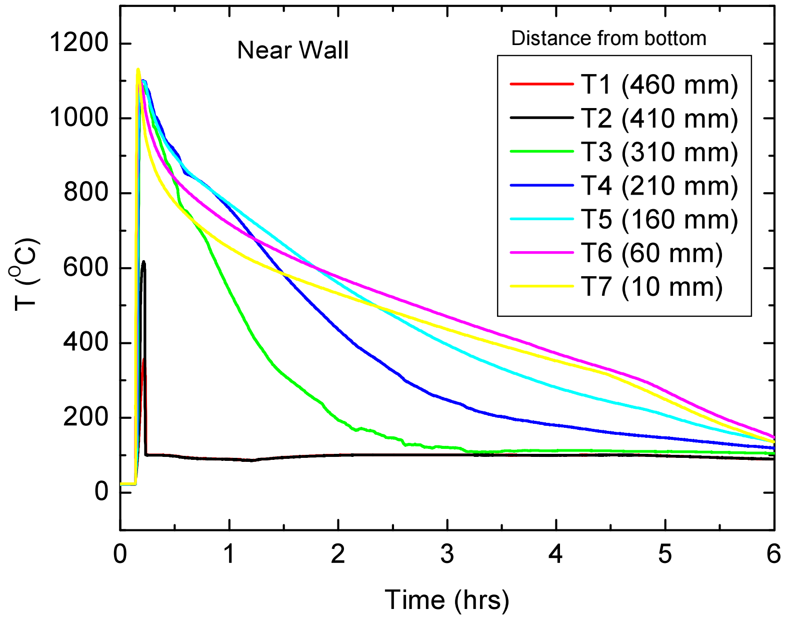

Figure 4.9 Temperature history from top flooding experiment

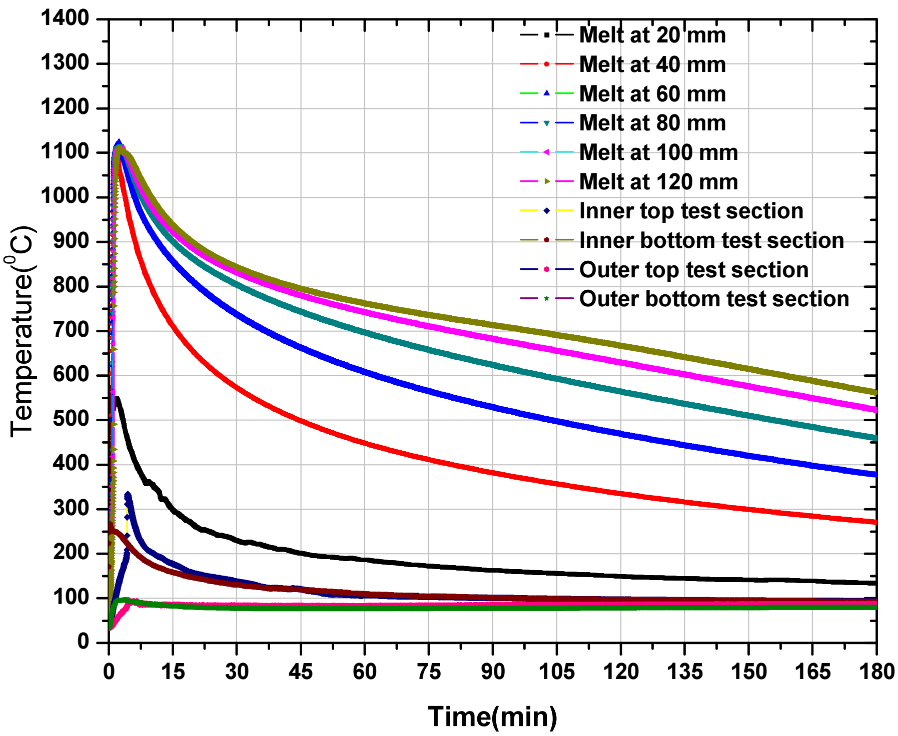

Figure 4.10 Temperature history from indirect cooling experiment

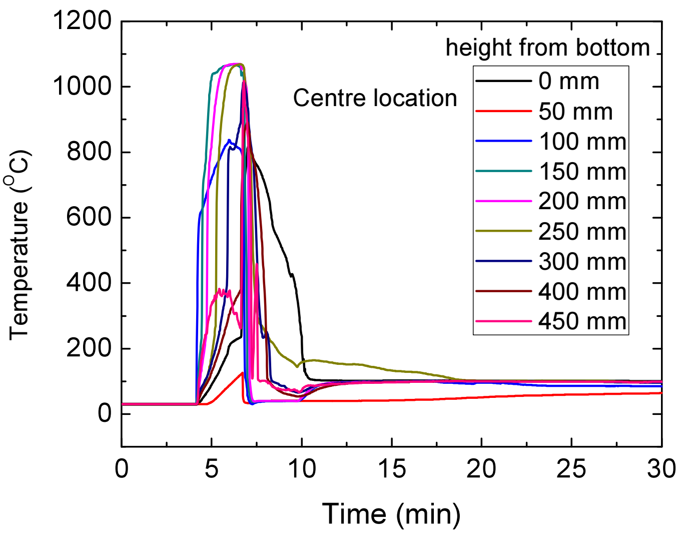

Figure 4.11 Temperature history from bottom flooding experiment

Figure 4.8 shows the different test sections used for the experiments. For top and bottom flooding, similar test section was used as discussed in chapter 2 and 3. For indirect cooling, the inside test section was of similar dimensions, but it was suspended horizontally and submerged in the water pool as discussed in the section 4.2.1. The initial depth of the melt was around 300 mm. Material of the melt was the same and its initial temperature was same in all the three tests.

Figure 4.9 Figure 4.11 show the measured temperature history in each of the tests. It can be seen that, in top flooding as well as in indirect cooling, it took several hours for quenching the melt whereas in bottom flooding, it took only a few minutes to cool the melt.

In order to have a quantitative estimate of the effectiveness of cooling amongst all the three methods, temperatures at the center of the pool were compared with each other for the three tests. Figure 4.12 shows the comparison plots. Undoubtedly, bottom flooding is the most effective technique where the melt is quenched in no time. Amongst indirect cooling and top flooding, initially, the rate of cooling is higher in indirect cooling. However, after some time the rate of cooling is found to increase in top flooding.

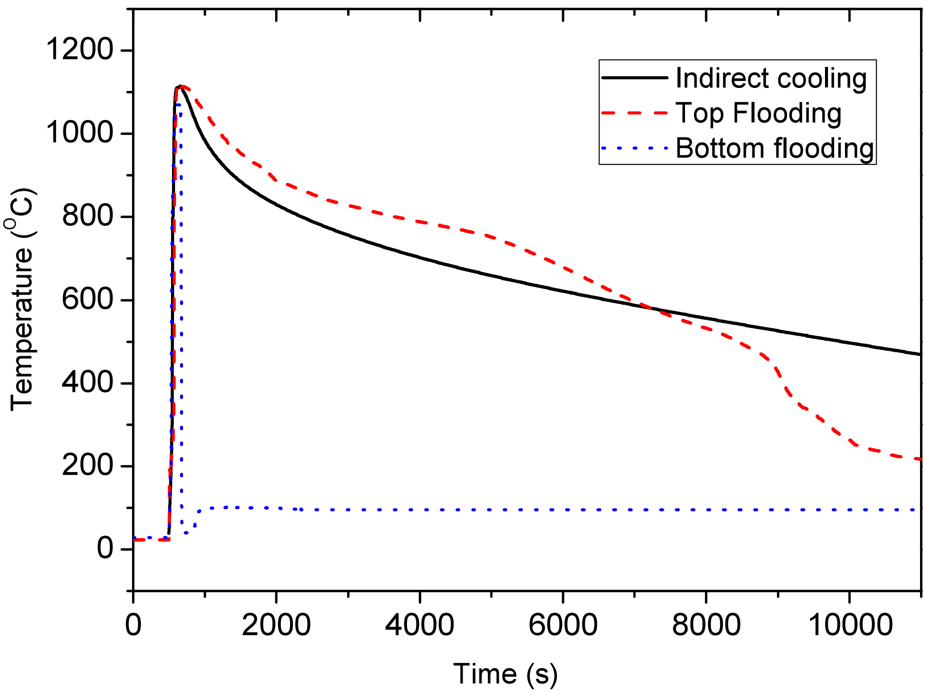

Figure 4.12 Comparison of all the three cooling strategies

4.4 Summary

Experiments were carried out wherein same mass of the simulant material at same initial temperature was cooled with different techniques. The experiments gave following insights

- Under top flooding condition, it took several hours to cool the melt under adiabatic conditions and water ingression occurred only upto 10 mm depth, below which a stable solid crust was formed which limited the heat transfer, which highlights that, top flooding is insufficient to quench the molten pool in case of severe accidents.
- In indirect cooling also, it took long time to cool the melt as a crust formed between melt pool and vessel acted as an insulation and resulted into poor heat removal.
- With bottom flooding, the steam formation below the melt and water backpressure induced porosity inside the otherwise impervious melt, which led to quenching of the melt in very short period of time. It took a few minutes to cool the melt to room temperature which otherwise took several hours in previous experiments.

Hence, it can be concluded that, bottom flooding is an effective way of quenching the molten pool in case of ex vessel severe accident scenarios.

5. Debris bed coolability under top and bottom flooding

5.1 Introduction

In the previous chapters, it was observed that, subsequent to flooding of molten pool from bottom or top, a porous debris bed is formed which still generates decay heat. Ensuring further long term coolability of such heat generating debris beds is very much important in the context of safety with respect to coolability as well as failure of cooling, yielding re-melting and subsequent attack of structures. To achieve long term coolability of the configuration, all evaporated water has to be replaced by water inflow due to natural forces. At the same time the produced steam must escape the porous structure driven by buoyancy forces. If the heat generation is too high and the coolant is unable to take out the heat, the bed reaches dryout condition where the temperature of the bed increases sharply. The heat flux corresponding to this is called as dryout heat flux (DHF). If there is an excessive pressure drop across the bed, water may not reach the entire length of the bed with the available gravity head and dryout may occur. Hence, in order to study the coolability of the debris bed, it is very important to know the DHF and pressure drop characteristics of the bed.

The hydrodynamics and heat transfer behaviour in debris bed is complex one influenced by many factors like

- The mean size of the particles,
- Porosity which is a function of the size and the shape of the particles which constitute the debris bed,
- Operating conditions such as water entry from the top or the bottom of the debris bed,
- Water temperature,
- Magnitude of non-condensable gases generated during MCCI
- Spatial distribution of the bed porosity

In a volumetrically heated top flooded debris bed, water flows down by gravity, takes away the heat by vaporization and the vapor again flows upwards by buoyancy. Thus, at steady state, for a given heat generation rate, there exists a counter current flow. As the heat input is increased, more vapor generation takes place and more heat flux is carried away by the vapor. But the increased vapor flow rate hinders the flow of water in the bed. At a particular heat generation rate, the upflowing vapor completely balances the water downflow. This is called as Counter Current Flooding Limit (CCFL). Beyond this point, no cooling is possible. The bed becomes dry and the bed temperature starts increasing rapidly. This heat flux is the maximum heat flux that can be removed from the bed. It is called as Dryout heat flux (DHF).

In case of bottom flooding, as the water and the vapor are flowing in the same direction, CCFL does not arise. However, if the bed is generating high heat flux and the water flow rate is very low, the water may evaporate even before it reaches the top of the bed. At that time, bed will experience dryout. The corresponding heat flux at a particular flow rate when first dry region is observed at the top of the bed is termed as dryout heat flux.

In coolability of debris beds, the bed characteristics play an important role. Debris beds with small particles also have small pores. This directly shows the higher pressure loss, and thus the increasing friction for flows with decreasing particle diameter. More resistance is acting against the flows of coolant and vapour for smaller particles. Thus, the dryout heat flux increases with the particle size.

The porosity influences the dryout heat flux in two ways. Firstly, in the case of higher porosity, more cooling liquid is inside the bed. So, more water can evaporate, and more heat can be removed. Secondly, and even more important for the long term coolability of the debris, is the fact, that with increasing porosity the friction losses of the fluid phases decreases. Geometrically this can already be seen by the larger available cross section for the fluid flows. The vapour can escape quicker from the bed, and the liquid coolant can easier penetrate into it. In any case, the higher the porosity, the better the overall coolability of the corium will be.

In real debris beds with irregular particle shapes and sizes, as to be expected for the fragmented corium, the porosity will additionally be influenced by the particle form and size distribution. The irregular shapes yield larger holes and thus higher porosity. On the other hand, different particle sizes will reduce the porosity, because the smaller ones can fill the holes of the bigger particles. This reduction of the porosity is dependent on the size distribution and on the local mixing.

Several experimental and theoretical programmes on debris coolability have been performed, especially in the beginning of the 1980's. The objective of most of these programmes had been to determine the maximum thermal power that can be removed from a heated particle filled column with a water reservoir on the top. The internal heating was produced either by resistance heaters [25], by inductive heating [26], or by direct neutron irradiation in a reactor [27].

The major tasks of the experimental investigations are the determination of local pressure drops for steady state boiling for checking friction laws, the determination of the Dryout Heat Flux (DHF) under various conditions for extension and comparison with existing data basis, and the analysis of the quenching process of dry hot debris bed. In the present work, dryout phenomena and pressure drop characteristics of top- and bottom-flooding condition have been reported which are very much important to predict the coolability of heat generating debris beds. Further, there are several models are available for prediction of dryout heat transfer as well as two phase pressure drop. However, a comparison of these models for prediction of dryout heat flux and two phase pressure drop of a single set of experimental data has not been reported earlier. In this chapter, the comparison of these models to select the best suitable model has been presented.

5.2 Experimental investigations on the coolability of the irregularly shaped heat generating homogeneous debris bed:

The emphasis of these experiments was to get an insight on the coolability of realistic debris beds. The fragmentation particles from the PREMIX-experiment [71] carried out at the Research Centre, Karlsruhe were used in these experiments, with particle diameters ranging from 2 mm to 10 mm with porosity of 30-40 %.

Experiments were carried out at DEBRIS test facility at IKE, University of Stuttgart, Germany. The test facility is as shown in Figure 5.1

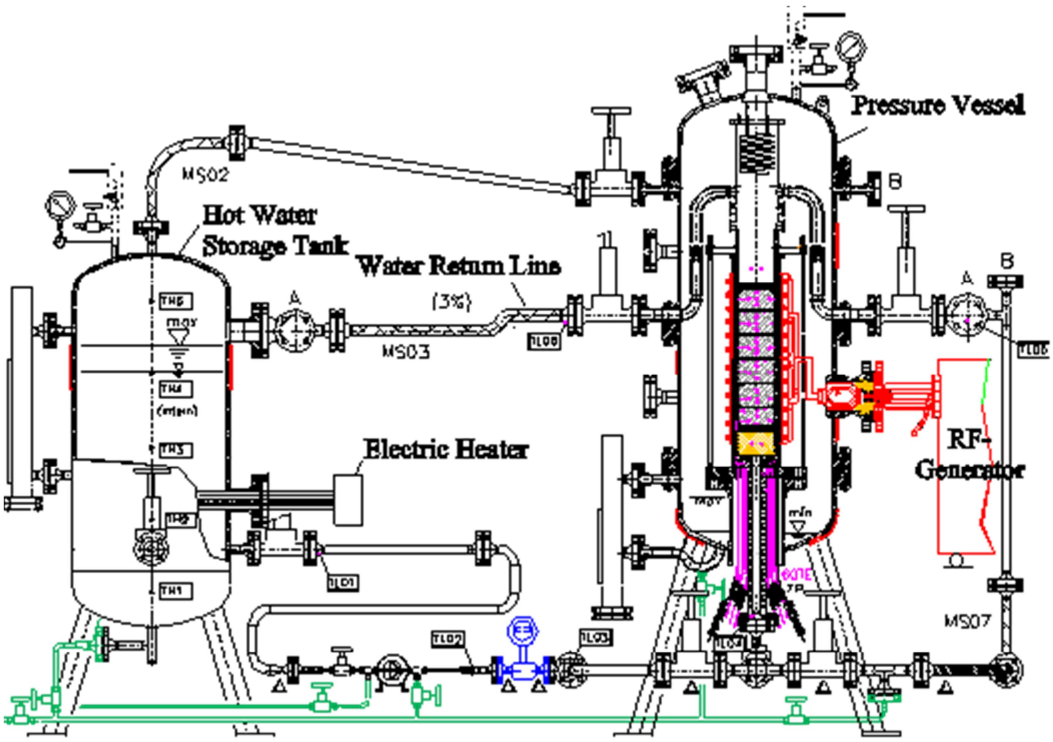

Figure 5.1 Experimental setup

The experimental set-up consists of a pressure vessel designed for pressures up to 40 bar in which the crucible filled with particles is mounted. The pressure vessel is connected to a storage tank filled with demineralized water and a pumping system, which allows performing boiling experiments with feeding water to the crucible at the bottom (bottom flooding) or at the top (top-flooding). Figure 5.1 shows the complete set-up including piping and heat removal system. The debris bed is heated via an oil-cooled 2-winding induction coil by an

RF-generator. The RF-generator operates at a frequency of 200 kHz and has a nominal output power of 140 kW. For boiling and dryout experiments, a crucible made of PTFE is used. It has a total height of 870 mm and an inner diameter of 125 mm. It is equipped with 60 thermocouples (1 mm, Type N), of which 51 are located in the debris bed on 25 levels. The thermocouples measure the temperature in the voids between the particles, which are filled by liquid, vapour or a mixture of both. For pressure measurements, 8 differential pressure transducers are used (100 mbar, class 0.1). The pressure taps are uniformly distributed in 100 mm intervals along the bed height (pressure transducer dp8 (not shown in figure) is used for measuring the pressure difference between level PL0 and PL7). The exact position of the thermocouples and pressure taps can be seen in Figure 5.2.

The bed configuration is as shown in Table 5.2 and bed physical properties are given in Table 5.3

Table 5.2 Bed Configuration

particles	Wt, g	Wt, %
6 mm steel spheres	11371.6	43.74
3 mm steel spheres	6442.5	24.78
5~10 mm Al_2O_3	5410.9	20.81
2~5 mm Al_2O_3	2775.0	10.67
Total	**26000.0**	100.00

Table 5.3 Bed physical properties

Bed Weight	26524.6 kg
Bed Volume	8.47 x 10-3 m3
Avg Bed Density	3131 kg/m3
Bed porosity (measured)	0.38

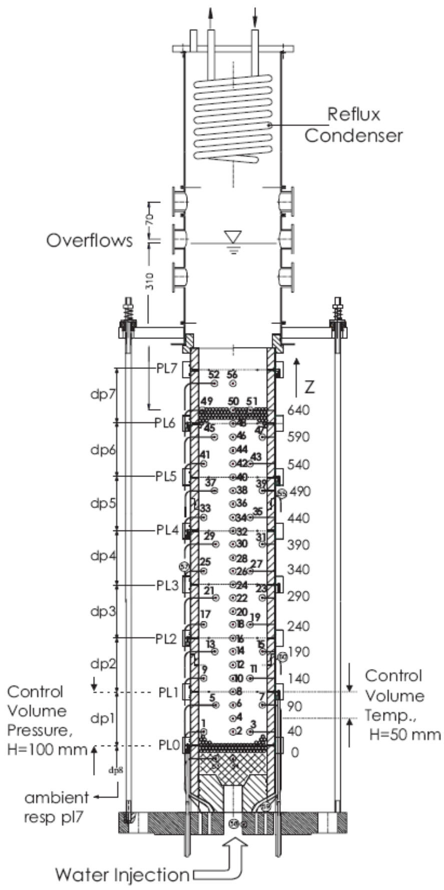

Figure 5.2 Position of measurement sensors

5.2.1 Evaluation of debris bed friction characteristics:

In order to determine the pressure drop characteristics of the bed and to determine the average particle diameter size, single phase pressure drop experiment has been carried out. The pressure drops were measured at different liquid superficial velocities (cross sectional average velocities) as shown in Figure 5.3. For each superficial velocity, 6 pressure drop readings were obtained from 6 DPT's located at positions as shown in Figure 5.2. For a given flow rate, the 6 data points correspond to 6 measurement positions, i.e. dp1 to dp6. The earlier experimental data on the beds with single-sized spheres (3 mm and 6 mm) and with polydispersed spheres (6/3/2 mm, 50% 6 mm spheres, 30% 3 mm spheres and 20% 2 mm spheres, in weight) are also shown in the figure. The pressure gradients for the irregular-particle bed are smaller than those for the polydispersed-sphere bed but higher than those for the 6mm-sphere bed. Surprisingly, the pressure drop behaviour of the irregular-particle bed and the 3mm-sphere bed are quite similar. The Ergun's equation is used to predict the single phase pressure drop of the particles.

$$-\frac{dp}{dz}-\rho_l g=150\frac{(1-\varepsilon)^2\,\mu u}{\varepsilon^3 d_p^{\,2}}+1.75\frac{(1-\varepsilon)^2\,\rho u^2}{\varepsilon^3 d_p} \tag{5.1}$$

$$-\frac{dp}{dz}-\rho_l g=150\frac{(1-\varepsilon)^2\,\mu u}{\varepsilon^3 d_p^{\,2}}+1.75\frac{(1-\varepsilon)^2\,\rho u^2}{\varepsilon^3 d_p} \tag{5.2}$$

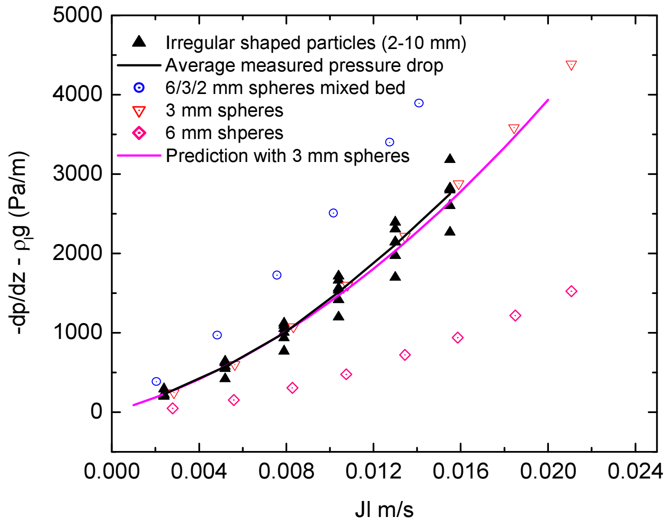

Figure 5.3 Single phase pressure drop characteristics of the bed

The Ergun equation prediction with measured porosity and average particle diameter 3 mm also matches with the experimental data with 3 mm particles and the average pressure gradient of all the DPT's. Hence, in all further calculations, average particle diameter of 3 mm has been used.

5.2.2 Experiments under boiling two phase conditions

In order to evaluate the friction laws under boiling conditions, two phase pressure drop experiments were carried out. Initially, the liquid in the test section is brought to saturation temperature. Then the pressure drops were measured for top flooding condition and bottom flooding condition for rising levels of heat input.

5.2.2.1 Top flooding condition

Once the liquid starts boiling, the reflux condenser at the top is started which helps in maintaining a liquid pool on the top of the bed and no additional water is pumped in the bed. The water flows down the bed by gravity and a counter current flow is established. Pressure drops are recorded once the steady state is reached. Pressure drop is measured at various heating levels in increasing order below the dryout heat flux. As the heating level increases, the vapor velocity increases. It limits the inflow of the liquid. Dryout occurs at a particular vapor velocity when the counter current flooding limitation is reached. The vapor velocity is calculated as follows.

$$J_g(z) = \frac{\int_0^z Q'''(z)\,dz}{\rho_g h_{fg}} \tag{5.3}$$

The experimental results are shown in Figure 5.4

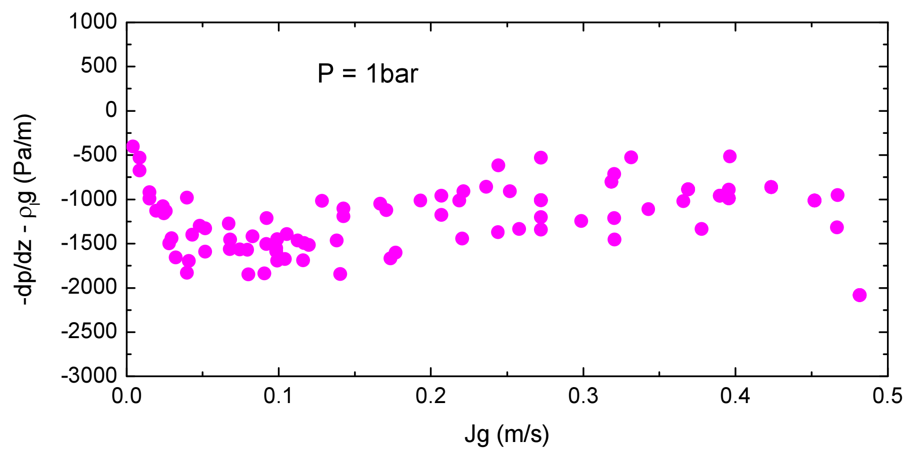

Figure 5.4 Measured pressure gradient at different heat flux conditions at 1 bar

As seen in Figure 5.4, the two phase pressure drop characteristic shows typical S shaped curve. Initially, at low vapor velocities, the pressure gradient is negative. It indicates the reduction in hydrostatic head of the water due to presence of a low density steam phase. The drag force between vapor and liquid plays important role in this region. As the vapor velocity increases, the drag force between vapor and particles becomes dominating which leads in increase in pressure gradient. At higher vapor velocities (implying higher powers,) the upflowing vapor creates resistance in the path of downcoming water resulting into lower cooling. At a particular power when the vapor balances the inflow of water, dryout occurs. It can be seen that, due to dryout, as there is no water present in the porous medium, the pressure gradient drastically reduces as shown in Figure 5.4.

Effect of System pressure:

In order to judge the effect of system pressure on the friction laws, experiment at slightly higher pressure (3 bar) was carried out. It can be seen from Figure 5.5 that, in the pressure drop characteristic remains almost same but the maximum vapor velocity reduces which can be attributed to the fact that, at high pressure, the density of the vapor is high which can limit the downflow of water at lower velocity only.

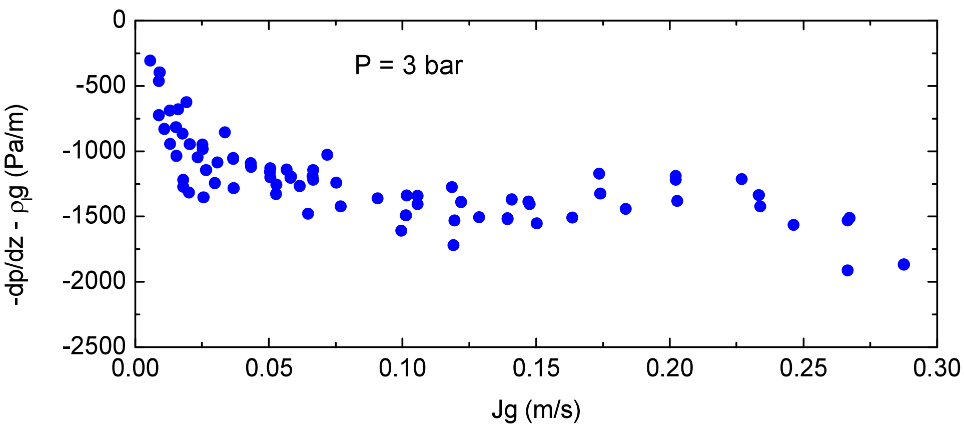

Figure 5.5 Effect of system pressure on measured pressure gradients

5.2.2.2 Bottom flooding condition

In bottom-flooding experiments, additional water is pumped into the bottom of the bed (forced flow condition), so a co-current flow of water and vapour will be established inside the debris. However, a pool of liquid was still maintained on the top of the bed. Experiments have been carried out at 1 and 3 bar pressures and for forced liquid inlet velocities of 0.5, 0.69, 1.2, 2.8 and 7.1 mm/s. In case of bottom flooding, it was observed that, due to heat losses, the inlet liquid temperature was below saturation. So it was necessary to add a correction while calculating the vapor velocities. It is given as follows

$$J_g(z) = \frac{\int_0^z \overset{'''}{Q}(z)\,dz - \overset{\circ}{G} C_{p,l}\left(T_{sat} - T_{in}\right)}{\rho_g h_{fg}} \tag{5.4}$$

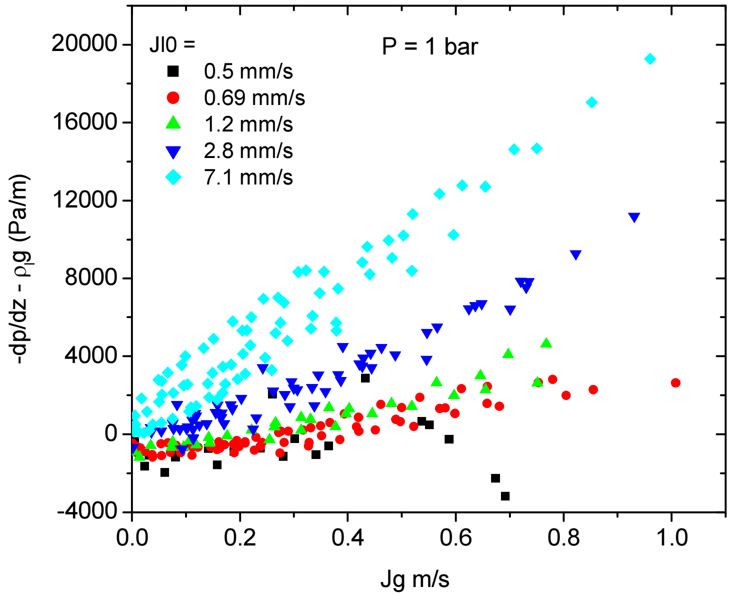

Figure 5.6 Measured pressure gradient at various inlet flow rates at increasing heat flux conditions

In Figure 5.6, it can be seen that, at very low bottom flow (0.5 mm/s), the pressure drop behaviour is almost similar to top flooding with small rise in maximum vapor velocity. As the bottom inflow rate increases, the pressure drop starts increasing with increase in vapor velocity. This is due to the co-current flow between vapor and liquid. In this scenario, the fluid particle drag is dominant component in overall pressure gradient which increases with increase in both liquid as well as vapor velocity. At very high liquid inflow (7.1 mm/s), there is almost linear relationship of pressure gradient with the vapor flow rate.

Effect of system pressure:

To see the effect of higher system pressure on two pressure drop, experiments were carried out for 3 bar pressure at liquid inflow velocities 0.33 mm/s and 2.72 mm/s. Figure 5.7 shows the experimental results.

It can be seen that, the results are similar to that of 1 bar and like in earlier case, there is decrease in maximum vapor velocity. Thus we can conclude that there is very small effect of system pressure on the pressure drop characteristics of debris beds.

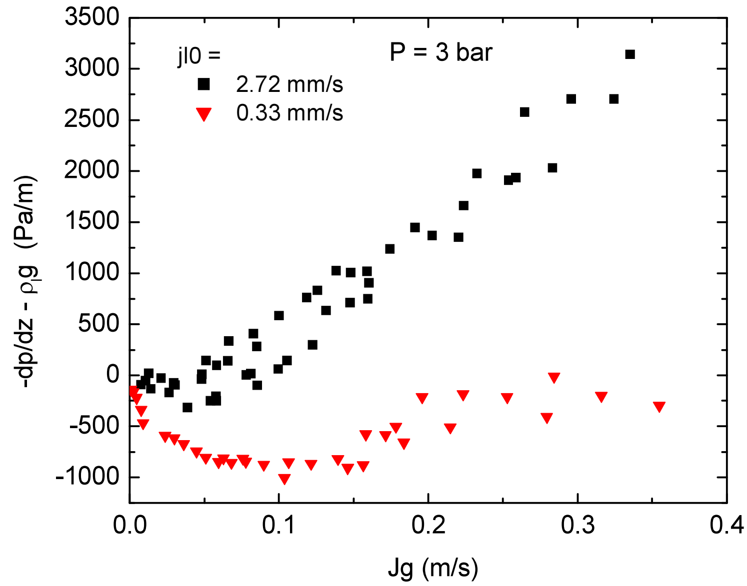

Figure 5.7 Bottom flooding pressure drop characteristics at 3 bar pressure

5.2.3 Dryout experiments

The top-flooding experiments are started with a water saturated bed and a water pool of 300 mm height. To determine the DHF, the heater power is increased in small steps. As the temperature approaches saturation, the step size is made finer. The vapour generated is condensed directly above the water pool, so the water level remains constant. At a particular power, when the upgoing vapor balances the water, dryout was found to occur. It is characterized by sudden rise in temperature of dry zone and sudden fall in the pressure drop of that zone.

Figure 5.8 shows the heat input, measured temperatures and pressure differences of a dryout experiment at 1 bar pressure with top-flooding. The initial dryout position and the dryout area shortly before the stop of heating are also shown in the figure. The heating power is increased in a small step. When the heat input increases from 9 kW to 9.56 kW, the pressure difference dp5 decreases to a negative value within a few seconds, and it decreases continuously, indicating that the counter-current flow limit at the position "dp5" (Figure 5.2) has been reached. With the heating going on, the counter-current limit is reached at lower bed positions ("dp4", "dp3" and "dp2"). Dryout does not occur immediately after the drop of dp5. The initial dryout is found to occur at about 1250 seconds after the application of the dryout heat flux (DHF) and at the position of "T13" (lower bed position) characterized by sharp rise in temperature above the saturation temperature when dp2 almost decreases to its lowest value.

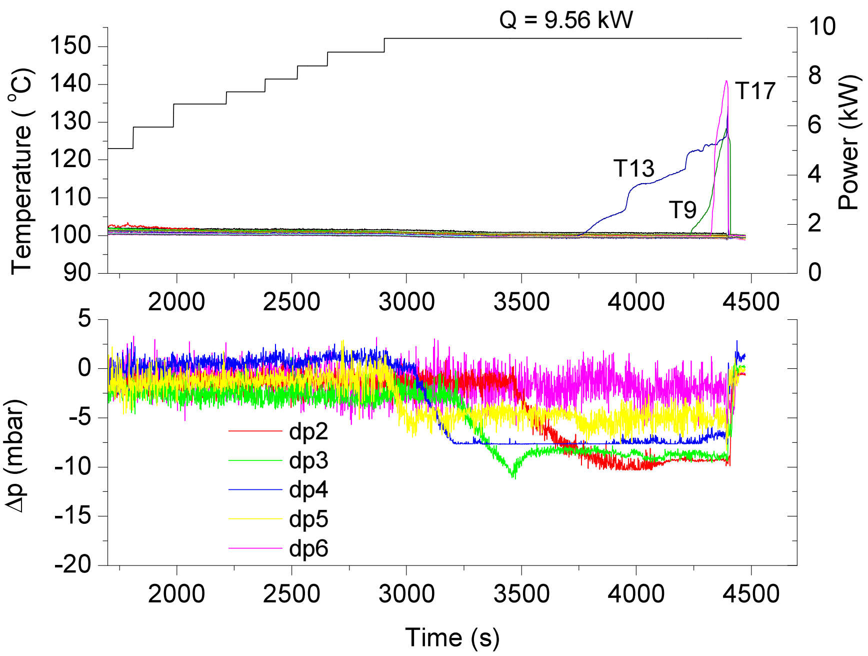

Figure 5.8 Typical dryout condition

The dryout experiments were carried out for top and bottom flooding condition under 1, 3 and 5 bar system pressures. A summary of the experiments is given in Table 5.4.

Table 5.4 summary of dryout experiments

Expt No	P Bar	Condition	Power kW	DHF kw/m^2
1	1	Top flooding	9.85	803
2	1	Bottom flooding, jl0 = 0.5 mm/s	14.435	1176
3	1	Bottom flooding, jl0 = 0.5 mm/s	15.16	1235
3	1	Bottom flooding, jl0 = 0.69 mm/s	19.9	1622
4	3	Top flooding	14.435	1176
5	3	Top flooding	15.9	1296
6	3	Bot flooding, Jl0 = 0.33 mm/s	19.9	1622
7	5	Top flooding	19.9	1622

Figure 5.9 shows the trend of dryout experiments. It can be seen that, as system pressure increases there is substantial increase in dryout heat flux. Also, dryout heat flux increases substantially with introduction of small bottom inflow of water.

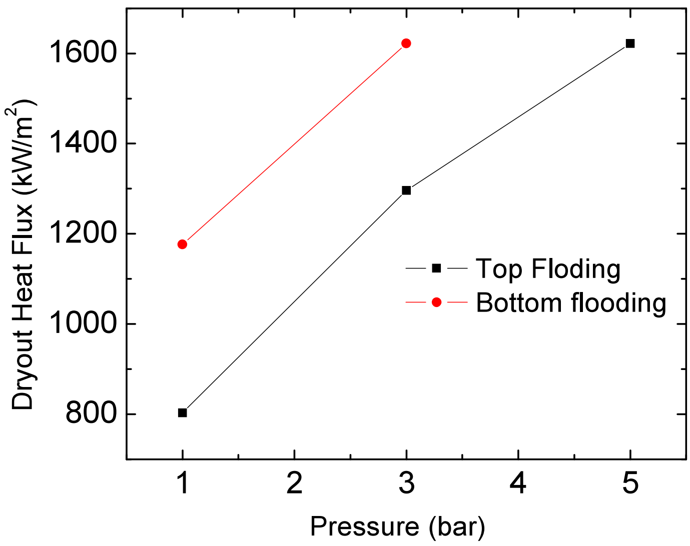

Figure 5.9 Dryout experiments

5.3 Assessment of Capability of Models for Prediction of Dryout Heat Flux and Pressure drop behaviour

Determination of the friction laws governing the two phase flow in the porous structure is very important aspect in prediction of dryout heat flux and pressure drop characteristics of a heat generating debris beds. Especially in case when there is counter current flooding observed, friction plays important role. There are several models available in the literature like Lipinski [28], Hu and Theophanus [25], Schulenberg and Mueller [45], Reed [43] and Tung and Dhir [46]. A comprehensive study of assessment of capability of these models for prediction of pressure drop and dryout heat flux was carried out. The predictions were compared with the experiments carried out earlier on the DEBRIS test facility.

5.3.1 Comparison of models with pressure drop data:

The pressure gradients of the bed with irregular particles are compared with various models found in literature describing the two-phase flow in porous media. Most models are based on extension of Ergun's equation for two phase flow and can be expressed in the form

$$-\nabla p = \frac{\mu}{K} j + \frac{\rho}{\eta} |j| j + \rho g \qquad (5.5)$$

where, K and η are the permeability and the passability of the porous media and are given as

$$K = \frac{\varepsilon^3 d_p^{\ 2}}{150(1-\varepsilon)} \quad and \quad \eta = \frac{\varepsilon^3 d_p}{1.75(1-\varepsilon)} \tag{5.6}$$

Equation (5.5) is valid for single-phase flow. For two-phase flows the Ergun-equation is set up for each phase separately. The mutual influence of the two phases (e.g. reduction of the flow path) is taken into account by the relative permeabilities $K_{rel,l}$, $K_{rel,g}$ and the relative passabilities $\eta_{rel,l}$, $\eta_{rel,g}$. The momentum equations for vapor and liquid phase are given as

$$-\nabla p_g = \frac{\mu}{KK_{rel,g}} j_g + \frac{\rho}{\eta\eta_{rel,g}} \left|j_g\right| j_g + \rho_g g \tag{5.7}$$

$$-\nabla p_l = \frac{\mu}{KK_{rel,l}} j_l + \frac{\rho}{\eta\eta_{rel,l}} \left|j_l\right| j_l + \rho_l g \tag{5.8}$$

In two phase flow, the permeability and passability are mainly dependent upon the void fraction of the vapor phase. There are several models available in literature to estimate these values. The models can be classified as the models with explicit interfacial drag force and those without interfacial drag force.

5.3.1.1 Models without interfacial drag force term:

Models by Reed, Lipinski and Hu and Theophanous express the permeabilities and passabilities in terms of void fraction and are without and explicit interfacial drag force term. Their expressions are summarized in Table 5.2.

Table 5.5 Relative permeabilities and relative passabilities of different models

Model	$K_{rel,v}$	$\eta_{rel,v}$	$K_{rel,l}$	$\eta_{rel,l}$
Reed	α^3	α^5	$(1-\alpha)^3$	$(1-\alpha)^5$
Lipinski	α^3	α^3	$(1-\alpha)^3$	$(1-\alpha)^3$
Hu and Theophanous	α^3	α^6	$(1-\alpha)^3$	$(1-\alpha)^6$

5.3.1.2 Models with explicit interfacial drag force term:

Models by Schulenberg&Mueller and Tung &Dhir havean additional term for interfacial drag. Schulenberg and Müller used the correlation obtained from air-water experiments to formulate the interfacial drag term. So equations (5.7) and (5.8) are modified as

$$-\nabla p_g = \frac{\mu}{KK_{rel,g}} j_g + \frac{\rho}{\eta\eta_{rel,g}} \left|j_g\right| j_g + \rho_g g + \frac{F_i}{\alpha} \tag{5.9}$$

$$-\nabla p_l = \frac{\mu}{KK_{rel,l}} j_l + \frac{\rho}{\eta\eta_{rel,l}} \left|j_l\right| j_l + \rho_l g - \frac{F_i}{(1-\alpha)} \tag{5.10}$$

Schulenberg and Müller developed the correlation for drag force term as

$$F_i = 350(1-\alpha)^7 \alpha \frac{\rho_l K}{\eta\sigma} \left(\rho_l - \rho_g\right) g \left(\frac{j_g}{\alpha} - \frac{j_l}{(1-\alpha)}\right)^2 \tag{5.11}$$

The expressions for permeability and passability are given as

$$K_{rel,v} = \alpha^3,\ K_{rel,l} = (1-\alpha)^3,\ \eta_{rel,l} = (1-\alpha)^5\ \eta_{rel,v} = \begin{cases} 0.1\alpha^4 & if\ \alpha \le 0.3 \\ \alpha^6 & if\ \alpha > 0.3 \end{cases} \tag{5.12}$$

Tung and Dhir also used a different approach to model the interfacial drag force based on the flow pattern in the porous medium. Based on visual observations in air-water flow experiment they defined flow patterns ranges for bubbly, slug and annular flow. The expressions for relative permeability and passability are defined as

$$K_{rel,v} = \left(\frac{1-\varepsilon}{1-\varepsilon\alpha}\right)^{4/3} \alpha^4,\quad \eta_{rel,v} = \left(\frac{1-\varepsilon}{1-\varepsilon\alpha}\right)^{4/3} \alpha^4\ for\ 0 \le \alpha \le 0.6 \tag{5.13}$$

$$K_{rel,v} = \left(\frac{1-\varepsilon}{1-\varepsilon\alpha}\right)^{4/3} \alpha^3,\quad \eta_{rel,v} = \left(\frac{1-\varepsilon}{1-\varepsilon\alpha}\right)^{4/3} \alpha^3\ for\ 0.6 \le \alpha \le 1 \tag{5.14}$$

and

$$K_{rel,l} = (1-\alpha)^4,\ \eta_{rel,l} = (1-\alpha)^4 \tag{5.15}$$

To compare the experimental data of the bed with irregular particles with the simulation models, an effective particle diameter of 3 mm is chosen, and the measured bed porosity of 0.38 is used.

A comparison is made between the above mentioned models and the experimental results for dryout heat flux (Table 5.6and Table 5.7) and pressure drop characteristics (Figure 5.10 - Figure 5.12). For top-flooding, the dryout heat flux is well predicted by the model of Reed. The Lipinski model largely overpredicts the DHF, while the Tung and Dhir model and Hu and Theophanous model underpredict the DHF value. For bottom-flooding, the Lipinski model gives better predictions of the DHF than the other models

Table 5.6 Comparison of predicted Dryout heat flux with experimental data for Top flooding condition

	Reed	Lipinski	Hu and Theophanus	Schulenberg and Mueller	Tung and Dhir	Experimental
1 bar	800	1075	640	729	518	**803**
3 bar	1184	1728	915	1068	864	**1296**

Table 5.7 Comparison of predicted Dryout heat flux with experimental data for bottom flooding condition

	Reed	Lipinski	Hu and Theophanus	Schulenberg and Mueller	Tung and Dhir	Experimental
1 bar, jl0* = 0.5 mm/s	1196	1312	1133	1171	1081	**1235**
1 bar, jl0 = 0.69 mm/s	1504	1523	1497	1497	1491	**1622**
3 bar, jl0 = 0.33	1376	1830	1139	1280	1024	**1622**

mm/s						

*Jl0 is inlet water velocity.

Although, the Reed model predicts the DHF very closely, like other models without explicit consideration of interfacial drag, fails to predict the two-phase-flow pressure drop below the dryout heat flux (Figure 5.10a). The better prediction is given by the Schulenberg and Mueller model, which is able to predict the pressure drop characteristic with typical lying-S shaped curve. For 3 bar pressure, the prediction by Schulenberg and Mueller is much better (Figure 5.10b). In two phase pressure drop in a porous medium, there are different types of pressure drops components like liquid-particle, vapour particle and vapour liquid drag. In case of top-flooding and low inflow bottom flooding, the vapor velocities are low and thus the interfacial drag between vapour and liquid plays an important role in the total pressure drop, which is taken into account in the Schulenberg and Mueller model. Hence it predicts the pressure drop well. However, as the liquid velocities increase, the liquid- particle drag becomes more dominant. The coefficients of Reed model are obtained from air-water flow rate at high inflows. Hence, Reed model predicts the pressure drop well. Although the variations in the predicted dryout heat fluxes among all the models are small, there is a significant difference in pressure drop characteristics under bottom flooding condition (Figure 5.11a-d). At a low inflow velocity of 0.70 mm/s, no model seems to be able to predict the pressure gradients accurately, except, the Schulenberg and Mueller model which captures the trend and predicts reasonably well in vary low vapor velocities range. For the inflow velocity of 2.8 mm/s, the Reed model gives the best prediction. The models of Hu and Theofanous and Lipinski give reasonably good predictions for the low vapour velocities, for a vapour velocity higher than 0.4 m/s the deviations become bigger. The predictions from the models of Schulenberg and Müller and Tung and Dhir are much smaller than the experimental values. When the flow velocity increases to 7.1 mm/s (Figure 5.11d), the particle-liquid drag becomes more dominant, the pressure gradients increase consistently with vapour velocity. All the models predict this tendency correctly, however the deviations are generally very high except for the model of Tung and Dhir. For 3 bar pressure, at low liquid inflow 0.33 mm/s, prediction by Schulenberg and Mueller model is in good agreement (Figure 5.12a) whereas, at a bit higher inflow (2.72 mm/s) Tung and Dhir model predicts well.

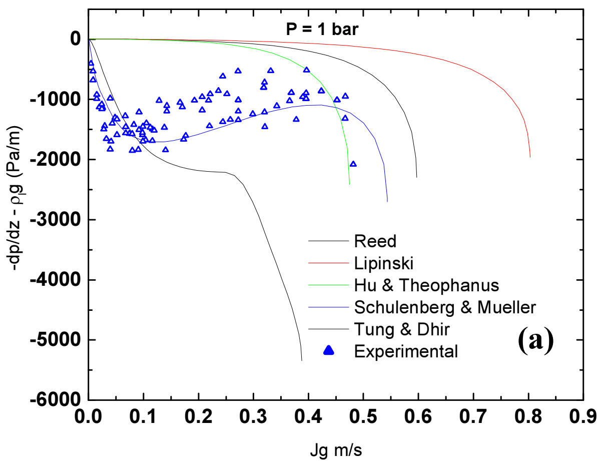

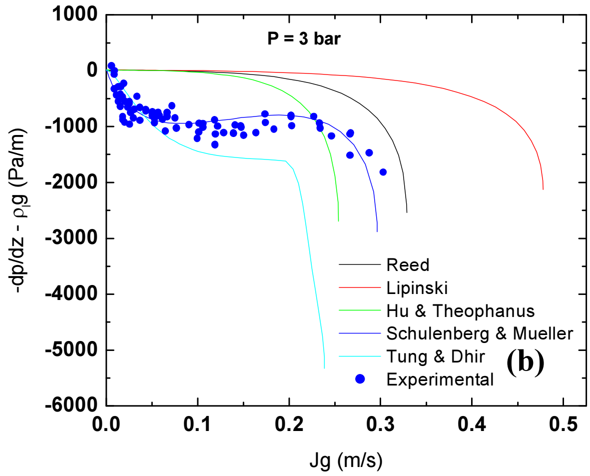

Figure 5.10 Predicted pressure drops under top flooding condition at 1 and 3 bar

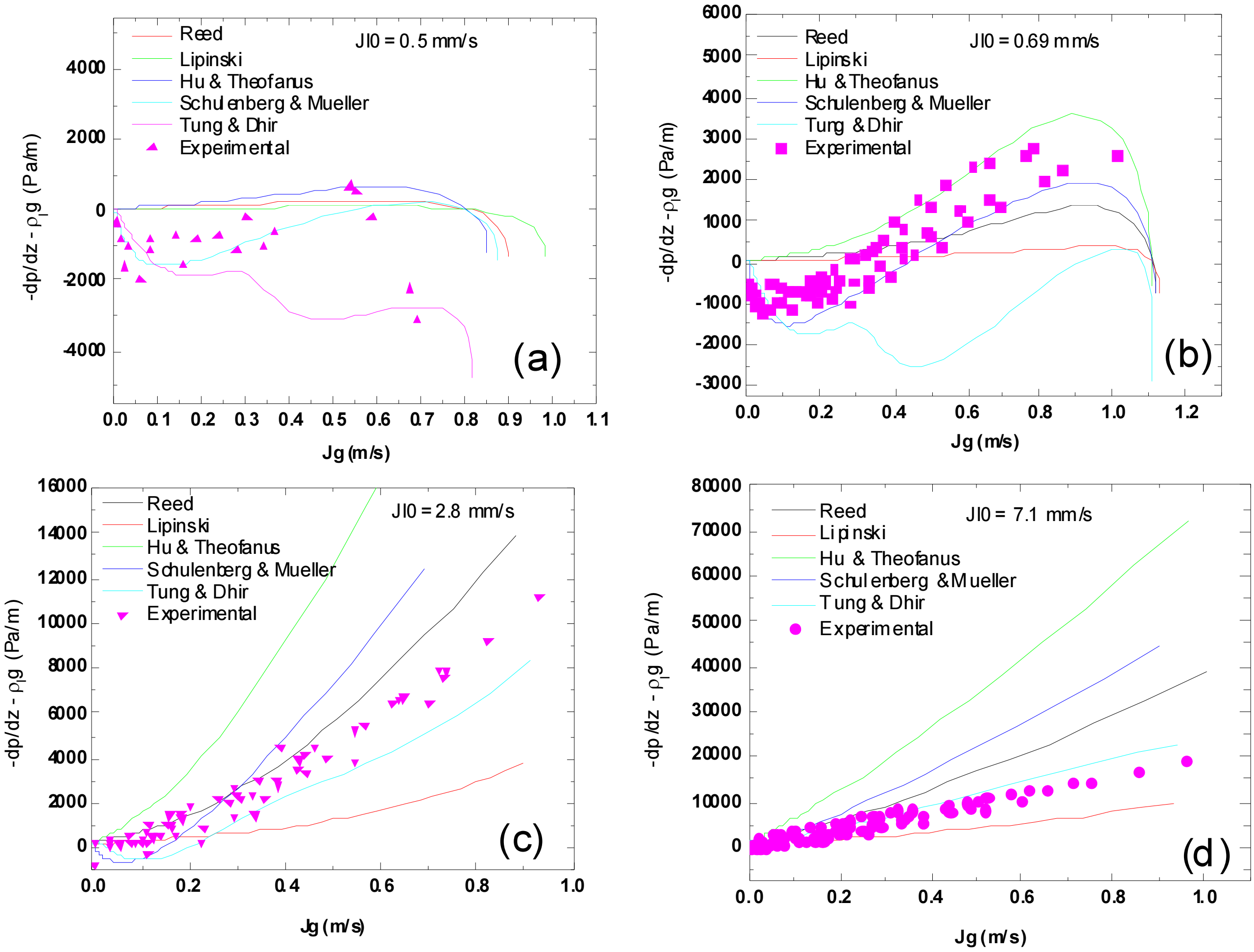

Figure 5.11 Predicted pressure drops under bottom flooding condition at 1 bar

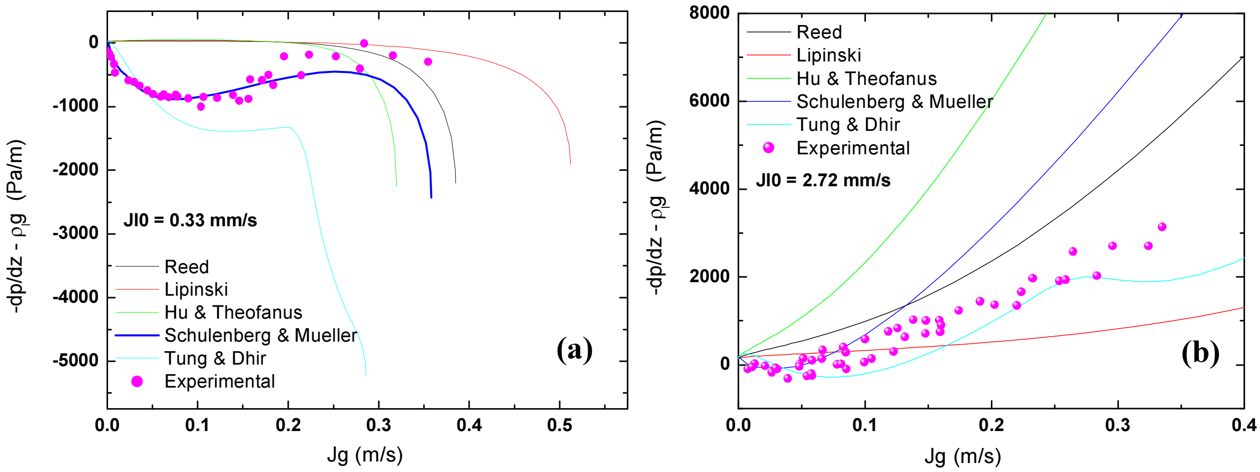

Figure 5.12 Predicted pressure drops under bottom flooding condition at 3 bar

5.4 Summary

In order to study the coolability of realistic debris beds, boiling and dryout experiments at top- and bottom-flooding flow conditions and different system pressures were carried out on debris beds consisting of irregularly shaped particles. The main findings are:

- For top flooding and bottom-flooding with very low inflow rates, the pressure gradient shows a typical lying S-shaped curve, indicating counter-current flow characteristics, where the vapour-liquid interfacial drag is important.
- For bottom-flooding with relatively high inflow rates, the particle-liquid drag becomes more dominant, the pressure gradient increases consistently with vapour velocity.
- The increase in system pressure substantially enhances the dryout heat flux. Also, the dryout is found to occur at upper location of the bed.
- Introducing a small bottom inflow brings about similar changes in dryout behaviour as an increase in system pressure, i.e. higher dryout heat fluxes and shifting dryout area to even higher location. In this context the inlet water temperature has significant effect on dryout time in bottom-flooding condition.
- Several classical 1-D models were applied to predict pressure drop characteristics and dryout heat fluxes.
- The modified model of Schulenberg & Müller with explicit consideration of interfacial drag between liquid and vapour phases is more suitable for top-flooding and low inflow rate bottom-flooding, whereas the models without interfacial drag like Reed model can better predict bottom-flooding with relatively high inflow rates.

6. Development of a core catcher for an advanced reactor

6.1 Introduction

In the previous chapters, models have been presented on melt coolability under top and bottom flooding, pressure drop and dryout heat transfer in porous heat generating debris beds. In this chapter, an integrated model has been presented which can simulate the coolability of molten pool in an ex-vessel situation in actual reactor condition. A conceptual design of a core catcher for a boiling light water cooled reactor has also been presented and its performance analysis has been evaluated.

6.2 Concept of a core catcher

In the event of complete core melt accident in a natural circulation light water cooled BWR, a core catcher has been conceptualized to terminate the severe accident progression and to quench the corium in the stipulated time besides providing long term cooling to the corium.

The design basis of the core catcher is

- Retention of the whole core melt in the cavity
- Quenching the molten mass within 30 minutes time
- Provide long term cooling for stabilization of the melt

The core catcher consists of a sacrificial concrete layer, high porosity concrete layer, riser tubes embedded in the sacrificial concrete, water pool and two down-comers from overhead tank supplying water to the water pool passively as shown in Figure 6.1 and Figure 6.2

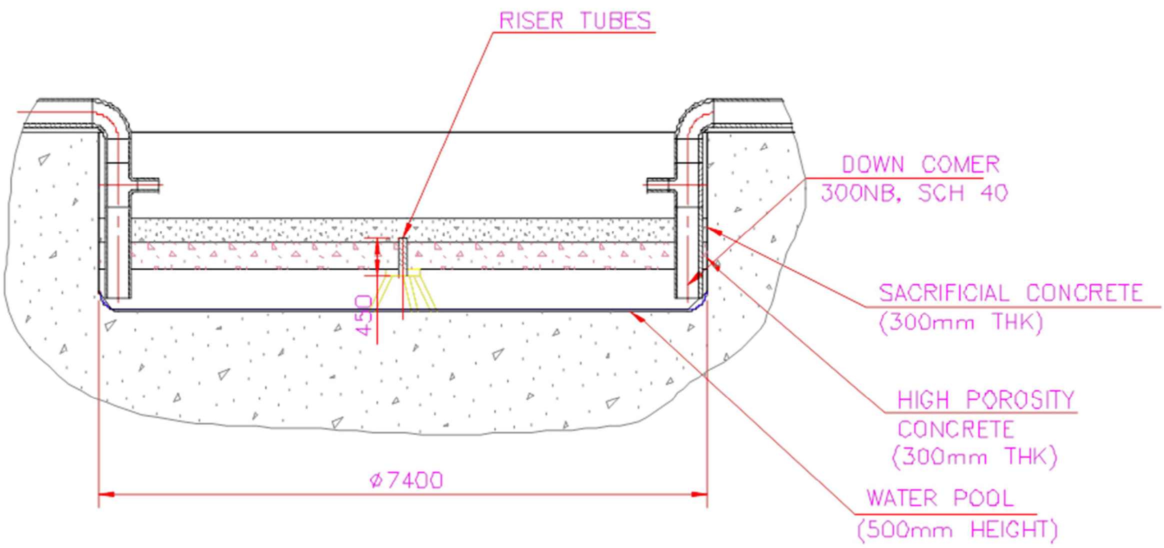

Figure 6.1 Schematic of the core catcher

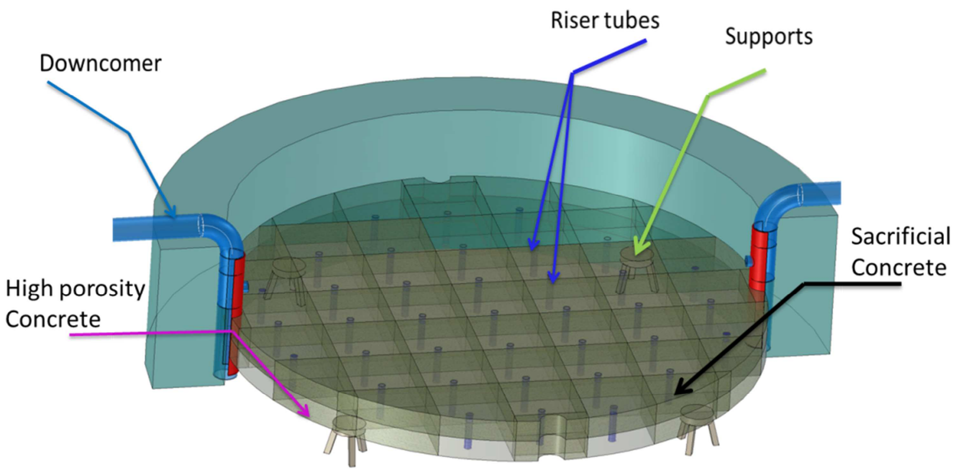

Figure 6.2 3-D layout of the core catcher

6.3 Phenomena taking place during cooling in core catcher

Molten core (corium) falls on the sacrificial concrete layer and causes its ablation. Mixing of concrete in the melt brings down its melting temperature drastically, changes its properties like density, viscosity which assists the corium-concrete mixture spreading on the large surface area. The melting of a large volume of the sacrificial material in the corium reduces the specific volumetric heat release. The endothermic interaction between the corium melt and the sacrificial material reduces a general temperature level in the final melt. As the sacrificial concrete is eroded, the corium comes to the level of the riser tubes near the high porosity concrete layer. By this time, corium is then flooded with water from bottom through the riser tubes. Flooding from bottom ensures porosity formation in the melt which can be cooled easily.

6.4 Integrated model for coolability of molten pool by bottom flooding

An integrated model has been developed for performance analysis of the core catcher considering following phenomena

- Molten core – concrete interaction (MCCI) which includes
    - Thermochemical interaction inside concrete
    - Concrete ablation
    - Mixing of corium – concrete and change in properties
- Bottom injection when the required ablation has taken place
- Coolability of melt/debris

Models for above phenomena are as presented below

6.4.1 Modeling of MCCI

A model has been developed for predicting the ablation of concrete, and evolution of gases due to thermal decomposition of concrete under heat load. The domain is as given in Figure 6.3

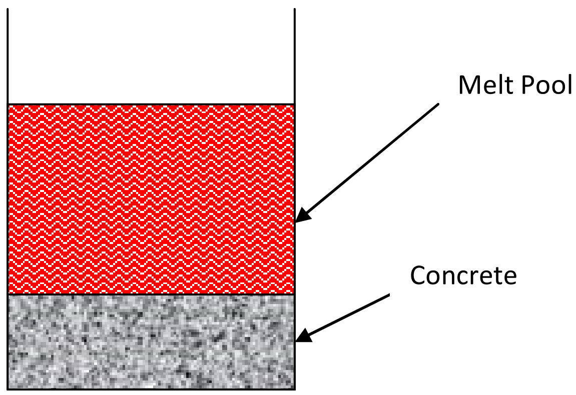

Figure 6.3 Domain for MCCI model

6.4.1.1 Governing Equations

2-D transient conduction equation in melt pool:

$$\rho C_p \frac{\partial T}{\partial t} = \frac{\partial}{\partial x}\left(k\frac{\partial T}{\partial x}\right) + \frac{\partial}{\partial y}\left(k\frac{\partial T}{\partial y}\right) + q''' \tag{6.1}$$

2-D transient conduction equation in Concrete layer:

$$\rho_{con} C_{p_{con}} \frac{\partial T_{con}}{\partial t} = \frac{\partial}{\partial x}\left(k\frac{\partial T_{con}}{\partial x}\right) + \frac{\partial}{\partial y}\left(k\frac{\partial T_{con}}{\partial y}\right) \tag{6.2}$$

Boundary conditions:

$$T_{i_{pool}} = T_{i_{concrete}}$$ Temperature continuity

$$k_p \left.\frac{\partial T}{\partial z}\right|_{pool} = k_{cn} \left.\frac{\partial T}{\partial z}\right|_{concrete}$$ Flux continuity

- Thermochemical reactions taking place during MCCI
  - At **T >100 ^{o}C:** Loss of evaporable water

$$H_2O_{(l)} \longrightarrow H_2O_{(g)} \quad \Delta H = 2258\, kJ/kg \tag{6.3}$$

  - **T ~ 500 - 600 ^{o}C**: Dehydration of $Ca(OH)_2$

$$Ca(OH)_2 \longrightarrow CaO + H_2O_{(g)} \quad \Delta H = 1340\, kJ/kg \tag{6.4}$$

  - **T > 750 ^{o}C:**Decomposition of lime

$$CaCO_3 \longrightarrow CaO + CO_{2(g)} \quad \Delta H = 1637\ kJ/kg \tag{6.5}$$

  - Melting of Concrete at about **1400 deg C**
  - Oxidation of Zirconium at temperatures of the order > 900 ^{O}C

$$Zr + 2H_2O \longrightarrow ZrO_2 + 2H_2 \quad \Delta H = -6300\, J/gZr \tag{6.6}$$

6.4.1.2 Solution Strategy:

Enthalpy Temperature hybrid method

The equations can be written in form of enthalpy-temperature hybrid form as follows

$$\rho_{con}\frac{\partial(h_{con})}{\partial t}=\frac{\partial}{\partial x}\left(k\frac{\partial T_{con}}{\partial x}\right)+\frac{\partial}{\partial y}\left(k\frac{\partial T_{con}}{\partial y}\right) \tag{6.7}$$

This method allows us to

1) Take into account the Cp of concrete as a strong function of temperaturewhich is converted into h = f(T) = $\int cpdT$ to take into account all the chemical reactions as shown in Figure 6.4 and Figure 6.5

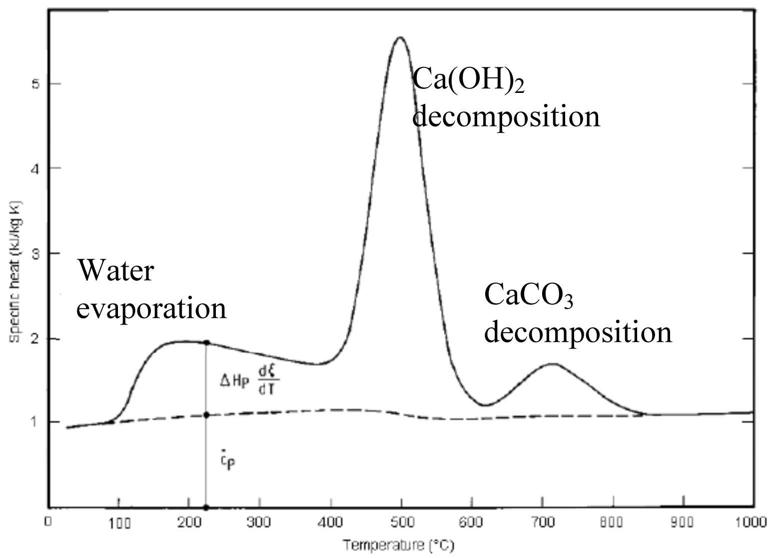

Figure 6.4 Cp vs Temperature of concrete

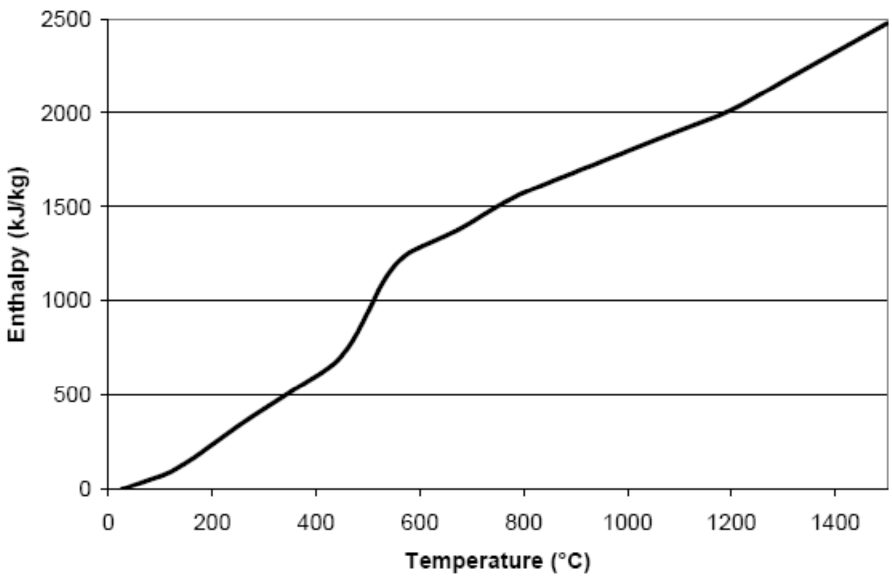

Figure 6.5 Enthalpy vs temperature for concrete

2) Ease in tracking the melt front in the concrete as enthalpy is continuous even though concrete may melt at different temperature.

The interface is tracked as follows:

If $h_{i,j}^{n} > h_{T_{solidus}} + \dfrac{h_{fusion}}{2}$ and $h_{i,j}^{n+1} < h_{T_{solidus}} + \dfrac{h_{fusion}}{2}$

$x = \dfrac{\dfrac{h_{fusion}}{2} + h_{solidus}}{h_{i,j}^{n+1} - h_{i,j}^{n}}$ which will give the contour position

These enthalpy-temperature relationships are specific for each type of concrete. There are three main types of concrete which can be taken into account.

1) Haematitic aggregates
2) Basaltic aggregates
3) Limestone and Common Sand (LCS)

The libraries contain the information regarding enthalpy – temperature data, density, thermal conductivity and mole fraction of main components of the concrete.

Figure 6.6 shows the difference in ablation for different concretes under same thermal load.

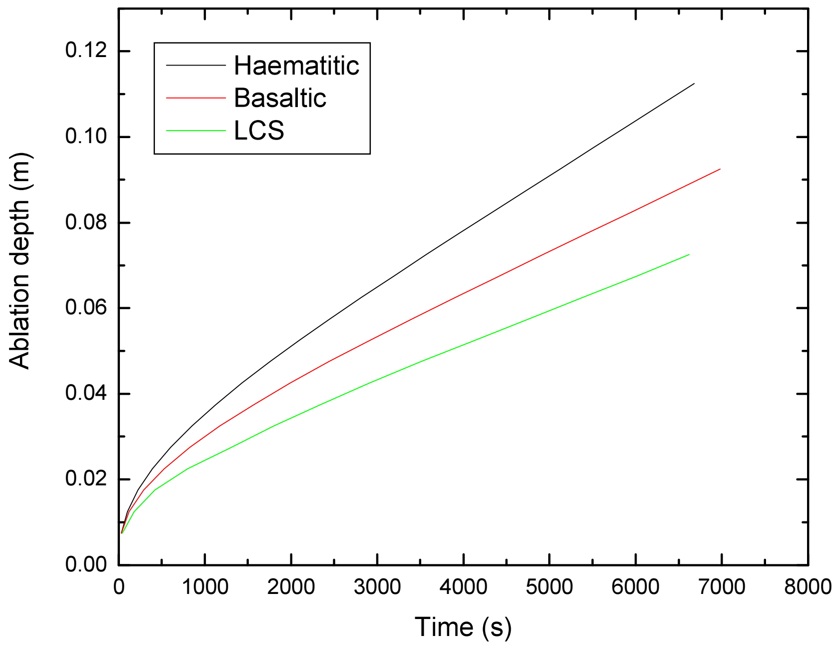

Figure 6.6 Ablation depths for different concretes

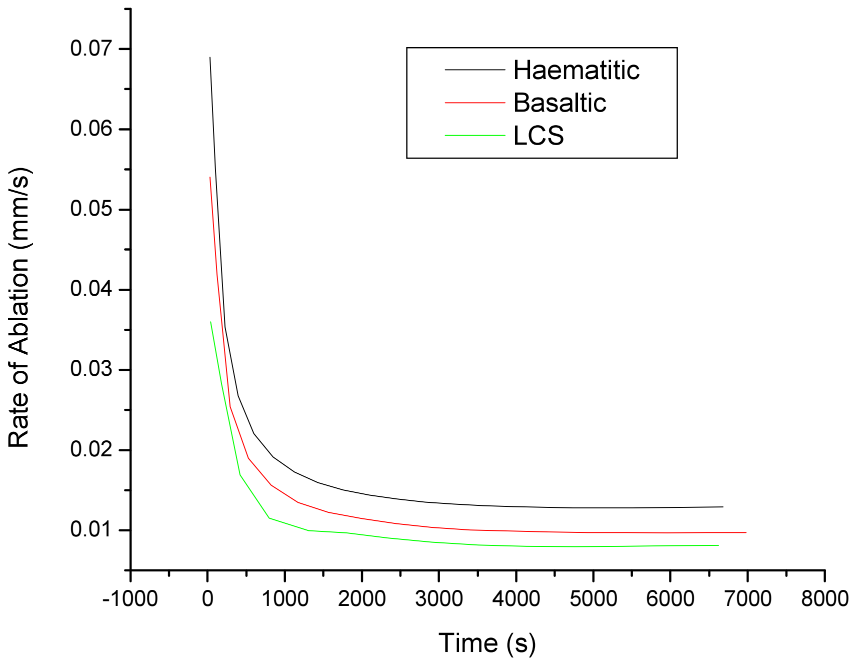

Figure 6.7 Ablation rates

From Figure 6.7, it is clear that Haematitic concrete has highest ablation rate which is helpful in bringing the concrete temperature down and spread it over large area quickly, hence it can be chosen in reactor configuration.

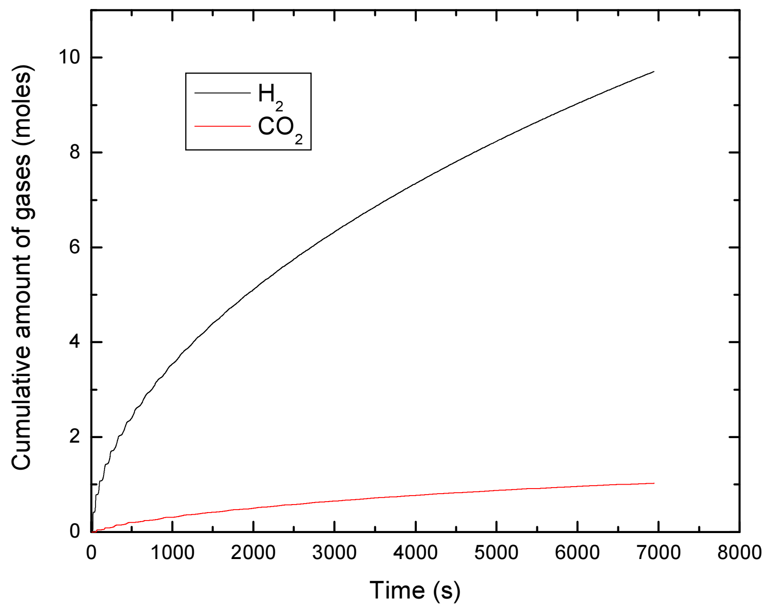

Figure 6.8 Non condensable gases evolution

Figure 6.8 gives the cumulative amount of non-condensable gases evolved during the MCCI progression. Using this, we can obtain the velocity of gases evolving at a particular time which can be used subsequently to determine its effect on Dryout heat flux.

6.4.1.3 Validation of MCCI model

The MCCI model has been validated using the ACE-L5 [72] and COTELS D8 [73] experiment where the known ablation data was available for a concrete under given thermal load. (Figure 6.9 Figure 6.10)

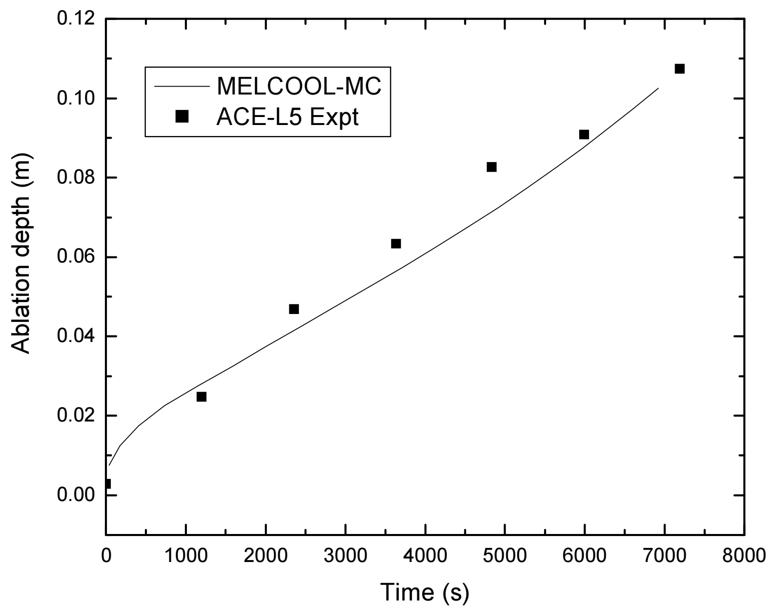

Figure 6.9 Validation with ACE L5 test

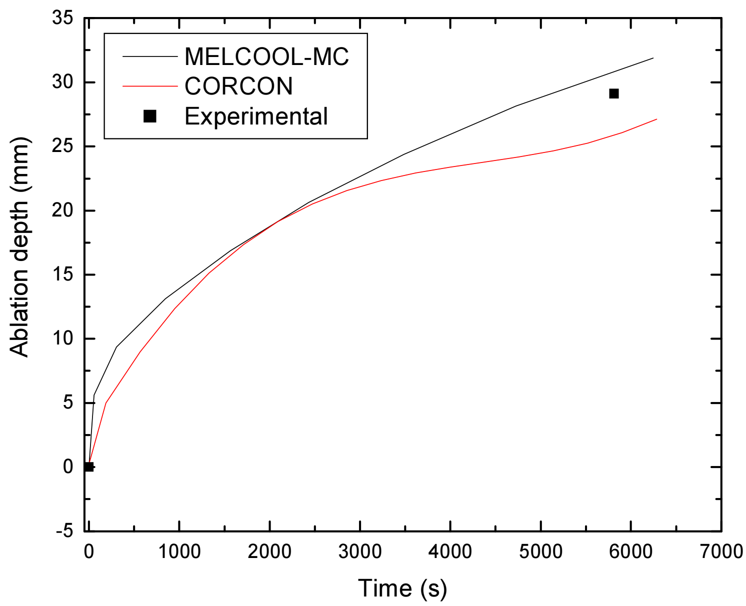

Figure 6.10 Validation with COTELs test D8-a

The model seems to be predicting the ablation in good agreement

6.4.2 Change of properties as a result of concrete addition

1) **Density:** The mixture density is evaluated by following formula

$$\rho_{mix} = \frac{\sum x_i M_i}{\sum \frac{x_i M_i}{\rho_i}} \tag{6.8}$$

Where x_i is the mole fraction of the component, M_i is the molecular weight and ρ_I is the density of the individual component

2) Specific Heat capacity:

$$Cp_{mix} = \sum x_i Cp_i \tag{6.9}$$

3) Thermal conductivity

$$k_{mix} = \sum x_i k_i \tag{6.10}$$

4) Heat of Fusion:

$$\Delta H_{fus,mix} = \sum x_i \Delta H_{fus,i} \tag{6.11}$$

5) Solidus and liquidus temperature: The solidus and liquidus temperature of the corium mixture containing UO_2 and ZrO_2 only is determined by the UO_2-ZrO_2 phase diagram given by Lam-Mueller. Then, due to addition of concrete, the change in solidus and liquidus is expressed in terms of the solid factor as given by Roche et al. as

$$T_{sol,mix} = T_{sol} + f * (T_{m,con} - T_{sol}) \tag{6.12}$$

Where, $T_{sol,mix}$ is solidus temperature of the mixture, $T_{m,con}$ is concrete melting point and *f* is the concrete solid factor. The value of *f* is obtained from experimental data by Roche et al as given by Epstein [74] as given in Figure 6.11

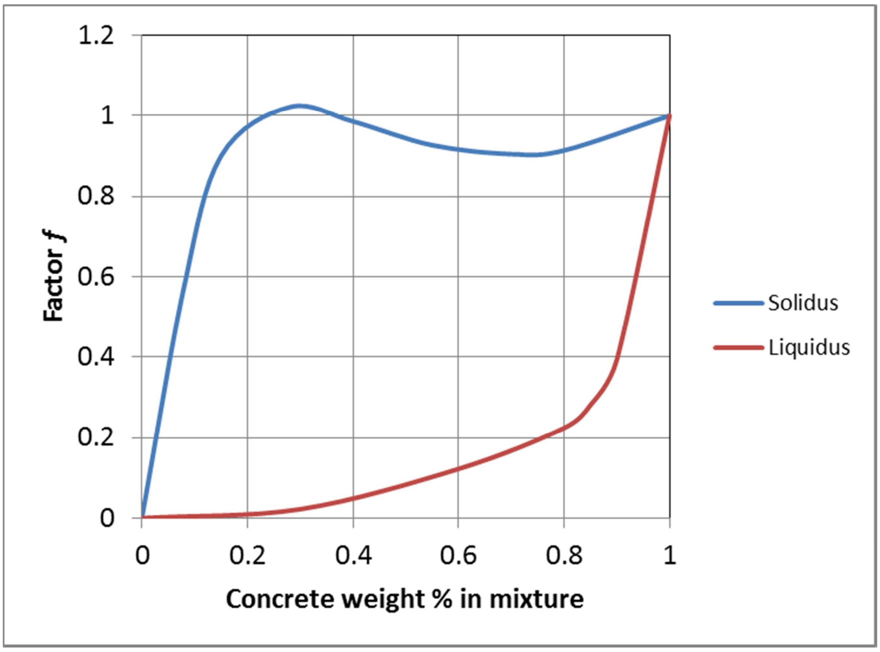

Figure 6.11. Determination of factor *f* for solidus and liquidus temperature of corium concrete mixture

6.4.3 Coolability of Corium under Bottom flooding:

Subsequent to the desired ablation has taken place, water is flooded from bottom. For prediction of the coolability, the bottom flooding model as given from equation 3.1 to 3.18 is used except equation 3.3. Instead, the two phase pressure drop in the debris bed as given by Schulenberg and Mueller model (Equation 5.9-5.11) is used.

6.5 Performance Analysis of the core catcher.

Performance analysis of the core catcher was carried out for a hypothetical accident scenario in a natural circulation tube type light water cooled BWR.

Assumptions:

- Whole core melt accident has been considered.
- 100 % Zr has been oxidized and No U-Zr-O reaction considered.
- The core melt consisting of only UO_2, ZrO_2 and structural steel of properties as given in Table 6.1 has been considered.
- The melt is assumed to be spreading uniformly over the core catcher

Table 6.1 Melt composition

	Value
Mass of melt	194 tonnes
Density	8000 kg/m^3
Melt height	0.6 m
Melt constituent	64 % UO_2, 5 % ZrO_2 (Inv15 % Unreacted Zr (PT/CT), Balance SS
Melt Initial Temperature	2900 K

The domain for analysis is as given in Figure 6.12. The computational domain is as shown. In x direction, 10 grids have been taken and in y direction, for melt, 30 grids and for each concrete block 10 grid points were taken.

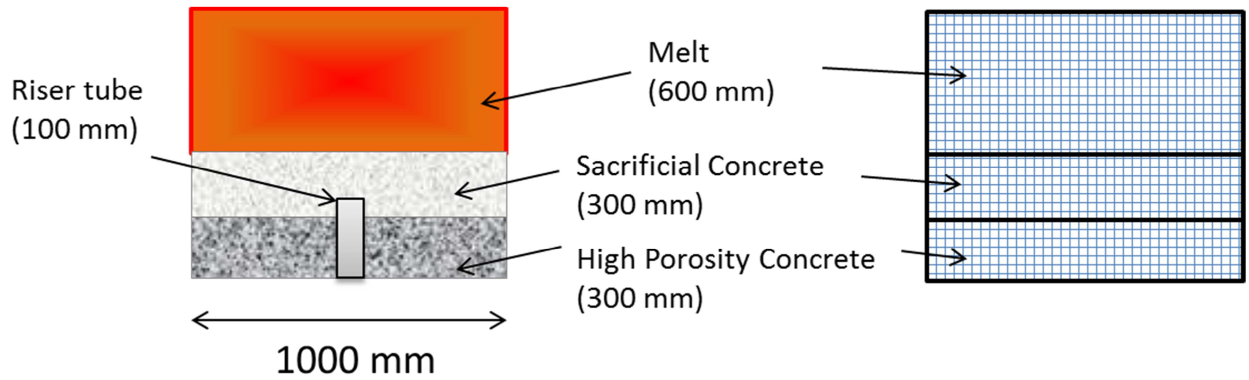

Figure 6.12 Domain for analysis: actual and computational

Results and discussion

Figure 6.13 shows the change in solidus and liquidus temperature of the melt as result of concrete addition. It is observed that, addition of about 20 % concrete by weight reduces the solidus temperature of the melt to as low as 1400 K.

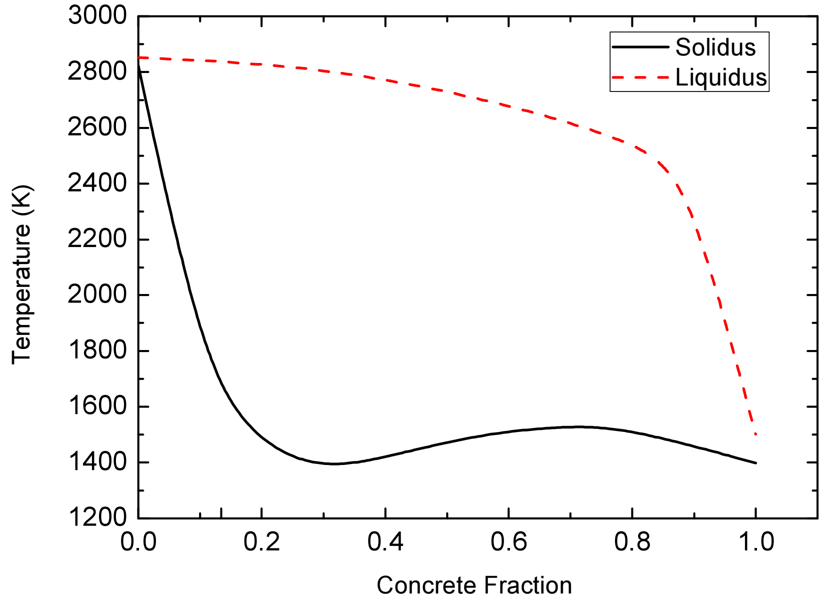

Figure 6.13 Solidus and liquidus temperature change as a result of concrete addition

Figure 6.14 shows the predicted temperature inside concrete layer. As the time progresses, different layers in concrete get ablated and mix with the melt which is at liquidus temperature. As a result of concrete addition, the liquidus temperature reduces from 2910 K to 2820 K. It takes about 3000 s to ablate the concrete upto 180 mm depth which is designated depth to start the flooding of water. Figure 6.15 shows that, the ablation is much above the high porosity concrete.

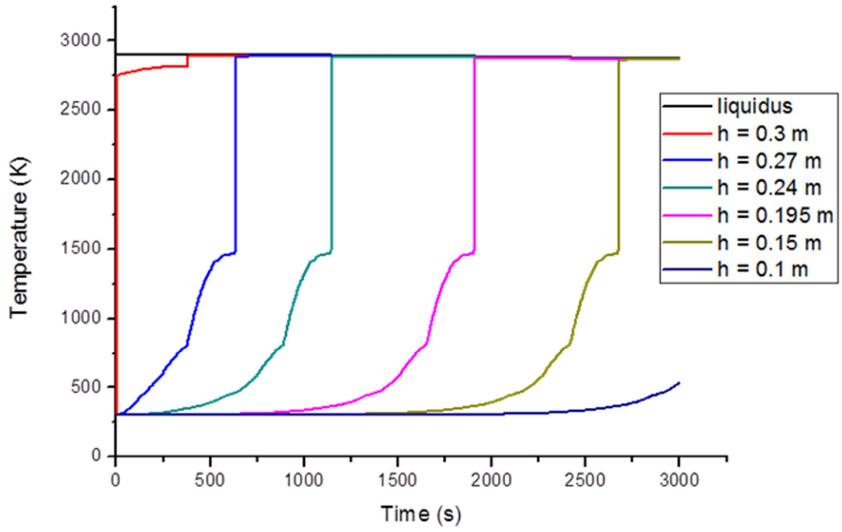

Figure 6.14 Concrete temperatures

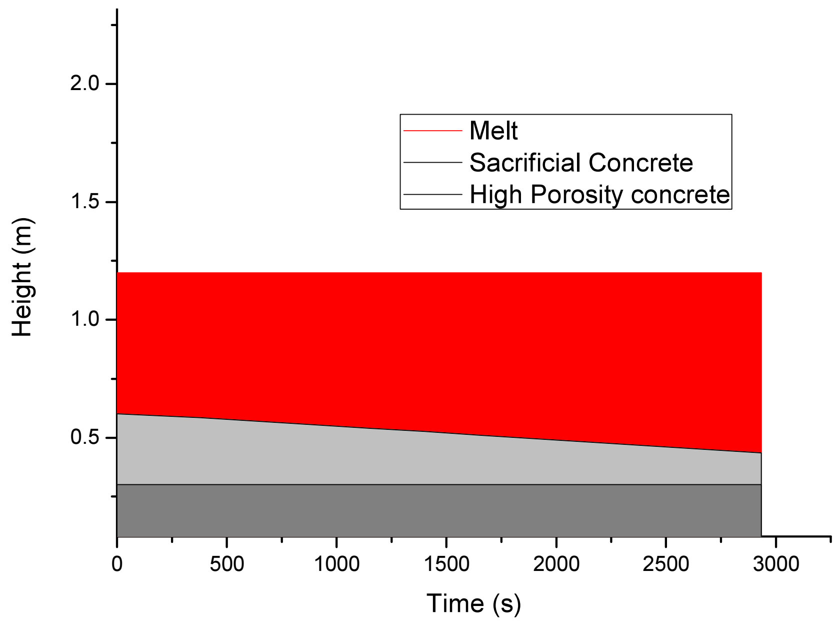

Figure 6.15 Ablation depth

The ablation with time is shown in Figure 6.16. During MCCI, lot of water vapour and CO_2 are generated. Figure 6.17 shows the amount of water vapour and CO_2 liberated during this reaction.

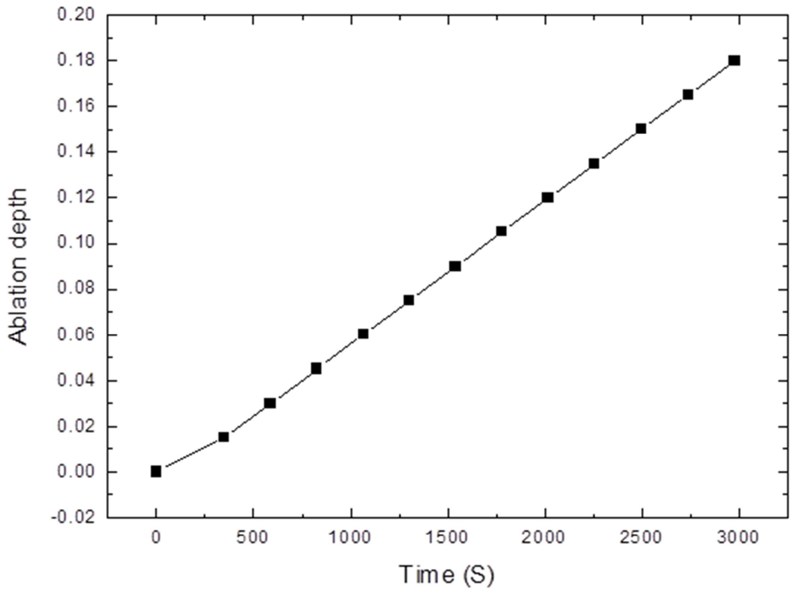

Figure 6.16 Concrete ablation

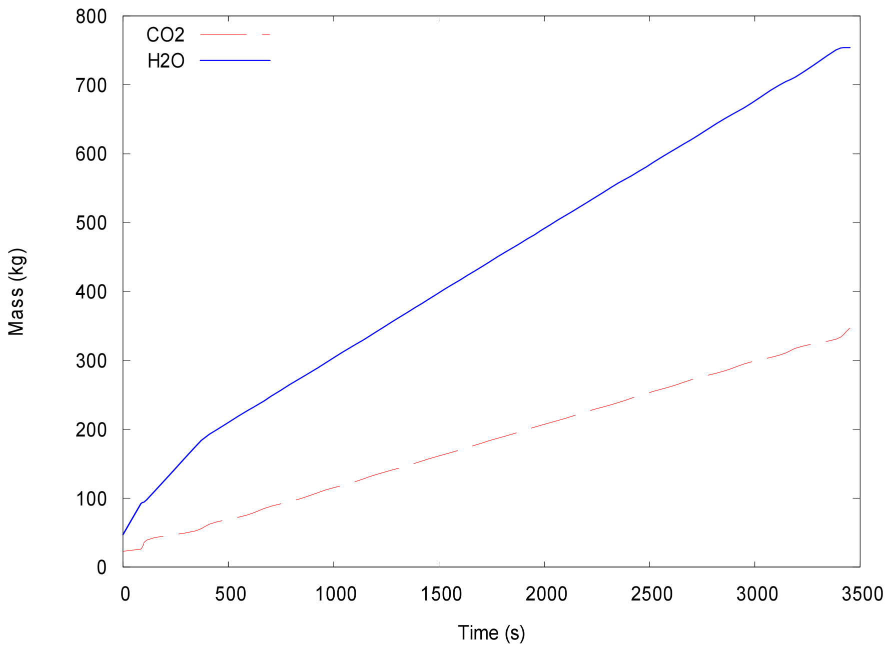

Figure 6.17 Water vapour and CO2 generated during MCCI

After the desired ablation has taken place, water is flooded from bottom. The bottom flooding model is activated. It is predicted that, within few seconds, the melt eruption takes place inside the melt. The resulting debris characteristics are given in
Table 6.2.

Table 6.2. Characteristics of debris post flooding

Parameter	Experimental
Diameter of eruption zone	1.3 m (Complete debris formation)
Maximum pressure pulse	1.4 bar
Debris porosity	0.4

It is assumed that the average debris particle size is 3 mm based on earlier experimental results. After the water is flooded, the temperature of the corium concrete mixture is drastically reduced. The model predicts complete coolability in 1000 s (total time 4000 s) by flooding it from bottom as shown in Figure 6.18. During the flooding, lot of steam is evolved. The steam flow rate is as given in Figure 6.19. Initially the steam flow rate is very high as the melt temperatures are high. After some time as the melt temperature reduces, the steam flow rate also reduces.

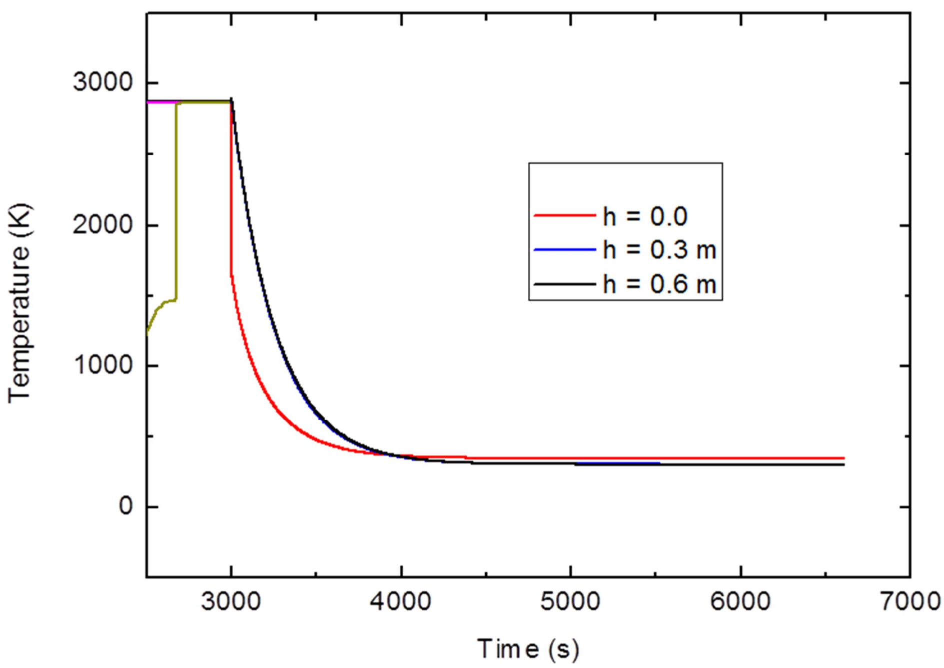

Figure 6.18 Temperature in corium concrete mixture post flooding

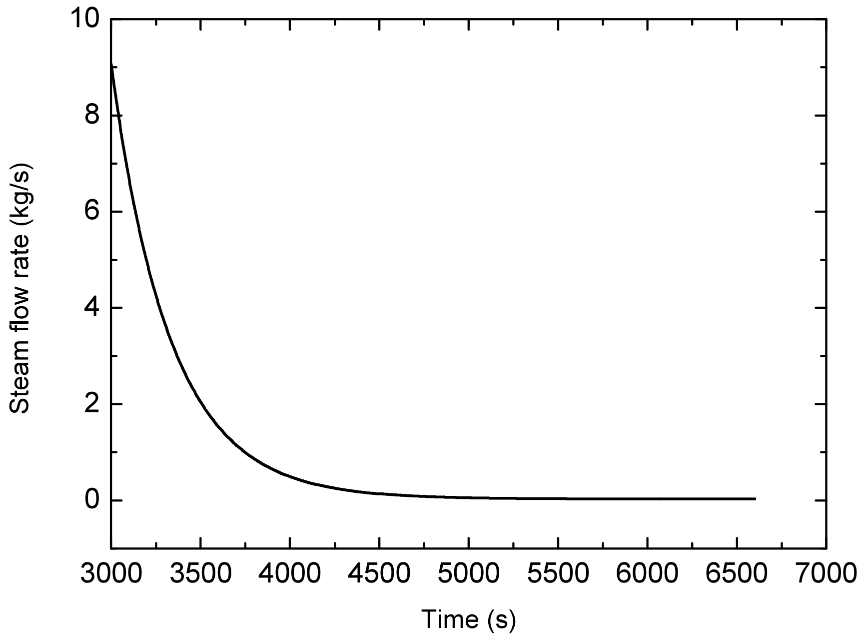

Figure 6.19 Steam flow rate during flooding

6.6 Summary

In this chapter, an integrated model has been presented for performance analysis of the core catcher during accidental condition. The model considers the molten core concrete interaction, concrete ablation, coolability of the molten pool/debris bed under bottom flooding condition. The model has been used for analysis of a natural circulation light water cooled BWR under accident condition. The model predicts complete coolability of the melt within 1000 s.

7. Conclusions and Recommendations

In this study, physics of coolability of top and bottom flooded molten corium pool with molten core –concrete interaction was brought out. The mechanism of coolability under top and bottom flooding was determined, quantification of the coolability was done, process parameters affecting the coolability were determined and finally, coolability in reactor severe accident conditions was predicted. Following conclusions were drawn from the study:

In Chapter 2, melt coolability under top flooding was studied. Following lessons were learnt from the study

- Water ingression plays an important role in melt coolability under top flooding
- Water ingression occurs when the thermals stresses in the crust exceeds the strength and fractures
- Extent of water ingression is determined by a dimensionless parameter $E\alpha/\sigma$
- Higher is the parameter, more is the coolability
- The physics of water ingression in top flooding has been successfully shown by our model
- Top flooding is not a reliable strategy to establish complete cooling

Subsequently, in Chapter 3, Melt coolability under bottom flooding was studied. Lessons learnt from the study were as follows

- When flooded from bottom, because of steam pressurization and subsequent eruption through melt, porous zones are formed.
- Water and steam pass through this zones taking away heat, hence complete coolability can be achieved
- Our model has captured the physics of melt coolability under bottom flooding

- After flooding from bottom, a porous zone of particles ranging from very fine mm to 10 mm were obtained with a porosity of 51 %
- Melt coolability under bottom flooding is scaled by thermal hydraulic parameters like inlet water temperature, pressure and the melt superheat.

In Chapter 4, Melt coolability under different strategies was presented to establish a comparison of different cooling mechanisms. From the study, it was concluded that,

- In indirect cooling, it took long time to cool the melt as a crust formed between melt pool and vessel acted as an insulation and resulted into poor heat removal
- Bottom flooding is the most effective technique for quenching the molten pool in case of ex vessel severe accident scenarios.

Subsequent to quenching of the melt, a heat generating debris bed is formed. In Chapter 5, coolability of Debris bed under top and bottom flooding condition was studied. The lessons learnt from the studies were

- In order to study the coolability of realistic debris beds, boiling and dryout experiments at top- and bottom-flooding flow conditions and different system pressures were carried out on debris beds consisting of irregularly shaped particles
- For top flooding and bottom-flooding with very low inflow rates, the pressure gradient shows a typical lying S-shaped curve, indicating counter-current flow characteristics, where the vapour-liquid interfacial drag is important.
- For bottom-flooding with relatively high inflow rates, the particle-liquid drag becomes more dominant, the pressure gradient increases consistently with vapour velocity.
- The increase in system pressure substantially enhances the dryout heat flux. Also, the dryout is found to occur at upper location of the bed.
- Introducing a small bottom inflow brings about similar changes in dryout behaviour as an increase in system pressure, i.e. higher dryout heat fluxes and shifting dryout area to

even higher location. In this context the inlet water temperature has significant effect on dryout time in bottom-flooding condition.

- Several classical models were applied to predict pressure drop characteristics and dryout heat fluxes.
- The refined model of Schulenberg & Müller with explicit consideration of interfacial drag between liquid and vapour phases is more suitable for top-flooding and low inflow rate bottom-flooding, whereas the models without interfacial drag like Reed model can better predict bottom-flooding with relatively high inflow rates.

Finally, as an outcome of the research work, development of a core catcher for an advanced reactor was presented in Chapter 6 with lessons learnt as follows

- An integrated model was developed for performance analysis of the core catcher which considers the molten core concrete interaction, concrete ablation, coolability of the molten pool/debris bed under bottom flooding condition
- The model predicts complete coolability for whole core melt within 1000 s.

Recommendation for future work

- In the current model for water ingression, the phenomenon of gap formation between the crust and the pool below is not considered. In future, advanced model may be developed considering the gap formation, gas generation during MCCI, and pressurization of the crust from bottom.
- At present, there is a single model for prediction of porosity which has been used in the current model. There is a need of development of generalized model for determination of porosity based on the enhancement factor (Ψ). For this, lot of small scale experiments are needed with different melt superheats and water inlet condition.

- For proper validation of the integrated model presented in chapter 3, data of integrated experiments having MCCI as well as coolability on bottom flooding is needed.
- For heat transfer and pressure drop in debris beds, models in literature were assessed. However, these models are typically one dimensional in nature which neglect multidimensional nature of the debris beds formed in actual reactor conditions. Hence is a need to develop models pertaining for actual debris beds. For this, there is a need of large amount of experimental data on multidimensional heat transfer in debris bed which demands comprehensive experimental program in the area of debris bed coolability

References

[1] M. Rogovin and G. T. Frampton, “Three Mile Island: A Report to the Commissioners and to the Public” NUREG/CR-1250, vols. I-II, (1980)

[2] IAEA, INSAG-7, “The Chernobyl Accident: Updating of INSAG-1” SAFETY SERIES No. 75-INSAG-7 (1992).

[3] IAEA, “IAEA International Fact Finding Expert Mission of the Fukushima Dai-Ichi NPP Accident Following the Great East Japan Earthquake and Tsunami” IAEA Mission Report (2011).

[4] Sehgal, B.R., 2000. Remaining issues in severe accident safety research. Proceedings of the OECD/NEA RASPLAV Project Seminar, Munich, November. 14–15

[5] Sehgal, B. R. 2006 , “Stabilization and termination of severe accidents in LWRs”, Nuclear Engineering and Design, 236, 1941–1952

[6] K. R. Robb, “Melt Eruptions during Molten Corium Concrete Interactions”, Ph.D. Thesis, University of Wisconsin- Madison, 2011.

[7] Farmer, M. T., Kilsdonk, D. J., Aeschlimann R. W., 2009. Corium Coolability Under Ex-Vessel Accident Conditions For LWRs, Nuclear Engineering and Technology, 41, 575-602.

[8] Alsemeyer, H., Spencer, B., and Tromm, W. 1998. The COMET concept for cooling of ex-vessel corium melts. ICONE-6, San Diego, USA.

[9] Sehgal, B.R., and Spencer, B.W., 1992, Ace Program Phase D: Melt attack and coolability experiments (MACE) Program. 2nd Specialist Meeting on Molten Core Debris – Concrete Interactions, Karlsruhe, Germany.

[10] Nagasaka, H., Kato, M., Sakaki, I., Cherepnin, Y., Vasilyev, Y., Kolodeshnikov, A., Zhdanov, V., Zuev, V., 1999 , “COTELS Project (1): Overview of Project to Study

FCI and MCCI During a Severe Accident," OECD Workshop on Ex-Vessel Debris Coolability, Karlsruhe, Germany, November 15-18,

[11] Blose, R. E., Gronager, J. E., Suo-Anttila, A. J., Brockman, J. E., 1987. "SWISS: Sustained Heated Metallic Melt/Concrete Interactions With Overlying Water Pools," NUREG/CR-4727

[12] Blose, R. E., Powers, D. A., Copus, E. R., Brockmann, J. E., Simpson, R. B., Lucero, D. A. 1993. "Core-Concrete Interactions with Overlying Water Pools - The WETCOR- 1 Test," NUREG/CR-5907

[13] Farmer, M.T., Aeschlimann, R.W., Kilsdonk, D.J., and Spencer, B.W. 2000. Results of MACE Test M3b posttest debris characterization. ACEX-TR-31.

[14] Nayak, A. K., Sehgal, B. R., Rao, R.S., 2005. Study on Water Ingression Phenomenon in Melt Coolability, The 11th International Topical Meeting on Nuclear Reactor Thermal-Hydraulics (NURETH-11) Paper: 449, Avignon, France.

[15] Farmer, M.T., Lomperski, S., and Basu, S. 2004. Results of reactor material experiments investigating 2-D core-concrete interaction and debris coolability. Proceedings of ICAPP-04, June 13-17, Pittsburg, USA.

[16] Alsmeyer, H., and Tromm, W., 1995. Concept of a core cooling system and experiments performed, Nucl. Engg. Des. 154, 69-72.

[17] Alsmeyer, H., Farmer, M., Ferderer, F., Spencer, B., Tromm, W., 1998. The COMET concept for cooling of ex-vessel corium melts. In: ICONE-6, San Diego, CA, May 10–14, paper 6086.

[18] Tromm, W., Alsmeyer, H., Schneider, H.,1993. Fragmentation of Melts by Water Inlet From Below. The 6th International Topical Meeting on Nuclear Reactor Thermal-Hydraulics NURETH-6 Grenoble, France.

[19] Foit, J.J., Bürger, M., Journeau, C., Alsmeyer, H., Tromm, W., 2008. Quenching ofmelt layers by bottom injection of water in the COMET core-catcher concept. In:European Review Meeting Severe Accident Res., ERMSAR, Nessebar, Bulgaria,23–25 September.

[20] Paladino, D., Theerthan, A. , Sehgal,B. R., 1999a. Experimental Investigation on Debris Coolability by Bottom Injection, ANS, Annual Meeting, Boston, USA

[21] Paladino, D., Theerthan, A., Yang, L. Sehgal,B. R., 1999b. Experimental Investigations on Melt-Coolant Interaction Characteristics During Debris Cooling by Bottom Injection, OECD Workshop on Ex-Vessel Debris Coolability, Karlsruhe, Germany.

[22] Widmann, W., Bürger, M., Lohnert, G., Alsmeyer, H., Tromm, W., 2006. Experimental and theoretical investigations on the COMET concept for ex-vessel core melt retention. Nucl. Eng. Des. 236, 2304–2327.

[23] Cho, D.H., Page, R.J., Abdulla, S.H., Anderson, M.H., Klockow, H.B., Corradini, M.L., 2006. Melt quenching and coolability by water injection from below: co-injection of water and noncondensable gas. Nucl. Eng. Des. 236, 2296–2303.

[24] Lomperski, S., Farmer, M.T., 2012. Performance testing of engineered corium cooling systems, Nucl. Engg. Des. 243, 311– 320

[25] Hu, K., Theofanous, T.G., 1991a. On the measurement and mechanism of dryout in volumetrically heated coarse particle beds. Int. J. Multiphase Flow 17, 519–532.

[26] Hofmann, G., 1984. On the location and mechanisms of dryout in top-fed and bottom-fed particulate beds. Nucl. Technol. 65, 36–45.

[27] Reed, A.W., Boldt, K.R., Gorham-Bergeron, E.D., Lipinski, R.J., Schmidt, T.R., 1985. DCC-1/DCC-2 Degraded Core Coolability Analysis. Technical Report NUREG/CR- 4390, SAND85-1967.

[28] Lipinski., R.J.1981. A one dimensional particle bed dryout model. ANS Transactions, Vol. 38: 386-387.

[29] Decossin. E. 1999. Experimental investigations on particulate debris bed coolability in a multi-dimensional configuration. In OCDE/CSNI-Workshop on EX-VESSEL DEBRIS COOLABILITY, 16-18 Nov.

[30] Atkhen K., G. Berthoud, 2006. SILFIDE experiment: Coolability in a volumetrically heated debris bed, Nuclear Engineering and Design, 236, 2126–2134.

[31] Sehgal, B.R., Konovalikhin, M.J., Yang, Z.L, Kazachkov, I.V., Amjad, M.and Li, G.J. 2001.Experimental Investigations on Porous Media Coolability, RIT/NPS Research report

[32] Jasiulevicius, A., Sehgal, B.R. 2003. Debris bed quenching with non-condensable gas addition from bottom. ICONE-11, 20–23 April.

[33] Nayak, A.K., Stepanyan, A. and Sehgal, B.R. 2004. Quenching Behaviour of a Volumetrically Heated Particulate Bed with Non-Condensable Gas Addition from Bottom. 42nd European Two-phase Flow Group Meeting, Genova, 23-25 June.

[34] S. Rahman, M. Buerger, M. Buck, G. Pohlner, R. Kulenovic, A. K. Nayak, B. R. Sehgal, "Analysis of Dryout Behaviour in Laterally Non-Homogeneous Debris Beds using the MEWA-2D Code", 13th International Topical Meeting on Nuclear Reactor Thermal Hydraulics (NURETH-13) Kanazawa City, Ishikawa Prefecture, Japan, September 27-October 2, 2009.

[35] Lindholm, I., Holmstroem, S., Miettinen, J., Lestinen, V., Hyvaerinen, J., Pankakoski, P., Sjoevall, H., 2006. Dryout heat flux experiments with deep heterogeneous particle bed. Nucl. Eng. Des 236, 2060–2074.

[36] Schäfer, P., Groll, M., Kulenovic, R. 2006. Basic Investigations on Debris Cooling. Nucl. Engg. Des. 236, 2104 2116.

[37] Lister, C. R. B., 1974, On the Penetration of Water into Hot Rock, Geophys. J. R. Astron. Soc., 39, 465-509.

[38] Bjornsson, H., et al., 1982, Penetration of Water into Hot Rock Boundaries of Magma at Crimsvotn, Nature, 295, 580-581.

[39] Jagla, E. A. and Rojo, A. G., 2002, Sequential Fragmentation: The Origin of Columnar Quasi-Hexagonal Patterns, Physical Review E, 65, 1-8.

[40] Epstein, M., 2006, Dryout Heat Flux during Penetration of Water into Solidifying Rock, J. Heat Transfer, 128, 847-850.

[41] Paladino, D, Theerthan, S. A., Sehgal, B. R., 2002. DECOBI: Investigation of Melt Coolability With Bottom Coolant Injection, Prog. Nucl. Ener, 40, pp. 161-206.

[42] Lipinski, R.J., 1982. A model for boiling and dryout in particle beds. Sandia National Laboratories, SAND 82-9765, NUREG/CR-2646.

[43] Reed, A.W., 1982. The effect of channeling on the dryout of heated particulate beds immersed in a liquid pool. PhD Thesis, Massachusetts Institute of Technology, Cambridge, USA.

[44] Hu, K., Theofanous, T.G., 1991. On the measurement of dryout in volumetrically heated coarse particle beds. Int. J. Multiphase Flow 17 (4), 519–532.

[45] Schulenberg, T., M¨uller, U., 1984. Zweiphasenstromung in Kugelschuttungen. Kernforschungszenrum Karlsruhe, KfK 3682.

[46] Tung, V.X., Dhir, V.K., 1988. A hydrodynamic model for two-phase flow through porous media. Int. J. Multiphase Flow 14 (1), 47–65.

[47] Schmidt, W. 2004, Influence of Multidimensionality and Interfacial Friction on the Coolability of Fragmented Corium, Ph.D. Thesis, Institut für Kernenergetik und Energie systeme, University of Stuttgart.

[48] Sinha, R., Nayak, A. K. and Sehgal, B. R., 2008, Modeling the Natural Convection Heat Transfer and Dryout Heat Flux in a Porous Debris Bed, ASME J. of Heat Transfer 130(10), 104503

[49] Berenson P.J., 1961, Film Boiling Heat Transfer from a Horizontal Surface, J. Heat Transfer, 83, 351-357.

[50] Rohsenow, W. H., 1952, A Method of Correlating Heat Transfer Data for Surface Boiling of Liquids, Trans. ASME, Vol. 74, 969-976.

[51] Ritchie R. D., Knott J. F. and Rice J. R., 1973, On the Relationship between Critical Tensile Stress and Fracture Toughness in Mild Steel, J. of Mechanics and Physics of Solids, Vol 21, 395 – 410.

[52] Beremin, F. M., 1983, "A local criterion for cleavage fracture of a nuclear pressure vessel steel", Metallurgical Transactions A, 14A, 2277-2287.

[53] Lomperski, S. and Farmer, M. T., 2007, Experimental Evaluation of the Water Ingression Mechanism for Corium Cooling, Nucl. Engg. & Design 237, 905-917.

[54] Timoshenko, S., and Woinowsky-Krieger, S., 1959. Theory of Plates and Shells, McGraw-Hill, New York.

[55] Zuber, N., 1958. On Stability of Boiling Heat Transfer, ASME Transaction, Vol. 80, pp. 711-720

[56] Khabensky, V. B.Granovsy, V. S.,Bechta, S. V., Gusarov, V. V. 2009, Severe accident management concept of the vver-1000 and the justification of corium retention in a crucible-type core catcher, Nuclear Engineering and Technology, 41, 561-574

[57] Westinghouse, 2009, AP1000 Pre-Construction Safety Report, https://www.ukap1000application.com/PDFDocs/Safety/UKP-GW-GL-732%20Rev%201.pdf

[58] Meneley, D.A., C. Blahnik, Rogers J.T.,. Snell V.G, Nijhawan, S, 1996, Coolability of Severely Degraded CANDU Cores, AECL 11110

[59] Wachowiak, R., 2006, Management of Severe Accident Phenomena in the ESBWR Design, Regulatory Information Conference, March 7, Session T2BC

[60] B.R Sehgal, A Theerthan, A Giri, A Karbojian, H.G Willschütz, O Kymäläinen, S Vandroux, J.M Bonnet, J.M Seiler, K Ikkonen, R Sairanen, S Bhandari, M Bürger, M Buck, W Widmann, J Dienstbier, Z Techy, P Kostka, R Taubner, T Theofanous, T.N D., 2003, "Assessment of reactor vessel integrity (ARVI)", Nuclear Engineering and Design, Vol. 221, pp 23-53

[61] Henry, R. E., Dube, D. A., 1994. Water in RPV: a mechanism for cooling debris in the RPV lower head, Proceedings of Specialist Meeting on Selected Containment Severe Accident Management Strategies, Stockholm, Sweden, June 13–15, pp. 93–104.

[62] Henry, R.E. 1996. A scaling and experimental approach for investigating in-vessel cooling, Proceedings of Twenty-Fourth Water Reactor Safety Information Meeting, Bethesda, MD, October 21–23, pp. 141–159

[63] X. Gaus-Liu, A. Miassoedov, T. Cron and T. Wenz, “The Coolibility of Melt Pool in PWR Lower Head – Results of LIVE Experiments” Journal of Energy and Power Engineering, Volume 4, No.3, 2010.

[64] Asmolov V. et al., "RASPLAV Application Report", OECD RASPLAV Seminar, Munich (Germany), 2000.

[65] Theofanous, T.G, Maguire, M., Angelini, S., Salmassi, T., 1997. The first results from the ACOPO, experiment, Nuclear Engineering and Design, 169, 49-57.

[66] Helle M.et al., 1999, Experimental COPO II data on natural convection in homogenous and stratified pools, 9th International Topical Meeting on Nuclear Reactor Thermal Hydraulics (NURETH-9), San Francisco, October 3-8.

[67] Bernaz L.et al., 1998. Thermalhydraulic Phenomena in Corium Pools: Numerical Simulation with TOLBIAC and Experimental Validation wit BALI, OECD/CSNI Workshop on In-Vessel Core Debris Retention and Coolability, Garching, Germany, March 3-6.

[68] Chu T. Y. et al., "Lower Head Failure Experiments and Analyses", NUREG/CR-5582, SAND98-2047, Sandia National Laboratories: Albuquerque, NM, 1998.

[69] Humphries L. L. et al., "OECD Lower Head Failure Project Final Report", OECD/NEA/CSNI/2(2002)27.

[70] Stepanyan, A. V., Nayak, A. K.,. Sehgal, B. R, 2005. Experimental investigations of natural convection in three layer stratified pool with internal heat generation, 11th International Topical Meeting on Nuclear Reactor Thermal-Hydraulics (NURETH-11), Avignon, France, October 2-6

[71] A. Kaiser, W. Schutz, W. Will, “PREMIX experiments PM12-PM18 to investigate the mixing of hot melt with water, FZKA 6380, 2001

[72] B. Spindler , B. Tourniaire, J. Seile, “Simulation of MCCI with the TOLBIAC-ICB code based on the phase segregation model”, Nuclear Engineering and Design 236 (2006) 2264–227

[73] Nagasaka, H., et al 1999. COTELS project (1): overview of project to study FCI and MCCI during a severe accident. In: Proceedings of the OECD Workshop on Ex-Vessel Debris Coolability, FZKA 6475, Karlsruhe, Germany, November 15–18, 1999, pp. 285–292.

[74] Epstein, M. 1998. Thermal Hydraulics of Molten Core–Concrete Interactions: Review and Comparison of Heat Transfer Models with Data, Interpretation of Rheologigal Data, and a Theory for the Onset of Concrete Spallation. Palo Alto: Electric Power Research Institute. (ACEX-TR-21.)

Appendix -1: Stream function approach:

The stream function is defined as

$$\frac{\partial \psi}{\partial y} = u$$

$$\frac{\partial \psi}{\partial x} = -v$$

This automatically satisfies continuity and gives rise to following equation

$$\frac{\partial^2 \psi}{\partial x^2} + \frac{\partial^2 \psi}{\partial y^2} = -\zeta$$

This can be solved independently to determine stream function.

The pressure gradient can then be calculated by

$$\left.\frac{\partial p}{\partial x}\right|_{wall} = \mu \left.\frac{\partial^2 u}{\partial y^2}\right|_{wall}$$

Appendix -2: Uncertainties in measurements

A2.1 Temperature measurement:

Temperature measurement was carried out with Inconel-600 sheathed ungrounded K type 1 mm thermocouples. The details of thermocouples, error and calibration are given in the following table.

Table A2.1. Temperature sensor details

Type	K, ungrounded
Sheath	1 mm OD
Insulation	MgO
Response time	175 ms
Calibration	With master RTD PT-100 with error 0.006 – 0.15 ^{0}C
Accuracy of the measurement	0.75 % of the measurement value upto 400^{0}C and 1 % upto 1300 ^{0}C
95 % Precision value	$\pm$1.04 ^{0}C
Total uncertainty in 95 % confidence measurement	$\pm$(0.0075*T + 1.04) ^{0}C T < 400 $\pm$(0.01*T + 1.04) ^{0}C T >= 400

As per the above table, the maximum error obtained in $\pm$13.04 ^{0}C at 1200 ^{0}C. This error bars are shown in figure below. As seen from the figure, there is not much influence of this error on the coolability prediction.

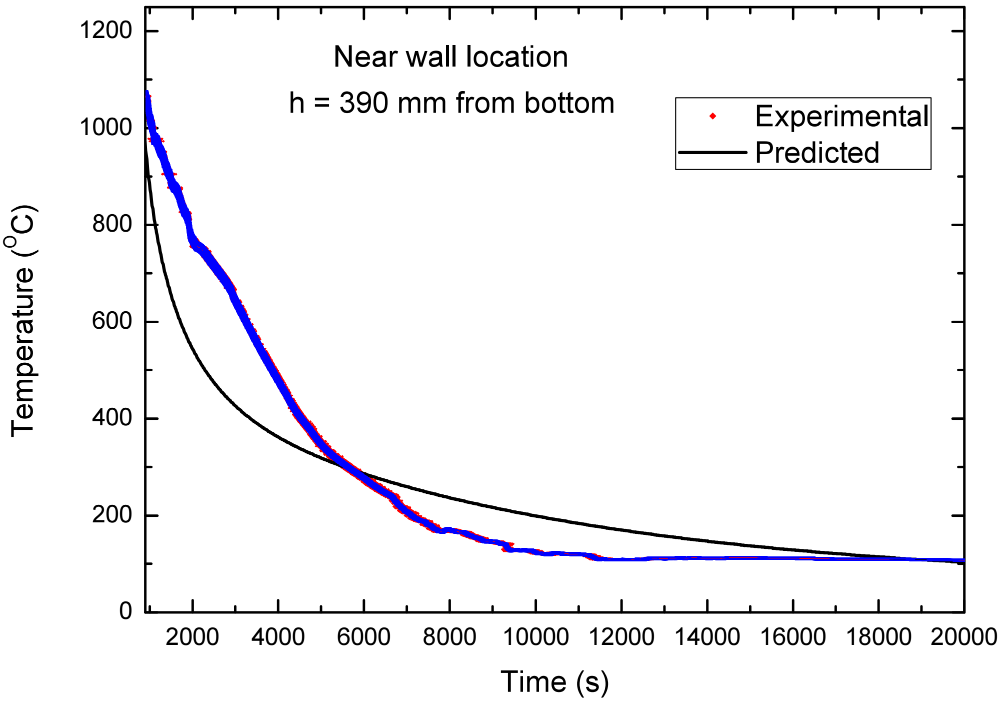

Figure A2. 1. Temperature plot with uncertainty in measurement

A2.1 Pressure measurement:

Table A2 2. Pressure senor details

Type	Nagano make Pressure Transducer
Response time	< 1ms
Calibration	Druck DPI 605 pressure calibrator with accuracy of 0.03 %
Accuracy of the measurement	0.1 %

A2.3 Differential pressure measurement

Table A2 3. Differential pressure sensor details

Type	Yokogawa make model EJA 110A
Range	–100 to 100 mbar
Time constant	0.3 s
Calibration	Druck DPI 605 pressure calibrator with accuracy of 0.03 %
Accuracy of the measurement	0.1 % of the value

A2.4 Flow rate measurement and level measurement are done with the same DPTs as above.

Hence the error in measurement is as specified above